Development and Evaluation of Some Semi-Metallic Oxide (TeO_2) and Semiconductor (CdTe) Films on Different Substrates for THz Device Applications

A thesis submitted to

University of Hyderabad

Towards partial fulfillment for the degree of

Doctor of Philosophy

in

Physics

By

M. Mahendar

(14ACPA04)

हैदराबाद विश्वविद्यालय
University of Hyderabad

प्रतिष्ठित संस्थान
INSTITUTION OF EMINENCE

Under the supervision of

Prof. Anil Kumar Chaudhary

Advanced Centre of Research in High Energy Materials (ACRHEM)

School of Physics, University of Hyderabad

Hyderabad 500046, Telangana, India.

December 2022

Dedicated to My

Mother

A thesis entitled

Development and Evaluation of Some Semi-Metallic Oxide (TeO_2) and Semiconductor (CdTe) Films on Different Substrates for THz Device Applications

Submitted to

University of Hyderabad

Towards partial fulfillment for the degree of

Doctor of Philosophy

in

Physics

हैदराबाद विश्वविद्यालय
University of Hyderabad

प्रतिष्ठित संस्थान
INSTITUTION OF EMINENCE

By

M. Mahendar

(14ACPA04)

Under the supervision of

Prof. Anil Kumar Chaudhary

Advanced Centre of Research in High Energy Materials (ACRHEM)

School of Physics, University of Hyderabad

Hyderabad 500046, Telangana, India.

December 2022

Certificate

This is to certify that the thesis entitled **"Development and Evaluation of Some Semi-Metallic Oxide (TeO_2) and Semiconductor (CdTe) Films on Different Substrates for THz Device Applications"** being submitted to the University of Hyderabad by **M. Mahendar** (Reg. No. **14ACPA04**), for the award of the degree of **Doctor of Philosophy in Physics**, is a record of bonafide work carried out by him under my supervision and is free of plagiarism.

The thesis has not been submitted previously in part or in full to this or any other University or Institution for the award of any degree or diploma.

27.12.2021

Prof. Anil Kumar Chaudhary

(Supervisor)

Dr. Anil Kr. Chaudhary
Professor (Physics)
Advanced Centre of Research in
High Energy Materials (ACRHEM),
UNIVERSITY OF HYDERABAD
HYDERABAD-500 046. T.S. INDIA.

Director

ACRHEM

Director
ACRHEM

Dean

School of Physics

I/c DEAN
School of Physics
University of Hyderabad
HYDERABAD - 500 046

Declaration

I, **M. Mahendar**, hereby declare that the work reported in this thesis entitled **"Development and Evaluation of Some Semi-Metallic Oxide (TeO_2) and Semiconductor (CdTe) Films on Different Substrates for THz Device Applications"** is original and has been carried out by me under the supervision of **Prof. Anil Kumar Chaudhary**, Professor in ACRHEM (School of Physics), University of Hyderabad, Hyderabad, Telangana, India, as per the Ph.D. ordinances of the University, which is also free from plagiarism. I further declare that this work has not submitted for the award of a research degree at any other University. I hereby agree that my thesis can be deposited in Shodhganga/INFLIBNET.

A report on plagiarism statistics from the University Librarian is enclosed.

M. Mahendar
27.12.22

(M. Mahendar)

Reg. No: 14ACPA04

27.12.2022

Prof. Anil Kumar Chaudhary

Thesis Supervisor
ACRHEM,
School of Physics,
University of Hyderabad.

Dr. Anil Kr. Chaudhary
Professor (Physics)
Advanced Centre of Research in
High Energy Materials (ACRHEM),
UNIVERSITY OF HYDERABAD
HYDERABAD-500 046. T.S. INDIA.

CERTIFICATE

This is to certify that the thesis entitled **"Development and Evaluation of Some Semi-Metallic Oxide (TeO_2) and Semiconductor (CdTe) Films on Different Substrates for THz Device Applications"** submitted by **M. Mahendar** bearing registration number **14ACPA04** in partial fulfillment of the requirements for the award of **Doctor of Philosophy in physics at ACRHEM, School of Physics, University of Hyderabad** is a bonafide work carried out by him under my supervision and guidance. This thesis is free from plagiarism and has not been submitted previously in part or in full to this or any other University or Institution for the award of any degree or diploma.

Further, the student has the following publications before submission of the thesis for adjudication:

1. **M. Mahendar**, A. K. Chaudhary, Ganesh Darmla, Vinay Gupta," Evaluation of cadmium telluride (CdTe) thin films grown at different annealing temperatures for efficient terahertz generation" Workshop on Recent Advances in Photonics (WRAP), Guwahati, 2019, DOI:10.1109/WRAPP47485.2019.9013662. **(Chapter 3).**
2. **M. Mahendar,** R, N Vamsi Krishna & A. K. Chaudhary, Femto Seconds Laser-Based Efficient THz Generation from Different Temperature annealed CdTe Thin films and Effects of carrier Concentration and Phase transition on Efficiency of Generation" submitted to the Indian Journal of Pure & Applied Physics (IJPAP) Vol.60, (2022) **(Chapter 3).**
3. **M. Mahendar**, P. Naveen Kumar, A.K. Chaudhary, SK. Ramiz Islam SoumenKanti Manna "Study of nucleotides using Terahertz Time Domain Spectroscopy", in URSI-RCRS (2022). **(Accepted) (Chapter 6).**
4. **M. Mahendar,** R, N Vamsi Krishna & A. K. Chaudhary, "Effect of Annealing Temperature on Structural, Morphological, and Nonlinear Optical Properties of TeO_2 films used for Efficient THz Generation", **(Communicated) (Chapter 5).**
5. **M. Mahendar,** Chandan Ghorui, & A.K. Chaudhary," Evaluation of terahertz (THz) based optical, dielectric, current density, conductivity and scattering, properties of Cd, Te, and CdTe films deposited on the GaAs substrate for device applications, (2022). **(Communicated) (Chapter 4).**

Also, made presentations at the following conferences:

1. **M. Mahendar,** A. K. Chaudhary, Ganesh Darmla, Vinay Gupta," Evaluation of cadmium telluride (CdTe) thin films grown at different annealing temperatures for efficient terahertz generation" in WRAP-2019, held at IIT Guwahati.

2. **M. Mahendar**, P. Naveen Kumar, A.K. Chaudhary, SK. Ramiz Islam Soumen Kanti Manna "Study of nucleotides using Terahertz Time Domain Spectroscopy", in URSI-RCRS (2022), held at IIT Indore.

The following courses have been taken as part of the coursework:

Course No.	Course offered at	Title of the Course	Credits	Pass/Fail
AC807	**ACRHEM**	Research Methodology	4	Pass
AC808	**ACREHM**	Non-linear Optics	4	Pass
AC810	**ACRHEM**	Introduction to High Energy Materials	4	Pass
MT803	**SEST**	Advanced Engineering Mathematics	4	Pass

27.12.2022

Supervisor,
Prof. Anil Kumar Chaudhary,
Physics,
ACRHEM, University of Hyderabad,
Hyderabad, India.

Dr. Anil Kr. Chaudhary
Professor (Physics)
Advanced Centre of Research in
High Energy Materials (ACRHEM),
UNIVERSITY OF HYDERABAD
HYDERABAD-500 046. T.S. INDIA.

Director,
ACRHEM,
University of Hyderabad,
Hyderabad,
India.

Director
ACRHEM

M. Shanashyam
27/12/22

Dean,
School of Physics,
University of Hyderabad,
Hyderabad,
India.

I/c DEAN
School of Physics
University of Hyderabad
HYDERABAD - 500 046

Acknowledgments

In these humble lines, I would like to express my gratitude to everyone who helped my thesis be successful.

My supervisor, **Prof. Anil Kumar Chaudhary**, is the first person I would want to thank on this list for his priceless guidance, powerful motivation, encouragement, and support. I would also like to extend my sincere personal gratitude to him. The extensive instruction I received while earning my Ph.D. will be very helpful to my academic career. In every way, without him, none of this effort would have been finished.

I would like to thank my doctoral committee members **Prof. Soma Venugopal Rao** and **Prof. M. Ghanshyam Krishna** for their invaluable suggestions in and out of the doctoral committee meetings.

It is my pleasure to thank the present director, **Dr. V. Kameswara Rao,** and former directors of ACRHEM for their support in all aspects towards the completion of this work. I also thank the Dean, School of Physics (SoP), UoH, for academic support.

I would like to thank Dr. Reshma and the late Prof. Vinay Gupta of Delhi University for donating the thermal deposition equipment required to fabricate the thin film.

I would like to thank the Defence Research and Development Organization (DRDO), India for providing me the financial support (through ACRHEM) all through my Ph.D.

I would like to thank Mr. Puspender Kumar and Dr. P. Sangra Ingole from IIT Kanpur for the Hall effect measurements.

I would like to thank the Former Director, Dr. Ajit Kumar Mohanty, and the present Director Dr. Gautam Bhattacharyya, Dr. Partha Saha Dr. Kaushik, Dr. Debasish mukhodhaya, Dr. Soumen Kanti Manna Dr. Chandrama Das, Dr. Sangram bagh, Dr. Oishee Chakravarthy, Dr. Raghu Raman, Mr. Raju Dutta, Mr. Arjit Da, Mr. Ajay Chakravarthy, Mr. Sanjay show, Mr. Shyamal Chandra Digar Mrs. Mahuya Dutta and administrative staff for SINP for their support.

I appreciate the experiments we performed with my senior and junior Drs. Vamsi Krishna, Chandan, Naveen Kumar, Kolla Rajesh Manchu, Dr. Venkatesh, Dr. Konda Srinivasa, Dr. Ganesh Damarla, these years would have been much harder without their support and company.

I wish to express my sincere thanks to the Former Executive Director General, Dr. N. R. Munirathnam, Dr. D.S. Prasad Dr. M.R.P. Reddy, Dr. U. Rambabu, Mr. R. Govindaiah,

Dr. Sandeep Mahajan, Dr. Mani Rokada Mr. B. Mahender, Mr. Ch. Sudheer, Mr. Bhaskar C-MET, Hyderabad for their support.

I would especially want to thank Lingam Murthy, Drs. E. Manikanta, Naga, Rajendra, Chandu, Yellu, Sai Shiva, Naga, Rajendra, and Chandu for their constant assistance, which enabled me to write my thesis and clear up a lot of my problems.

I would like to thank my friends/roommates Dr. Rajendra, Dr. Chandu, Dr. Naga, Dr. Kalam, and Mr. Sampath for their help in carrying out this research work, sharing their joy and my pain over these years. Without their company and help, these years would have been much tougher.

I also thank my endearing friends Mr. K. Vishnu Vardhan, Mr. Vijaysri Kumar, Mr. Partha Sarath, Mr. Vipin Singh, Mr. C. Palanivel, Mr. VenuGopal Rao, Dr. Nilkamal Barai, Mr. Pranay Raju, Dr. Pagidi Srinivas, Dr. Ramesh Manda, Mr. Kali Suresh, Mr. Vipin Singh, Dr. Saran, Mr. Bharath, Mr. Hari Babu, Mr. Jagan, Mr.Ajay, Mr. Giri, Mr. Deepak, for their motivation and support throughout my education career. Their support at all odd times in my personal life is invaluable.

My loving family is my top priority, and I sincerely appreciate them. I owe my parents, the Late **Mrs. M. Yadamma, Mr. M. Bikshapathi**, and my wife, **Mrs. M. Malathi**, for their unwavering love, devotion, and prayers over the course of my life. My power comes from them.

Finally, I would like to thank the almighty God for his blessings throughout my entire life.

List of Abbreviations

OR	**Optical Rectification**
TDS	**Time domain spectroscopy**
CdTe	**Cadmium telluride**
TeO_2	**Tellurium dioxide**
SDF	**Surface depletion field**
PDE	**Poto Dember effect**
EO	**Electro-optic**
EOS	**Electro-optic sampling**
PC	**Photoconductive**
PCA	**Photoconductive sampling**
THz	**Terahertz**
EFIOR	**Electric Field-Induced Optical Retification**

Table of Contents:

List of Figures

List of Tables

Chapter 1: Introduction

1.1 The Basics of Terahertz radiation

The terahertz (THz) frequency range of the E.M. spectrum is an order of = 10^{12} Hz. As per the international telecommunication guideline the frequency ν = 0.1 to 10 x10^{12}. It bridges the gap between electronics (MW), and the Photonics (FIR) spectrum of E.M radiation. As a result, it provides a smart tool to exploit the technology of two important regions. The THz frequency window finds potential use in defence, academic, medical science, and industries Fig.1- 1: depicts the location of the Terahertz frequency range of E.M. spectra [1].

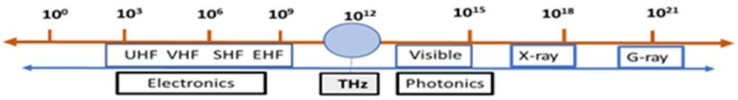

Fig. 1- 1: The Electromagnetic spectrum shows the THz area.

It possesses a very high absorption in water and high reflection from the metallic surface [2]. Laser-based optical techniques are employed for efficient generation and detection of wide-range THz radiation. The frequency domain spectra can be obtained by taking FFT of the time domain signal, similar to FTIR spectroscopy [3-4]. David Auston's research group, for the first time, they have demonstrated the role of short lifetime photo excited charge carriers in GaAs for the THz generation.-T-rays in present from name important properties potentially in the area of homeland security, defence, spectroscopy, and semiconductor industries [5]. Due to low photon energy (0.4 - 4.1meV). Moreover, it can penetrate through rubber, paper, fabric, polymer, etc., and also be treated as a non-destructive and non-ionizing means of analysis. Its spectral features match with the weak vibrational rotational modes of the organic molecules, an intraband transition from the semiconductor. The absorption bands in the THz domain are also treated as "fingerprints" of the test molecules [6-13].

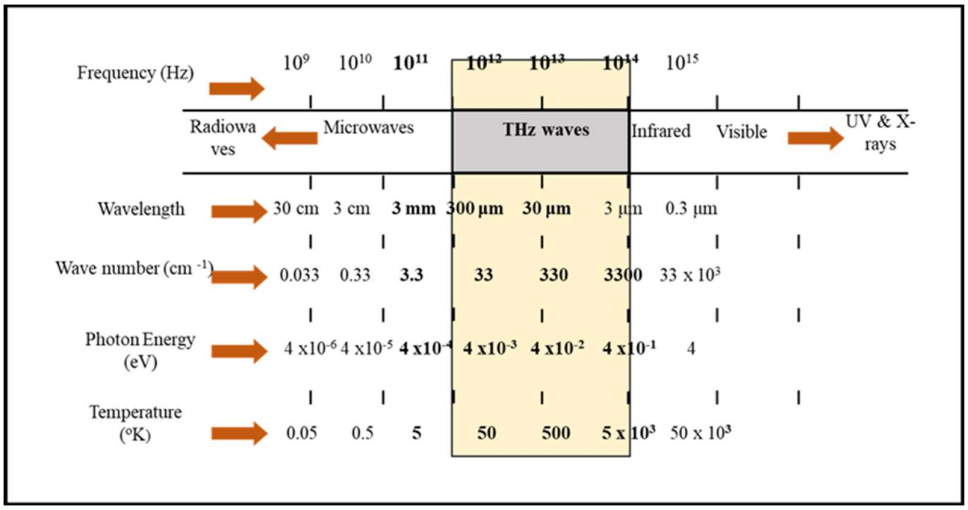

Fig. 1- 2: Terahertz is plotted in the units of frequency, wavelength, wavenumber, photon energy, and Temperature.

1.2 THz Generation Mechanism:

It can be generated by using different types of electronic and optical sources follows various mechanisms [14-23]. Among them, some prominent techniques are used for THz generation are ultrafast optical excitation of PCA, nonlinear crystals, and semiconductor surfaces. Photoconductive (P.C.) switching and optical rectification technique for the generation of terahertz radiation from antennas and nonlinear crystals. Semiconductor surfaces can generate THz radiation employing surge currents and non-linear effects. We have employed all types of aforesaid techniques for generating THz radiation.

1.2.1 GaAs Photoconductive antenna (PCA):

PCA is widely used as a source for Terahertz generation and the detector in the Time-Domain spectroscopy system. It consists of two metallic strips separated by a small gap of 5-10 microns on the LT/SI GaAs (III-IV direct band gap semiconductors) substrate. Also, this is treated as electrodes. These electrodes are externally biased with ~10 V. In a Photoconductive switch/ antenna, ultrafast lifetime photo-excited charge carriers are generated using ultrafast femtoseconds laser pulses. The incident laser pulses should posses higher energy than the bandgap of the semiconductor. The photo-excited ultra-short charge

carriers generate a transient current. The time derivative of the transient current as shown in Fig.1- 3 which is responsible for the generation of THz pulses [24-25].

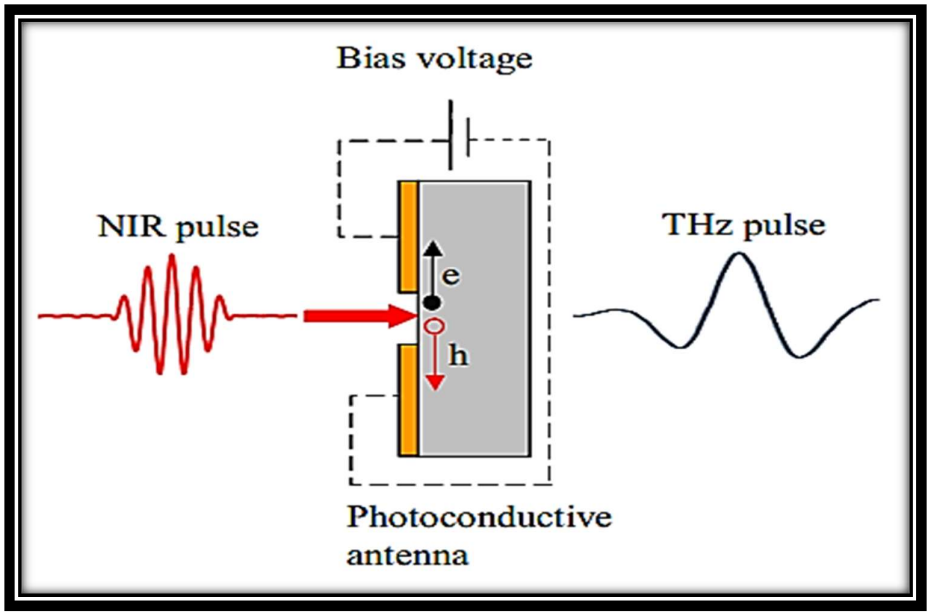

Fig.1- 3: Schematic diagram of the generation of THz radiation from PCA

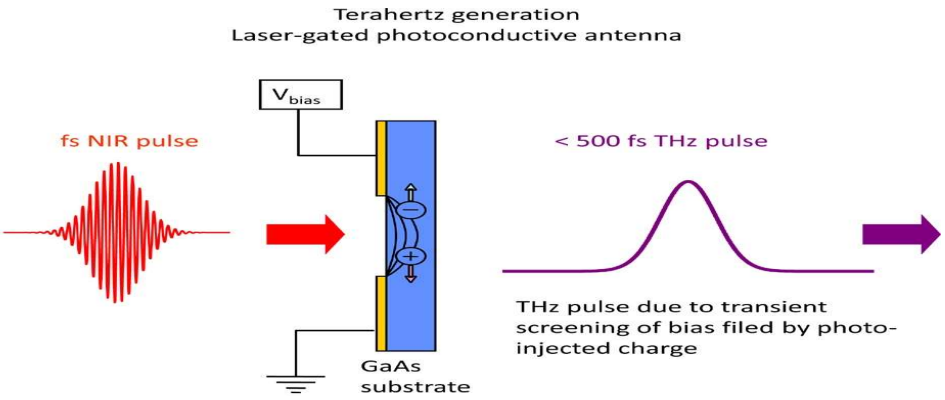

Fig.1- 4: Diagram of the THz generation mechanism induced by a femtosecond laser pulse in PC anntena.

$$\mathbf{E}_{\mathrm{THz}} = \frac{\mathrm{Ae}}{4\pi\varepsilon_o c^2 z}\frac{\partial^2 \mathrm{N}(t)}{\partial t}\mu\ \mathrm{E_b} \qquad (1.1)$$

Where A, "e", 'ε_o', is 'c' t 'z' represent the area under the beam electron charge is the vacuum permittivity, velocity and "Pulse penetration" in the semiconductor, where "N" stands for photo carrier density, " μ " for carrier mobility, and "Eb" for bias field.

There are multiple types of designed PC antennas used for THz generation. The first one depends on the distance between the metallic electrodes and the center frequency to produce THz radiation. The second one has variable gap distances and provides a broader frequency of Terahertz emission [26]. There are many reasons for using a Photo conductive antenna for Terahertz generation and their applications metallic, explosive, and organic molecular or imaging.

1.2.2 Optical Rectification Techniques:

Generally, optical Rectification (OR) is based on a nonlinear optical response of the materials with respect to the incident optical field associated with ultrashort laser pulses. When incident E electric field some isotropic and anisotropic materials show the under the influence of strong 2nd and 3rd order nonlinear response. The conversion of A.C. voltage is converted the process is in electronic into D.C. voltage known as rectification. Similarly, when subjected to intense laser beam, a nonlinear response varying with respect to optical field (electric field) component and optical materials is induced a time-dependent D.C. polarization, this phenomenon is called optical rectification. The ultra-short pulses produce DC polarized waves of sub picoseconds duration.–The generated time-dependent (transient) second-order wave polarized is associated with an electromagnetic field which lies in THz domain (as per maxwell equation). In another words, the optical rectification is another form of a difference frequency mixing, where two very closed spectral components present in a single ultrashort laser pulse are mixed in the optical. Some most well-known nonlinear crystals such as GaAs, InSb, InAs, LiNbO3, LiTaO3, ZnTe, DAST, BNA etc., are used for THz generation. The process of Optical rectification and DC polarized are given by Eqns (1.2-1.5).

Generally, all dielectric medium is transparent for small electric fields is associated with optical radiation, treated as a source of linear susceptibility of the medium and measured

in terms of refractive index however, when the number of photons very high and intense the nonlinear effects come into the picture, which can be represented as Taylor's expansion of the polarization wave in the Nonlinear optical medium.

$$\vec{\mathrm{P}}(\mathrm{t}) = \varepsilon_0\left(\chi^{(1)}e^{-i\omega t}\vec{\mathrm{E}}(t) + \chi^{(2)}\vec{\mathrm{E}}^2(\mathrm{t}) + \chi^{(3)}\vec{\mathrm{E}}^3(\mathrm{t}) + \cdots..\right) \quad \textbf{(1.2)}$$

Where χ(1): linear susceptibility and χ(2), χ(3), respectively, stand for second and third order nonlinear susceptibilities. Optical rectification is a second-order process, If applied electric field E(t) has two frequency components ω1 and ω2 then :

$$\vec{\mathrm{E}}(t) = \vec{\mathrm{E}}_1 e^{-iw_1 t} + \vec{\mathrm{E}}_2 e^{-iw_2 t} + C.C. \quad \textbf{(1.3)}$$

The second-order polarization is directly proportional to

$$P^2(t) \propto \varepsilon_0\chi^2\left[E_1^2 e^{-i2w_1 t} + E_2^2 e^{-i2w_2 t} + 2E_1E_2e^{-i(w_1+w_2)t} + 2E_1{E^*}_2 e^{-i(w_1-w_2)t} + C.C.\right]$$
$$+2\chi^2[E_1{E^*}_1 + E_2{E^*}_2] \quad \textbf{(1.4)}$$

where C.C. -Complex Conjugate of all the components. The remaining other two components i.e. sum and difference frequency waves are associated with Second Harmonic (S.H.), "Sum Frequency (SFG) E ($\omega_1+\omega_2$)", "difference frequency (DFG) E(ω1-ω2) of E_1 and E_2":

Essentially, the generated THz is related to the derivative of second-order polarization.

$$E_{THz}(t) \propto \frac{\partial^2 P^2(t)}{\partial t^2} \quad \textbf{(1.5)}$$

The generated THz field is directly proportional to second order derivative of polarized wave [27].Since the Refractive index of the medium and group velocity based dispersion are the function of frequency. Therefore, group refractive index mismatches with the refractive index of the THz velocity. Consequently, it violets the conservation laws which prevents the proper exchange of energy and momentum between incident optical pulse and generated THz waves. The coherence length provides an equal path for effective interaction between optical and THz pulses in the medium and given by :

$$L_c = \frac{\lambda_{THz}}{2(n_{group}-n_{THz})} \quad \textbf{(1.6)}$$

Where n_{group} is given by:

$$n_{group} = n_{optical} - \frac{\partial n_{optical}}{\partial \lambda_{optical}}\lambda_{optical} \quad \textbf{(1.7)}$$

Here $\lambda_{optrical}$, $n_{optical}$ are the Optical wavelength and refractive indices of the pump beam.

1.2.3 Semiconductor or Metallic Thin Films:

(a) Transient Current Effect:

THz radiation on semiconductor surface can also be generated by means of surge current mechanism which is also known as transient current effect. The surge current mechanism on the semiconductor surface is a linear effect that is further separated into two parts: the first one is the surface field effect [28] and the second one is the Photo Dember Effect [29-30]:

Surface field Effect:

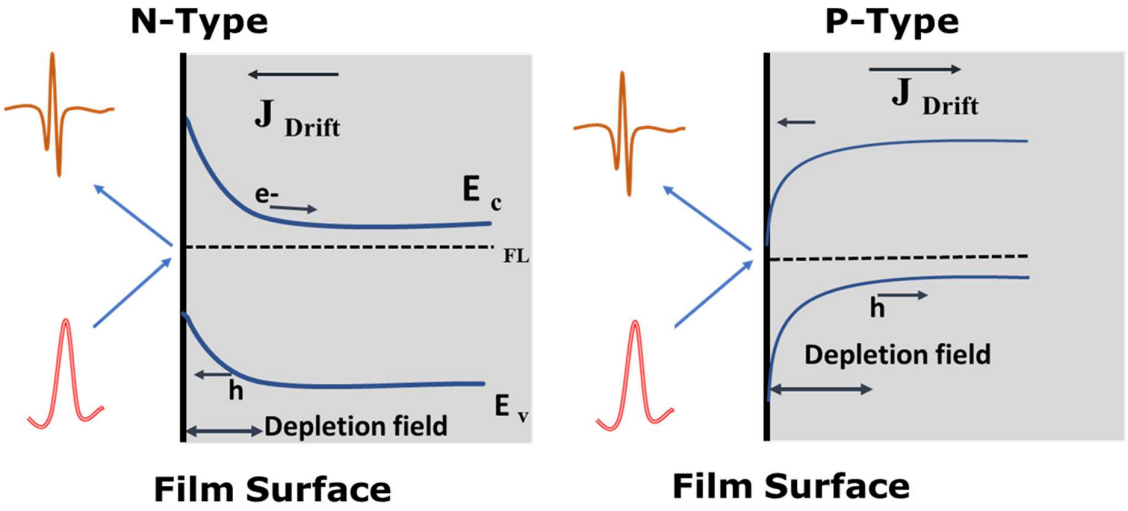

Fig. 1- 5: Energy diagram of surface field effect in p-type and n-type semiconductor materials (E_c-conduction band, E_v-valence band, W-depletion width, surface field-SF, Jdrift-drift current, e-electron, h-holes, and FL-fermi level).

The banding of conduction (C.V.) and valence (V.B.) bands along with mid level pinning of Fermi-level in many direct band semiconductors are responsible for the surface-depletion filed effect. If the energy of the excitation of femtosecond pulse is above the bandgap, the charge carriers present in form of electro-hole pairs get freed on the semiconductor surface. The generated field due to optical pulses mobilized the two

types of charge carriers in opposite directions. It generated photocurrent with associated dipole formation normal to surface direction behave like a transient dipole and emits polarized waves in THz domain.

The nature of the surface field effect totally based on the intrinsic field which opposed the biasing effect created by ultrashort pulses during photoconductive (P.C.) emission. Furthermore, in the case of the P. C. effect the direction of current flow and field lie in and normal to the surface plane.-The strength of surface depletion field depends on the type of doping and location of Fermi level. Generally, the band bending at the p-type to n-type materials are downwards and upwards, respectively [28].

The generated THz field E_{THz} is directly proportional to the drift current associated with the photoexcited carriers and given by Eqn (1.8)[32].

$$E_{THz} \propto \frac{\partial J_{drift}(t)}{\partial t} \quad \textbf{(1.8)}$$

$$J_{drift} = eE(n\mu_n + n\mu_p) \quad \textbf{(1.9)}$$

Where: $J_{drift}(t)$ is the drift current of carriers driven by the depletion field. The generated transient current is written as [31].

The E_d represents the surface depletion filed as a function of the distance x perpendicular to the surface can be represented as [29].

$$E_d = (eN/k)(W - x) \quad \textbf{(1.10)}$$

where "W" stands for the depletion width and "N" stands for the impurity concertation, and they can be expressed as

$$W = \sqrt{(2k/eN)\{V - (kT/e)\}} \quad \textbf{(1.11)}$$

Where Thermal energy is denoted by the symbol "kT/e", while "V" is the potential barrier.

b) Photo Dember Effect:

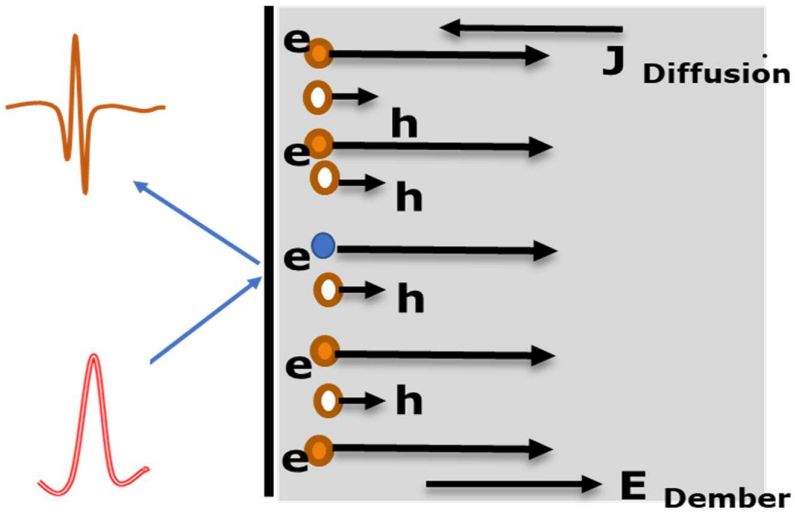

Fig.1- 6: Schematic of Diffusion field effect (EDember-photo dember effect, J diffusion -diffusion current, e-electron, h-hole)

The Photo Dember effect is the formation of a charge dipole in the proximity of the semiconductor surface due to ultra-fast laserbased photo generated charge carriers. The dipoles are formed owing to the difference in the diffusion rate of mobilities for holes and electrons. The electrons diffuse away from the surface rapidly due to their high mobility rate as compared to holes which possess low mobility and remains vicinity of the surface. In addition, holes combined with broken symmetry provided by the surface, leads to create effective charge separation in perpendicular direction of the surface. The macroscopic passage of an electric current is forbidden in an isolated sample, which causes the rapid carriers (typically the electrons) to slow down. An electric field accelerates the slow carriers (usually the holes), called the Dember field.

The electron and hole diffusive currents (Jn and Jp, respectively) can be shown as below [31].

$$J_n \propto eD_e \frac{\mathrm{d}\Delta n}{\mathrm{d}x} \text{ and } \quad J_p \propto -eD_h \frac{\mathrm{d}\Delta p}{\mathrm{d}x} \qquad \textbf{(1.12)}$$

Here, n and p represent the electron and hole densities, respectively, and D_e and D_h stand in for the electron and hole diffusion coefficients.

$$D = K_B T\mu/e \quad \textbf{(1.13)}$$

where K.B, μ , T, and represent the constant (Boltzmann), carrier temperature, mobility of the carrier concentration,

Hence, the diffusion current $\mathbf{J_{diffusion} = J_n + J_p}$ is proportional to the carrier mobility.

$$\alpha \ \ e\left(D_{\mathrm{e}} \frac{\mathrm{d}\Delta n}{\mathrm{d}x} - D_{\mathrm{h}} \frac{\mathrm{d}\Delta p}{\mathrm{d}x}\right) \quad \textbf{(1.14)}$$

$$\alpha \ \ K_{\mathrm{B}} \left(T_e \mu_e \frac{\mathrm{d}\Delta n}{\mathrm{d}x} - T_h \mu_h \frac{\mathrm{d}\Delta p}{\mathrm{d}x}\right) \quad \textbf{(1.15)}$$

Further, the diffusion current of the electrons is much larger than holes due to the electrons' significant mobility and kinetic energy compared to the holes. Hence, the THz radiation amplitude is directly proportional to the electron mobility.

$$J_{\mathrm{diffusion}} \ \alpha \ \ K_{\mathrm{B}} T_e \mu_e \frac{\mathrm{d}\Delta n}{\mathrm{d}x} \alpha \ \mu_e \quad \textbf{(1.16)}$$

$$E_{THz} \ \alpha \ \frac{\partial J_n}{\partial t} \propto \ \mu_e \quad \textbf{(1.17)}$$

From the above equations, the generated terahertz electric field is directly proportional to carrier temperature, mobility, and carrier density. The Photo Dember Effect is more pronounced in narrow bandgap semiconductors, such as InAs and InSb, due to higher electron mobility, weak depletion field, and short absorption depth [31-32].

1.3 The Electro-Optics Sampling techniques:

Electro-optic sampling (EOS) is an optoelectronics technique for detecting THz radiation, and the linear electro-optic effect is called the Pockels effect. By applying an electric field, the optical properties of electro-optic (E.O.) crystal can be changed in terms of birefringence even in many centrosymmetric crystals like ZnTe [34-35].

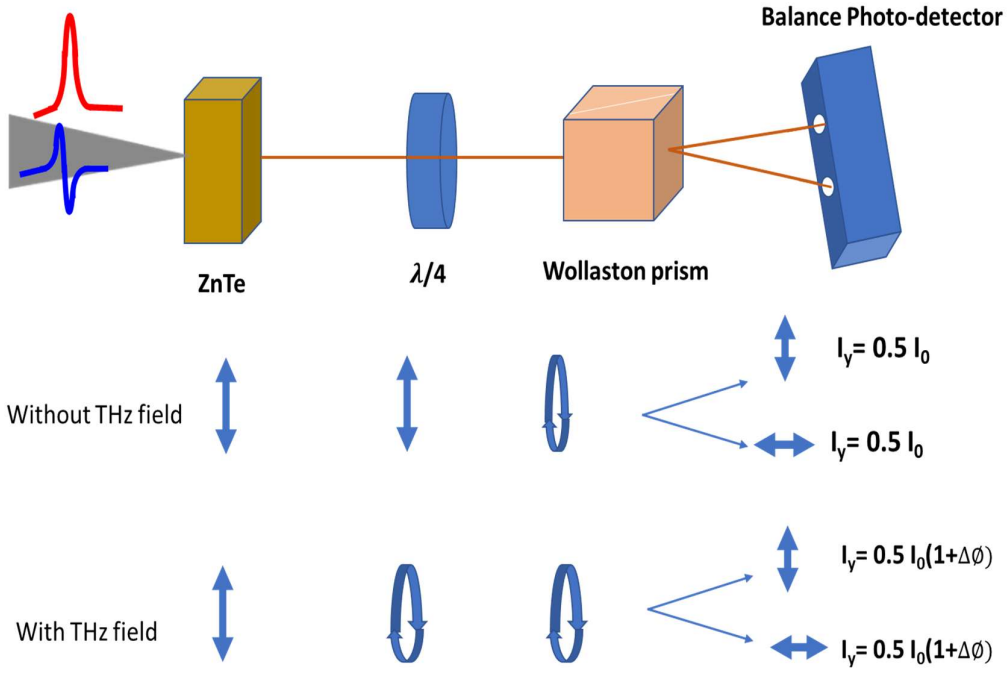

Fig.1- 7: Schematic of THz detection using Electro-optic sampling technique.

Coherent detection is an electro-optic (E.O.) sampling-based technique frequently used to detect THz time-domain spectroscopy [36-37]. In this technique, the effect of generated THz radiation is realized in the nonlinear detection crystal, such as ZnTe, which changes the induced polarization state of the transmitted optical pulse.

Fig. 1- 7: (a) Ultrashort pulses of wavelength of 800 nm obtained from femtoseconds laser are split into two parts in the ratio of 90:10 using a beam splitter. The first part of the incident beam acta as a pump and other part as a probe beam. The pump beam is used for the THz generation and recording of spectroscopy data using four numbers of off axis parabolic mirrors (OA). Finally it was directed and focussed towards the ZnTe crystal based balanced detector system. The system is made of ZnTe crystal, quarter waveplate Wollaston prism and pair of balance photo diodes [39-40]. The probe beam is rooted through delay stage and collimated with generated THz radiation using a perforated OA parabolic mirror and directed to ZnTe crystal.

In the absence of incident THz signal and optical probe beam which is linearly polarized is passed through the ZnTe and Quarter wave plates (QWP) convert it

into a –into circularly polarized plane. The circularly polarized probe beam splits into two equal and cross polarized components using a Wollaston prism. The output of the balanced detector remains zero due to equal strength of two optical components of probe beam, as shown in Fig. 1- 8. However, in the presence of THz radiation, due to the Electro-optic effect the ZnTe crystal rotates the polarization of the probe beam into circular polarized. The circularly polarized light is converted into an elliptical polarized using a QWP, and finally split into two unequal parts using a Wollaston prism.-The BPD gets unbalanced output in form of volts is fed to the lock-in amplifier (Model No. SR830) for the recording time-relative frequency and time-relative time-domain spectra of probe beam with respect to THz pulse.

1.4 Terahertz Application:

Terahertz part of the electromagnetic spectrum is employed in all branches of science such as physics, chemistry, pharmaceutical, bio medical, environmental research including defense and homeland securities. However, the majority of explosives organic polymers and biomolecules and their corresponding groups and orientation along with rotational and vibrational modes possesses signature in THz regions [38-39]. Therefore, it finds potential applications as a biomarker for cancerous cells. The biomarkers cells and tissue are small, and the tissue contains hundreds of other substances. This makes it challenging to identify the absorption peaks of biomarkers in mixed spectra. The typical peaks of biomarkers for various diseases have been established by numerous research teams. THz spectroscopy has several advantages over common spectroscopic techniques. THz-based 2D and 3 D time/ frequency domain imaging is another new area of research, specially imaging of historical artifacts, explosives, drugs and metallic implements under concealed conditions along with plant leaf and biological samples.

The image mapping will be carried out by measuring the temporal delay in the reflected signal. The refractive index of each thin layer of the paint material is different, causing a delay in the reflected signal. THz radiation is completely harmless, so T- ray imaging can be treated as an excellent alternative to X-ray imaging which is ionizing in nature.

The present thesis mainly focuses on the art of developing thin semimetal and Semiconductor films for making efficient terahertz sources without applying any external biasing voltage or magnetic fields. The C.W./pulsed terahertz radiation can be generated by means of several techniques such IMPATT and Gun diodes, Nonlinear crystals using Difference Freq. Mixing (DFM) technique, Optical Rectification (OR) technique using the femtoseconds laser pulses from N.L. crystals, semiconductors materials such as metallic oxide TeO_2 and semiconductor CdTe films deposited on glass substrates, etc. The annealing of these materials at a certain temperature range help to modify the structural and linear and nonlinear optical properties. We made an attempt to study the variation in the crystal structure, orientation, and thickness of films along with optical and morphological properties. A multipurpose THz generation cum spectroscopy setup was used for recording the time/frequency domain spectra. The set-up can further be modified according to the nature of test sample available in from of solid or liquid. The measurement of the refractive index, absorption coefficients, etc. has been carried out using terahertz time-domain spectroscopy. Additionally, one goal of the current investigation is to learn more about the many kinds of linear and nonlinear optical properties by using these materials to generate terahertz radiation.

In the present study, we have investigated the role of active and passive substrates such as GaAs wafers and glass plates for the growth of different types of semiconductors and semimetal films. GaAs wafer was selected as an active substrate for the growth and THz-based optical characterization of 3N and 5N Te, CdTe, and Cd films. Time-domain THz spectroscopy in transmission mode confirmed the role of interaction of free charge carriers of newly formed crystallographic structures of GaAs and CdTe films under the influence of applied THz field and resulted in the enhancement of the carrier concentration, the conductivity of the CdTe on GaAs substrate. It also influenced optical characterizations like absorption coefficients, dielectric constants, refractive index, and scattering in the terahertz domain.

Similarly, TeO_2 film was deposited on the glass substrate and subjected for annealing at 400^oC temperature. We used thermal evaporation techniques to deposit thin films as it is the only available technique that gives contradictory results compared to other techniques. Thermal evaporation techniques have their own merits in producing high-

quality TeO_2 and CdTe films. We can control the thickness of the thin film, which was understood from early works. The impact of deposition parameters By individually altering a number of development factors, such as film thickness, rate of deposition, substrate and source distance, growth pressure, source evaporation temperature, and substrate temperature, the structure of TeO2 and CdTe products has been examined. Hence, optimizing the deposition conditions is crucial to obtain thin films of high quality. Finally, these films were subjected to femtoseconds laser pulses and specially designed THz generation and detection setup for evaluating their performance as an efficient source of THz generation. The annealing carried out above 400 to 450^{o}C has made significant phase changes in the TeO_2 films. As a result, newly phase-transferred films were able to generate efficient and enhanced THz signals with respect to changes of temperature and incident laser power.

Finally, in the last part of the thesis, we have shown some applications for the recording of time/ frequency domain spectra of ribo-and deoxyribonucleosides constituting RNA and DNA biomolecules in aqueous solution using time-domain THz spectroscopy in reflection mode geometry. Between the range of 0.1 and 2.0 THz, each molecule has a unique absorption coefficient, refractive index, and extinction coefficient. Large atomic groups in the molecule's low-frequency vibration modes are thought to be the cause of the change in optical characteristics of macromolecules in the THz spectral band.

1.5 Overview of Thesis

The flow chart below provides a summary of the thesis (Fig.1 -8). Below are the specifics of the chapter discussion.

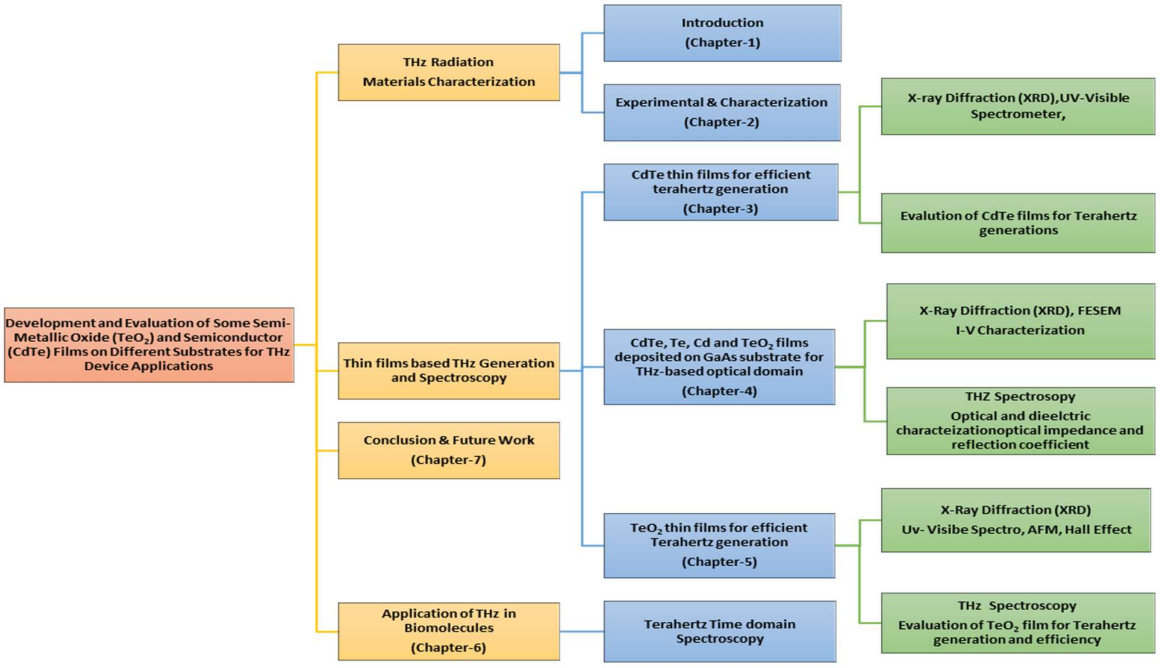

Fig. 1- 8 Overview of thesis

Chapter 1: **Introduction:**

The main topics covered in this chapter are related to the production, detection, and characteristics of THz radiation. The fundamental mechanisms underlying THz generation from photoconductive antennas (PCA), nonlinear organic and semiconductor-based optical rectification (OR), and metallic or semiconductor films based on the photo-dember (P.D.) effect are also covered in this chapter. It also concludes a brief discussion on detection techniques such as electro-optics sampling. An overview of the THz applications are mentioned at the end.

Chapter 2: Experimental & Characterizations Techniques:

This chapter primarily focuses on the fundamentals of the thin film deposition methodology (thermal evaporation) and the structural characterization of these films using well-known lab methods. Using techniques including (AFM), Hall effect measurements, UV-Visible NIR spectrometer, XRD, and (FESEM). In the third step, we have employed femtoseconds laser pulses for the evaluation of these films as a THz device. Additionally, the current transmission/reflection mode THz time-domain spectroscopic facility was employed for

the characterization of thin films. The experimental details of THz experiments using semiconductor and metallic thin films are briefly elucidated. It is also detailed how to measure terahertz power using an incoherent Pyroelectric detection approach.

Chapter 3: Elaboration of Thermal Annealing of the Structure and Optical Properties of CdTe thin films for Efficient Terahertz Generation

This chapter, discussed the process of thin-film preparation on a glass substrate using the evaporation technique under vacuum (at 10^{-5} mbar pressure) and investigated their X-ray diffraction (XRD) and UV/Vis/NIR spectrophotometer, respectively, are used to measure structural and optical properties. The as-deposited films were annealed at 200, 300, and 400ºC temperatures, respectively for a period of 30 min. Some of the important structural parameters such as grain size, dislocations density, and macro strain of thin films were also investigated. The absorbance and transmission data were recorded between 400–900 nm wavelength range which also reveals the effect of annealing in terms of shift in the bandgap between 1.35 to 1.45 eV. Whereas the XRD data confirms the significant effect of temperature on the change of structural properties which include crystallinity and preferential orientation. Finally, these films were subjected to 800 nm wavelength of 50fs pulses obtained from Ti: sapphire amplifier at a 1kHz repetition rate for evaluating their potential as a THz generator. The incident power of the laser was focused and tuned between 150-350 mW range and generated THz signals was recorded using calibrated Pyroelectric detector at 22.5 Hz frequency. The intensity of the generated signal was increased from 254.8 nW/cm2 to 1082.8 nW/cm2 reported at 200ºC annealed film. The highest efficiency of the generated THz signal was of the order of 3.41E-5% at 180mW incident laser power. We have also explained the effect of carrier concentration and phase transition with respect to temperatures for the efficient generation of the THz signal.

Chapter 4: Studies on Structural and Electrical properties of CdTe, Te, and Cd Deposited on GaAs Substrate for THz Domain.

This chapter deals with the systematic study on the role of GaAs wafer selected as an active substrate for the growth and THz-based optical characterization of 3N and 5N Te, CdTe, and Cd films. An indigenously designed THz spectrometer tunable between 0.1- 2.5 THz range was employed for the optical

characterization of deposited thin film samples. The 800 nm wavelength 140 femtosecond pulses obtained from Ti: sapphire femtosecond laser at 80 MHz repetition rate were used as a pumping source. Time-domain THz spectroscopy in transmission mode confirmed the role of interaction of free charge carriers of newly formed crystallographic structures of GaAs and other semiconductor films under the influence of applied THz field that which resulted in the enhancement of the charge carrier concentration, conductivity of the CdTe on GaAs substrate. It also influenced optical properties such as refractive index, absorption coefficients, dielectric constants, and scattering in the terahertz domain. Further, X-ray diffraction (XRD) also confirms the variation in crystallographic properties in terms of average crystallite size, lattice constant, micro-strain, dislocation densities, etc., during the growth process. This is also confirmed by the I-V characteristics graphs of these films in terms of enhancement current charge density (j). Finally, we have made an attempt to ascertain the conductivity, optical impedance surface roughness (g), and ϱ values, along with the reflection coefficient for both T.E. and T.M. modes of improvised semiconductor structures for the first time.

Chapter 5: Temperature-Dependent Annealing Effect on Structural, Morphological, Optical, and Electrical properties of TeO_2 Thin films for Efficient Terahertz Generation

In this chapter, we have discussed this temperature-dependent annealing on structure, morphology, optical, and electron properties of tellurium dioxide thin film prepared on a glass substrate using the evaporation technique under a vacuum (at 10^{-5} mbar pressure). The as-deposited TeO_2 films were annealed at 400 and 450ºC for 30 minutes. TeO_2 thin film of 120 nm thickness as a function of temperature. The structural properties were investigated by X-ray diffraction (XRD). The optical properties were determined, which are transmittance, absorbance, and the energy band gap. These films have a direct allowed transition with optical energy of 3.66, 3.64, and 3.54 eV at different annealing temperatures. The electrical properties of this film are determined using Hall measurements such as conductivity and Hall coefficient. The Hall effect measurement results show that the TeO_2 Thin-film is a p-type semiconductor, and carrier concentration and Hall mobility strongly depend on the effect of temperature at 310 to 355 K. The surface roughness and film morphology were analyzed by AFM. The optical

parameters of this film were determined by the refractive index and absorption coefficient in the terahertz domain. Finally, these films were subjected to 800 nm wavelength of 50 fs pulsed obtained from Ti: sapphire amplifier at 1kHz repetition rate. The incident power of the laser beam was focused and tuned between 65-115 mW range, and generated THz signals were recorded using a calibrated Pyroelectric detector at 22.5 Hz frequency. The highest power of the THz signal was 210nW for 450^{o}C annealed film with respect to the incident power of 115mW.

Chapter 6: Application of Terahertz Spectroscopy in Biomolecules

This chapter mainly focused on the time-domain THz spectroscopy of ribo- and deoxyribonucleosides constituting RNA and DNA in the aqueous solution. They play pivotal roles in the biological information cascade and functioning of the cell. The specified molecules' collective low-frequency vibrational modes are examined using terahertz spectroscopy. THz fingerprint spectra of DNA and RNA molecules are isolated from the cells which could provide crucial information about the basic constituents and conformations. These modes may provide information about the biomolecule fingerprint in the THz domain. In addition,We also determined the optical characteristics of these molecules in the 0.1-2.0 THz spectral range, including their refractive index, absorption, and extinction coefficients.

Chapter 7: Conclusions and Future plan

This chapter comprises the summary of the thesis work, conclusion and future scope. Our new investigation on the annealing effect can play a crucial role in improvising the structural, surface, and optical properties of semiconductor and semi-metallic films. Which can be used for developing simple and less expensive THz generation sources for future applications.

1.6 References:

1. Ashish Y. Pawar, Deepak D. Sonawane, Kiran B. Erande, Deelip V. Derle, Terahertz technology and its applications,Drug Invention Today, Volume 5, Issue 2, 2013, Pages 157-163, ISSN 0975-7619, https://doi.org/10.1016/j.dit.2013.03.009.

2. Mira Naftaly and Richard Dudley, "Terahertz reflectivities of metal-coated mirrors," Appl. Opt. 50, 3201-3204 (2011)

3. Fülöp, J. A., Tzortzakis, S., Kampfrath, T., Laser-Driven Strong-Field Terahertz Sources. Adv. Optical Mater. 2020, 8, 1900681. https://doi.org/10.1002/adom.201900681

4. Namje Kim, Sang-Pil Han, Hyunsung Ko, Young Ahn Leem, Han-Cheol Ryu, Chul Wook Lee, Donghun Lee, Min Yong Jeon, Sam Kyu Noh, and Kyung Hyun Park, "Tunable continuous-wave terahertz generation/detection with compact 1.55 μm detuned dual-mode laser diode and InGaAs based photomixer," Opt. Express 19, 15397-15403 (2011)

5. Terahertz Spectroscopy, Matthew C. Beard, Gordon M. Turner, and Charles A. Schmuttenmaer, The Journal of Physical Chemistry B 2002 106 (29), 7146-7159, DOI: 10.1021/jp020579i.

6. T. Globus, B. Gelmont, I. Sizov, 10 - Overview of terahertz spectral characterization for biological identification, Biological Identification, Woodhead Publishing, 2014, Pages 281-312, ISBN 9780857095015, https://doi.org/10.1533/9780857099167.3.281.

7. Fu Xiaojian, Liu Yujie, Chen Qi, Fu Yuan, Cui Tie Jun, Applications of Terahertz Spectroscopy in the Detection and Recognition of Substances, Frontiers in Physics, 10, 2022, http://:doi.org/10.3389/fphy.2022.869537, ISSN=2296-424X.

8. R. W. Boyd. Nonlinear Optics. (San Diego, USA: Elsevier Science) (2003).

9. H. Park, J.-H. Son, and C.-B. Ahn, "Enhancement of terahertz reflection tomographic imaging by interference cancellation between layers," Opt. Express (2016).

10. P. F. Taday, I. V. Bradley, D. D. Arnone, and M. Pepper, "Using Terahertz pulse spectroscopy to study the crystalline structure of a drug: A case study of the polymorphs of ranitidine hydrochloride," J. Pharm. Sci. (2003).

11.Siegel P.H THz technology: an overiew .Int.J. High Speed Electron.syst.2003; 13(2): 352-394.

12. Shen Y. C., Lo T., Taday P. F., Cole B. E., Tribe W. R., Kemp M. C. Detection and identification of explosives using terahertz pulsed spectroscopic imaging. Appl.Phys. Lett. 2005; 86(24): 241116.

13. Y. S. Lee, Principles of Terahertz Science and Technology (2009).

14. P.R. Smith, D.H. Auston, M.C. Nuss, IEEE J. Quant. Electron. 24, 255 (1988).

15 A.Rice, Y. Jin, X. Ma, X.C. Zhang, D. Bliss, J. Larkin, M. Alexander, Appl. Phys. Lett. 64, 1324 (1994).

16 X.C. Zhang, D. Auston, J.Appl.Phys. 71, 326 (1992). [35] G.H. Welsh, N.T. Hunt, K. Wynne, Phys. Rev. Lett. 98, 026803 (2007).

17. L. Ozyuzer, A. Koshelev, C. Kurter, N. Gopalsami, Q. Li, M. Tachiki, K. Kadowaki, T. Yamamoto, H. Minami, H. Yamaguchi, Science 318, 1291 (2007).

18 P.C. Planken, M.C. Nuss, I. Brener, K.W. Goossen, M.S. Luo, S.L. Chuang, Phys. Rev. Lett. (1992).

19 C. Waschke, H.G. Roskos, R. Schwedler, K. Leo, H. Kurz, K. Köhler, Phys. Rev. Lett. 70, 3319 (1993).

20 M.C. Beard, G.M. Turner, C.A. Schmuttenmaer, J. Phys. Chem. A 106, 878 (2002).

21 D.J. Hilton, R. Averitt, C. Meserole, G.L. Fisher, D.J. Funk, J.D. • ompson, A.J. Taylor, Opt. Lett. 29, 1805 (2004).

22 J. Shen, X. Fan, Z. Chen, M.F. DeCamp, H. Zhang, J.Q. Xiao, Appl. Phys. Lett. 101, 072401 (2012).

23 D. Cook, R. Hochstrasser, Opt. Lett. 25, 1210 (2000).

24. Tani M., Matsuura S., Sakai K., Nakashima S. Emission characteristics of photoconductive antennas based on low-temperature grown GaAs and semi-insulating GaAs. Appl.Opt. 1997; 36(30): 7853-7859.

25. Shen Y. C., Upadhya P.C., Linfield E. H., Beere H. E., Davies A. G. Gregory I. S.Generation and detection of Ultra-broadband terahertz radiation using photoconductive emitter and receivers. Appl. Phys. Lett. 2004; 85(2):164-166.

26. Shen Y. C., Upadhya P.C., beere H. E., Linfield E. H., Davies A. G. Gregory I. S. Ultra-broadband terahertz radiation from low-temperature-grown GaAs photoconductive emitters.Appl. Phys. Lett.2003; 83(15:3117-3119.

27. X.-C. Zhang and D. Auston, 'Optoelectronic measurement of semiconductor surfaces and interfaces with femtosecond optics', J. Appl. Phys.71, 326 ~1992.

28. H Takahashi, A Quema, M Goto, S Ono, and N Sarukura. "Terahertz radition mechanism from Femtosecond-laser irradiated InAs (100) surface", Japanese Journal of Applied Physics, 42, L1259-L1261 (2003).

29. P Gu, M Tani, S Kono, K sakai, and X-C Zhang. " Study of terahertz radiation from InAs and InSb", Journal of Applied Physics, 91 (9), 5533-5537 (2002).

30. S Kono, P Gu, M Tani, and K Sakai. " Tempearture dependence of terahertz radiation from n -type InSb and n-type InAs surfaces," Applied Physics B, 71 (6), 901-904 (2000).

31. J N Heyman, N Coates, A Reinhardt and G Strasser. " Diffusion and drift in terahertz emission at GaAs Surfaces", Applied Physics Letters, 83 (26), 5476-5478 (2003).

32. K Liu, J Xu, T Yuan, and X-C Zhang. "Terahertz radiation from InAs induced by carrier diffusion and drift", Physical Review B, 73 (15), 155330 (2006).

33. Wu Q., Zhang X. C. Ultrafast electro-optic field sensor.Appl.Phys.Lett. 1996; 68(12): 1604-1606.

34. Kono S., Tani M., Sakai k. Ultra-broadband Photoconductive detection: Comparison with free-space electro-optical sampling. Appl.Phys. Lett. 2001; 79(7): 898-900.

35. C. Bernerd, P. Segonds, J. Debray, T. Notake, M. Koyama, H. Minamide, H. Ito, and B. Boulanger, "Quadratic nonlinear optical properties of the organic N-benzyl-2-methyl-4-nitroaniline (BNA) biaxial crystal," Opt. Lett. (2018).

36. F. D. J. Brunner, O.-P. Kwon, S.-J. Kwon, M. Jazbinšek, A. Schneider, and P. Günter, "A hydrogen-bonded organic nonlinear optical crystal for high-efficiency terahertz generation and detection," Opt. Express (2008).

37.R. Beigang, S. G. Biedron, S. Dyjak, F. Ellrich, M. W. Haakestad, D. Hübsch, T. Kartaloglu, E. Ozbay, F. Ospald, N. Palka, U. Puc, E. Czerwinska, A. B. Sahin, A. Sešek, J. Trontelj, A. Švigelj, H. Altan, A. D. van Rheenen, and M. Walczakowski, "Comparison of terahertz technologies for detection and identification of explosives," in Terahertz Physics, Devices, and Systems VIII: Advanced Applications in Industry and Defense (2014).

38. V. A. Trofimov, S. A. Varentsova, M. Szustakowski, and N. Palka, "Efficiency of the detection and identification of ceramic explosive using the reflected THz signal," in Terahertz Physics, Devices, and Systems VI: Advanced Applications in Industry and Defense (2012).

Chapter 2: Experimental and Characterization Techniques

Abstract:

This chapter primarily focuses on the fundamentals of the thin film deposition methodology (thermal evaporation) and the structural characterization of these films using well-known lab methods. Using techniques including (AFM), Hall effect measurements, UV-Visible NIR spectrometer, XRD, and (FESEM). In the third step, we have employed femtoseconds laser pulses for the evaluation of these films as a THz device. Additionally, the current transmission/reflection mode THz time-domain spectroscopic facility was employed for the characterization of thin films. The experimental details of THz experiments using semiconductor and metallic thin films are briefly elucidated. It is also detailed how to measure terahertz power using an incoherent Pyroelectric detection approach.

Experimental Thin-film Deposition Technique:

2.1.1 Thin films:

Thin film deposition is a procedure that alters a surface's physical properties by depositing very thin layers of material that range in thickness from a few micrometers (μm) to a few nanometers (nm). The principal benefit of applications of thin films are availed by the semiconductors electronics industry and optical coating units. Thin film is used in fabricating solar cells, batteries, dye-sensitized, etc.

Since a long time ago, thin metal films on solid substrates have drawn interest due to their peculiar physical and chemical characteristics. These attributes are mostly governed by the microstructure and morphology, which are strongly influenced by the deposition technique and substrate characteristics [1–5]. Thin polycrystalline metal films are the subject of current research due to their widespread use in the production of various electronics. For the dependability and performance characteristics of such device production and the use of integrated circuits, thin dielectric and metal films must be thermally stable. There are different types of techniques used to grow thin films. Physical methods and Chemical methods are the two basic groups into which these approaches fall. For the present application, we have mainly utilized the Thermal Evaporation Process, which is a physical method used for depositing desirable films. The basic principle of this method is based on vacuum technology.

Many new areas of solid-state physics and chemistry research that are based on phenomena that are exclusively characterized by the thickness, structure, and morphology of the films have been influenced by thin films, either directly or indirectly [6-7]. Such thin films need to be produced, hence the depositing process needs to be well-regulated. It aids in the deposition of an atomic monolayer in exceptionally clean, specific-free circumstances. Due to the requirement that individual deposition particles be allowed to travel a considerable "mean free path" from a source to the substrate with little to no touch with gas molecules. Therefore, a high vacuum is used throughout the thin film deposition process.

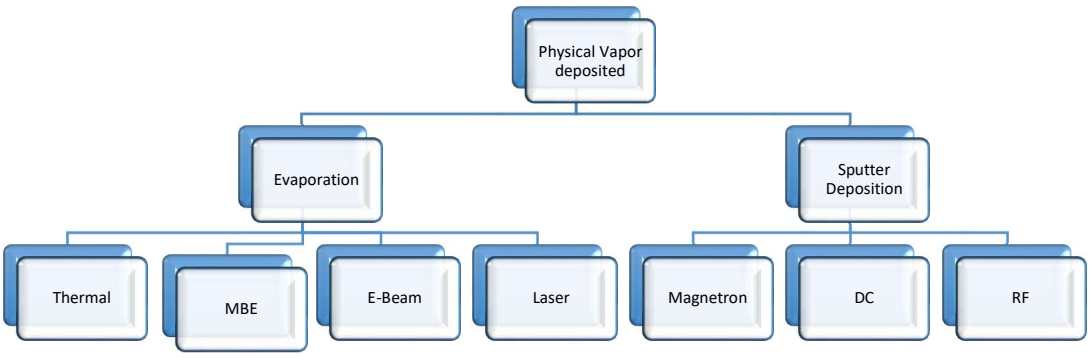

Fig.2- 1. Physical vapor deposition techniques

2.1.2 Physical Vapour Deposition:

The steps that physical vapor deposition takes are as follows:

a) The to-be-deposited solid materials are physically changed into the vapor phase.
b) The solid materials to be deposited are physically converted to the vapor phase.
c) The vapor phase is transferred from the source to the substrate via a region of low atmospheric pressure.
d) Thin sheets' vapor condenses onto the substrate.

The solid phase is changed into the vapor phase by physically moving the surface atoms, either by transferring momentum in the case of sputter deposition or by adding heat in the case of evaporation deposited.

A thin film is created by physical vapor using mechanical or thermodynamic methods. The primary mechanical method uses the sputtering technique, which involves bombarding a target made of the desired film materials with energetic noble gas ions, such as argon. When a shell strikes the ground, it creates a target-like shower of earth that emits a plume of material that embeds itself into the substrate's surface. the process starts by heating a solid piece of the material for the desired film until it melts, evaporates, or

sublimes. Under a strong vacuum, the vapour moves straight to the substrate, where it condenses to form a thin coating.

2.1.3 Thermal Evaporation:

The word "Thermal" implies that a high thermal temperature is essential for this procedure. All evaporation systems operate at the same "thermal high temperature," but they use different methods to melt the source materials. Thermal Evaporation or sublimation techniques are widely used to prepare thin layers. One technique for creating thin films in a high vacuum environment is thermal vacuum deposition, often known as the "thermal evaporation method." With this technique, the target is melted or sublimated at high temperatures into a vapor state. It is necessary to have a vacuum for molecules to be able to freely evaporate in the chamber and condense on substrate surfaces.

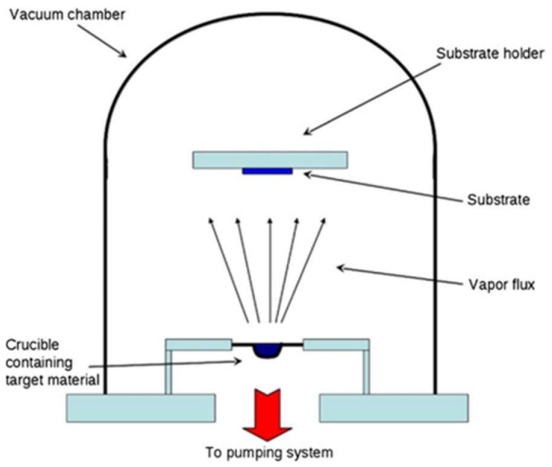

Fig.2- 2.Schematic diagram of Thermal evaporation unit [8]

The solid material is heated to a temperature that generates vapor pressure inside a high vacuum (10^{-6} Torr) chamber during the thermal evaporation process, which is shown in Fig. 2-2. Even very low vapor pressures inside the vacuum chamber can result in the production of a vapor cloud. These components are now moving through the chamber as a stream of vapor. lands on the substrate adhere to it and then condenses into a film or coating. Most materials are placed near the chamber's base, commonly in the shape of an

upright filament or crucible, because they must be heated to their melting point in order to become liquid. The vapor then rises above the chamber due to the source, which is at the bottom. It finally reaches the substrate, which was held upside-down in a suitable fixture at the top of the chamber with the coated surfaces pointing downward toward the ascending vapor.

To guarantee film bonds and regulate various film assets as needed, various steps were conducted. For factors, example, grain structure, homogeneity, stress adhesion strength, thickness, and optical qualities. The evaporation system design allows for the handling of many parameters to achieve favorite outcomes. Thermal evaporation systems will occasionally use quartz crystal deposition control to monitor and control the deposition rate in real-time to achieve the required layer thickness (2 nm to a few microns). Thin-film evaporation systems can provide comparatively high deposition rates, controllable thickness, and superior evaporation stream directional control for a variety of applications.

2.1.4 Thin-film Annealing Process:

Heat is utilized during the process of annealing to change the microstructure of materials with respect to gradual change of temperature. It helps to change its micro-strain and sometimes chemical properties to increase the ductility and reduce the hardness of materials. We used muffle furnace to anneal a given thin film under atmosphere conditions for the period of 30 minutes. In the first step, the sample was kept in the furnace, and temperature was set at 400^{o}C. After reaching the desired temperature of the thin film, we have waited for 30 minutes. To follow the slow-down cooling process the temperature of the furnace was set to 100^{o}C at a given time interval (one hrs). Generally, the cooling process takes 10 to 12 hours time to reach at room temperature.

2.2 Characterization Techniques:

Characterization of prepared materials is an important issue before their use in various device applications. the present work, the following characterization techniques were used for their optoelectronic characterization.

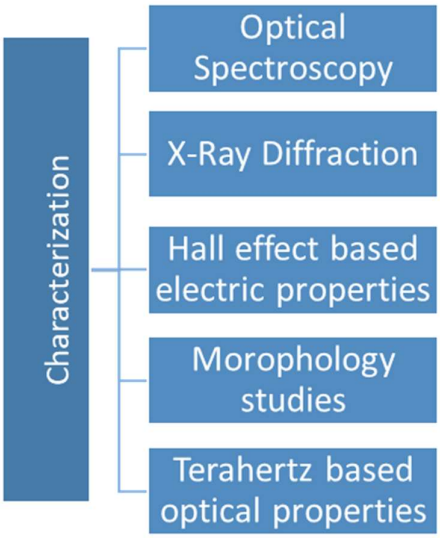

2.2.1 Optical Spectroscopy:

UV-Vis-NIR Spectroscopy:

Incoming light can cause an atom to respond. Light can either be absorbed or scattered by it. Light may be redirected or have its direction changed during scattering. In the case of absorption, the atom absorbs light and then undergoes a quantum leap to one of its higher energy levels. The absorption coefficient is the property of a substance that governs the amount of light that it absorbs. The absorption coefficient's inverse tells us how far on average a photon travels before it is absorbed.

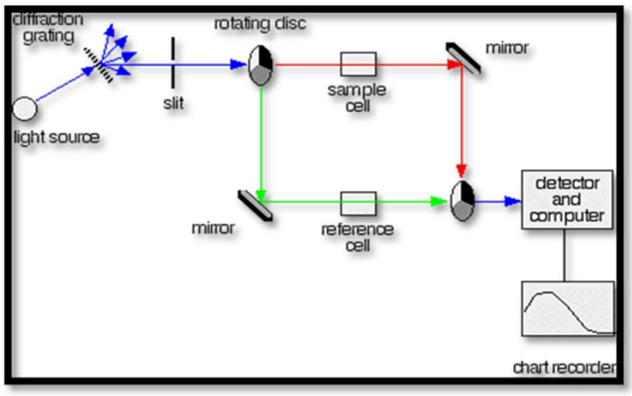

Fig.2- 3.Schematic diagram of UV-Visible spectrophotometer [9].

Energy variations in the range of 10^2 to 10^3 kJ mol^{-1} are related to electron transitions between the outermost energy levels. These energies, which range from near-infrared through visible to ultraviolet, are frequently linked to color. Numerous electronic transitions take place and can be found via spectroscopy.

A basic form for the absorption coefficient can be obtained from a straightforward consideration of the absorption process.

$$\alpha h\nu = (h\nu - E_g)^n \qquad \textbf{(2.1)}$$

Depending on the type of transition, n has values of 1/2 - allowed and 3/2 -forbidden for direct transitions and 2-allowed and 3 -forbidden for indirect transitions forbidden. Here, E_g stands for the material's energy bandgap. The direct bandgap energy is therefore obtained from a plot of $(\alpha h\nu)^2$ verses $h\nu$.

According to conventional wisdom, inorganic semiconductors can only excite electrons from the V_b -V.b to the C_b -C.b by absorbing radiant energy that is equal to or greater than the system's bandgap, Eg. As a result, when a quantum of energy ($h\gamma$) equals E_g, light is absorbed.

$$E_g = h\gamma_g = hc/\lambda_g = (1240/\lambda_g)\ eV. \qquad \textbf{(2.2)}$$

Since all of our thin-film samples behave like semiconductors, λ_g is calculated at the location where the slope of the absorbance versus wavelength graph abruptly changes. However, the approximate energy gap values that were acquired much aid in understanding the band structures of the thin films as they were formed.

2.2.2 X-ray Diffraction (XRD):

In crystalline materials, ions/atoms are arranged in regular periodic order, leading to different types of structures. XRD is one of the essential tools for the crystallographic structural investigation of materials. This technique is helpful for phase identification and the measurement of crystallite size. The X-ray scattering from numerous atoms and ions present in the lattice parameter (a b c) and Miller Indices (h, k, l) of that plane is the basis for the principle underlying this technique. Because of the periodic arrangement of ions and atoms in a crystal lattice, X-rays that are scattered by

them have clear phase relations between them; because of these phase relations, constructive interference only occurs in certain directions, resulting in diffracted beams.

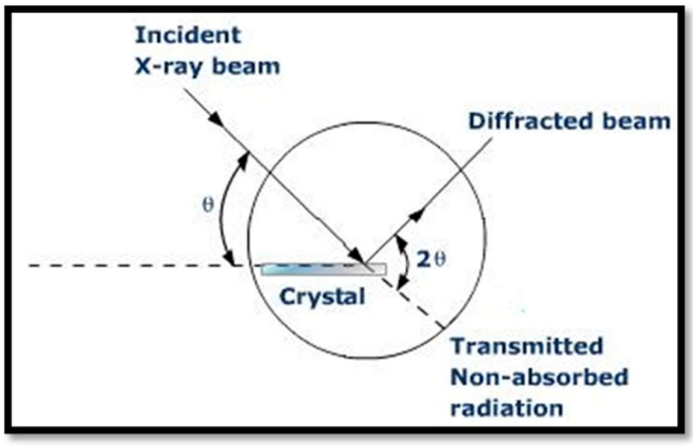

Fig.2- 4.A simple representation of x-ray diffraction is shown as follows [9].

Most solids are crystalline in nature, with crystal sizes ranging from 1/10 to 1/1000 nm. Understanding the details of the crystalline structure is vital not only for scientific reasons but also for practical applications. One of the simplest methods for obtaining structural information about the nanocrystallites contained in the amorphous matrix is the X-ray diffraction technique. Only when the Bragg condition is met can the X-Ray beam from a lattice be diffracted. The state of Bragg is described by

$$n\lambda = 2d_{hkl}\sin\theta \text{ (Bragg's law)} \qquad \textbf{(2.3)}$$

where "n" is the order of diffraction, "λ" is the incident wavelength, X-ray's "d_{hkl}" is the interplanar distances, and θ = angle of incidence.

The powder XRD technique uses a powder specimen to diffract monochromatic X-rays. In this collection of randomly oriented crystals with respect to the incident X-ray beam, a few of the crystals will be perfectly oriented so that their (h k l) planes reflect the incident X-ray beam in diverse directions and according to Bragg's law. Since the single crystal is not always available, this technique is preferred over the Laue method. Polycrystalline samples may be analyzed non-destructively without any preparation. It is a useful technique for structural determination because it gives the polycrystalline material structure and crystallite size. Using the diffractometer, one can also monitor the effect of doping, iodization, etc.

Using a Rigakuminiplex powder X-ray diffractometer, all of the samples used in this experiment were characterized by XRD. The Cu-Kα radiation was used as the X-rays source, and the diffraction patterns were recorded at room temperature in the 2θ (degree) range of 4-70º with a step size of 0.02º. Using Scherrer's equation, the materials in the thin film's crystallite sizes or grain sizes might be predicted from the intense diffracted line's full width at half-maximum (FWHM) [10].

$$D = \frac{0.9\lambda}{\beta \cos\theta} \qquad \textbf{(2.4)}$$

Where **λ** denotes wavelength (**λ= 1.5406 A°)** β (in radian) refers to Full Width at Half Maxima (FWHM) obtained from the XRD spectra at fact, k symbolizes the shape factor, which is=0.94, and θ (in degree) is the diffraction angle.

2.2.3 Measurements of the Hall Effect:

When a current-carrying wire or semiconductor is exposed to a perpendicular magnetic field, the Hall Effect states that a voltage can be created at a right angle to the current route. This voltage is known as the hall voltage.

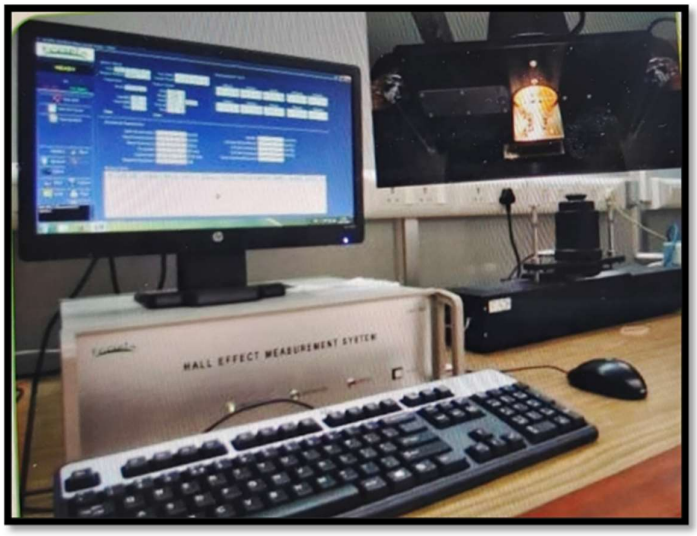

Fig.2- 5.Experimental image of Hall effect measurement system Ecopia HMS.

By studying the Hall effect, we can identify semiconductors i.e., the type of 'N' or 'P'-type, and the concentration of electric charge carrier concentration of the film between

room to 300° K temperature a perpendicular continuous magnetic field (B) was applied to the film for a generation of the Hall magnetic field given by Eqn. (2.5) using this, The Hall coefficient (R_H value) can be found in the following situations:

$$R_H=(V_H*I)/(t*B) \quad \textbf{(2.5)}$$

Further, the values of hall coefficient R_H were used to measure the charge carrier concentration using the given Eqn (2.6).

$$n=A/|R_H|e \quad \textbf{(2.6)}$$

If the Hall factor A is one, then e is an electron's charge.

The Hall mobility (μ_H) at room temperature can be calculated from Eqn (2.7).

$$\mu_H = |R_H| \sigma \quad \textbf{(2.7)}$$

The equation yields the Hall voltage, denoted by V_H:

$$V_H=IB/qnd \quad \textbf{(2.8)}$$

Where: I stand for the current passing over the device, B for magnetic field strength, q for the charge, n for charge carriers per unit volume, and d for sensor thickness.

The mathematical formula for the Hall Coefficient R_H is

$$R_H=E/jB \quad \textbf{(2.9)}$$

2.2.4 Atomic force microscopy:

Atomic force microscopy (AFM), which measures surface topography on a scale from angstroms to 100 microns, is used. The method entails photographing a sample with a probe or tip that has a radius of 20 nm. A feedback mechanism that studies interactions between the surface and tip at the nanoscale keeps the tip a few nanometers above the surface. As the tip is repeatedly scanned across the sample, variations in tip height are noted, creating a topographic representation of the surface[9].

The imaging apparatus of the Microscopy Suite is capable of creating pictures in a wide range of modes, including basic AFM modes including pulsed, magnetic, electrical, and tapping forces. The tip oscillates over the sample surface in tapping mode, allowing measurements of interactions with surface topography, stiffness, and adhesion. It

generates more picture contrast approaches than normal AFM. Magnetic domains on the material are found using the magnetic force mode imaging technique. To detect and capture variations in surface charge, electrical force mode imaging employs a charged tip. Pseudo-force-distance curves are produced while the sample oscillates beneath the tip in pulsed force mode (Wintec). Pseudo-force-distance curves are generated as the sample oscillates in pulsed force mode beneath the tip (Wintec). The ability to separate sample topography, stiffness, and adhesion values enables the creation of three independent images or data sets at once.

This device can also be utilised with an STM head, or scanning tunnelling microscope. STM makes use of electron quantum mechanical tunnelling to scan conducting surfaces. A clear, microscopic representation of the surface topography of a small object is provided by atomic force microscopy, in contrast to all imaging techniques that use the diffraction of electron and light beams at crystal lattices, which are incapable of resolving local structures and flaws. AFM is a variation of the (electron) scanning tunneling microscope, whose main drawbacks are the need for a conducting sample surface and reasonably stable measurement conditions. AFM analyses the deflection of a small cantilever with a small tip due to the interatomic interactions between the tip and surface atoms.

In addition to these two main modes, there is also a contact mode and a non-contact mode that both touch and do not touch the surface being probed. While the soft layer can be penetrated in non-contact mode necessitates being very close to the surface to operate with rigid samples covered in soft adsorbates. and must be clean otherwise the results may differ depending on how dynamically the surface is touched. As a result, tip and surface damage is minimised.

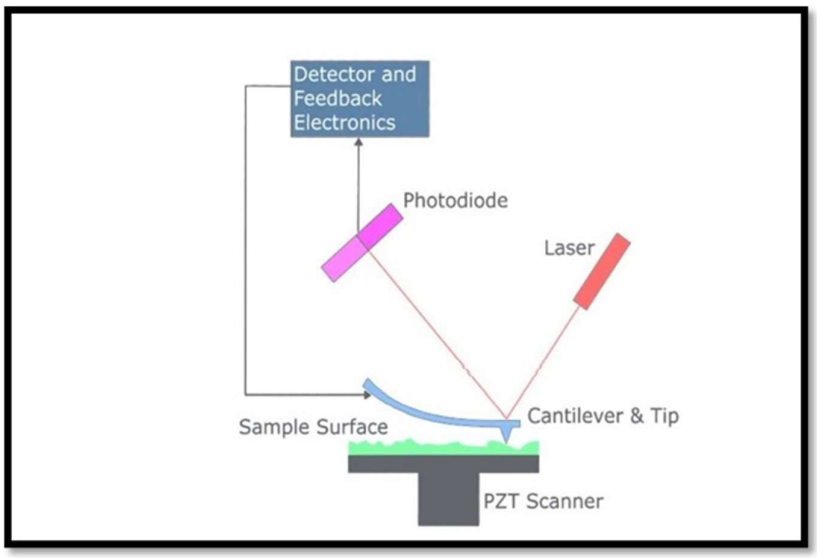

Fig.2- 6.Atomic force microscope block diagram

2.2.5 Field Emission Scanning Electron Microscopy (FESEM):

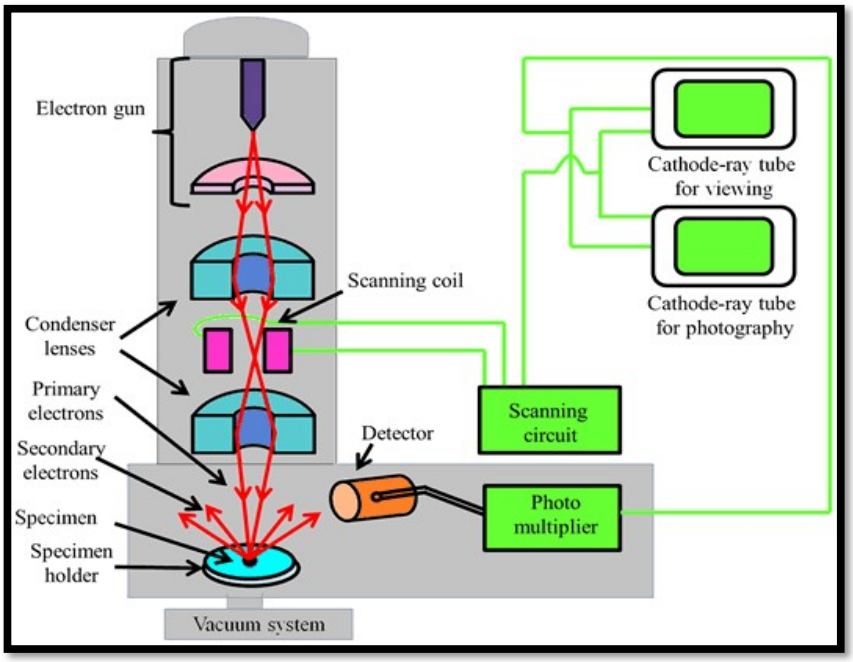

Fig.2- 7.Schematic diagram of FESEM Setup [11].

As a result of the field emission source's discharge of electrons, a powerful electric field gradient accelerates them. Within the high vacuum column, electron lenses concentrate and deflect primary electrons to create a focused beam that scans the area and bombards the targets. A section of the object, therefore, emits secondary electrons. The speed and

inclination of these secondary electrons are dependent on the item's surface shape. An electrical signal is produced once the secondary electron is collected by a detector. A video scan is created from this signal once it has been amplified. This picture can be seen on the monitor or as a digital picture that can be saved and enhanced. Field ionisation One type of electron microscopy, known as scanning electron microscopy (FESEM), creates images when scanning an electron beam focussed by field emission. A strong electric field that is applied over the source results in a gradient electric field. The electron is released, and the field then accelerates and channels it. This electron beam is focused on the sample under investigation using electromagnetic lenses. The interaction of the electron beam with the electrons in the samples results in a variety of electron types and characteristic X-rays. Secondary electrons are created when a high-energy electron beam interacts with atoms on or near the sample's surface. Electron detectors take these in. These electrons are synchronized with the incident beam and then analyzed to produce high-resolution images of the sample surface.

2.3 Brief description of the femtosecond laser system:

Two commercially available Ti: Sapphire Laser systems were utilized to perform the terahertz experimental (a) Laser pulses with a 140fs duration and an 80 MHz repetition rate produced by the oscillator laser (Chameleon Ultra-II). b) Amplifier femtosecond (fs) laser (coherent LIBRA) having a 1 kHz repetition rate and 50 fs-long pulses.

2.3.1 Oscillator Laser (Chameleon Ultra-II)

Compact, adjustable between the visible -680 nm and near-infrared 1080 nm ranges, and producing laser pulses with a 140fs length at an 80 MHz repetition rate is the oscillator laser (Chameleon Ultra-II). At 800 nm, the pulse has a 4 mW average power. The essential components of the laser are the laser head, power supply, chiller, and miniature-recirculating unit (MRU). As seen in Fig.2- 7, A Verdi, Verdi pumped ultrafast (VPUF) laser head, and power track mirrors are included in the laser's schematic. Neodymium vanadate (Nd: YVO4) serves as the gain medium in the Verdi laser and is pumped by fiber optics using a dual-end pump configuration. For the second harmonics generation kept at 150°C, an LBO crystal with a type-I cut that is non-critically phase-matched is employed. The Pump 532 nm beam from Verdi Leaser is guided into VPUF by Pump power track (PPT) mirrors mounted on piezo-controlled feedback loop electric transducers (PZT). Power track mirrors (CPT) inside the VPUF cavity position the Laser pump beam inside the cavity.

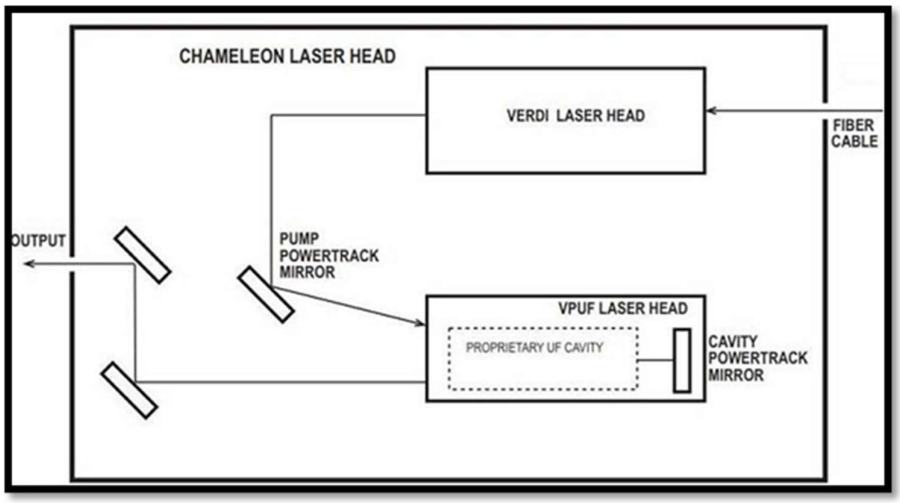

Fig.2- 8.Chameleon Ultra II Laser Head (image adopted from the coherent manual)

A chiller outside circulates a pre-mixed fluid to keep the baseplate's temperature within UPUF at 20°C. Ti: sapphire is utilized as a gain medium, and the Kerr Lens Mode locking method is used to emit ultrashort femtosecond pulses. When Kerr lensing occurs, the medium's refractive index varies with a distinctive intensity. The cavity length can be altered to tune chameleon lasers.

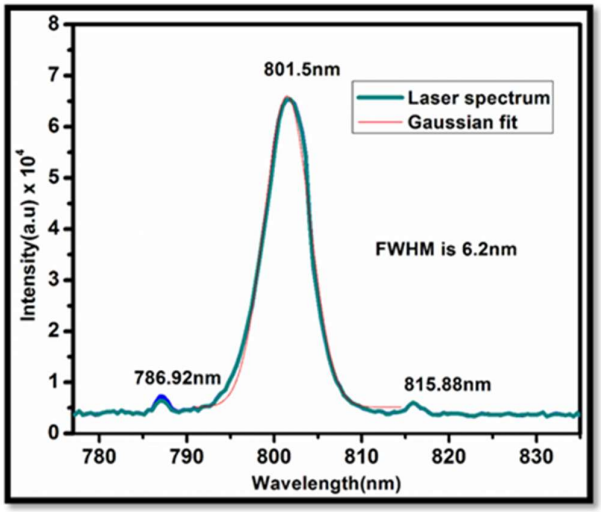

Fig.2- 9.The output spectrum of the laser wavelength at 800 nm

The humidity of a laser is conditioned, cleaned, and maintained using MRU. To track the laser's emission wavelength, a built-in spectrometer is fastened to the laser head. Manufacturers offer a straightforward GUI that shows the output and regulating process. At line width $\Delta\lambda$ 6.2 nm at FWHM, the Chameleon oscillator emits the most power at an output

wavelength of 800 nm. The Maya 2000 Pro spectrometer's output spectrum at 800 nm is displayed in Fig.2- 9.

2.3.2 Coherent LIBRA (amplifier)

The optical bench installation is depicted in Fig.2- 9, and the femtosecond needed for Terahertz studies was produced using a commercial compact fs laser system (Coherent LIBRA) [12]. An ultrafast laser (Ti: Sapphire) system with a beam diameter of about 9 mm, operating at 800 nm as the wavelength's centre and a repetition rate of 1 kHz. It emits pulses with a maximum energy of 4 mJ/pulse, which translates to a pulse width of about 35 fs and an average power of 4 W. Four modules make up the optical bench assembly. a stretcher, a compressor, a regenerative amplifier (RGA), a Vitesse seed laser, an evolution pump laser region merged into a single box, and so on.

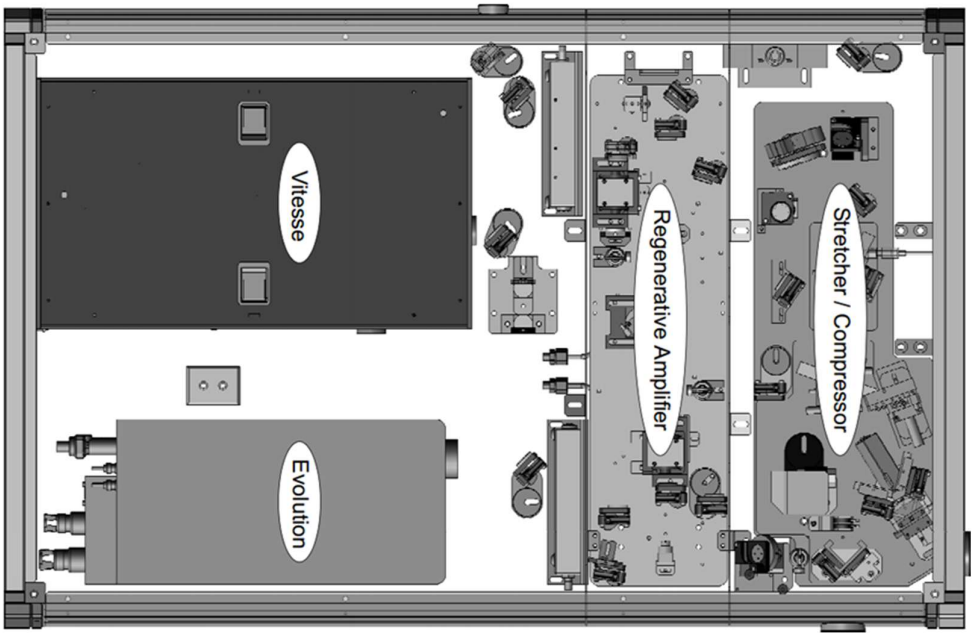

Fig.2- 10.The optical bench assembly of the Libra fs laser system.

2.3.2 (a)Vitesse seed laser

The cavity power track mirrors are the only difference between the Vitesse and Chameleon laser schematics, as seen in Fig.2- 10. A green diode laser (Coherent Verdi) with a power range of 2 to 5 W pumps the Ti: sapphire oscillator laser Vitesse. Fig.2- 11

depicts the components of Verdi, which also comprise an astigmatic compensator, two pump mirrors, two cavity end mirrors, LBO (SH crystal), and Etalon.

The wavelength produced by Neodymium Yttrium Orthovanadate (Nd:YVO4) is 1064 nm. The second harmonic of 1064 nm, or 532 nm, green in colour, is produced by the lithium triborate (LBO) NLO crystal and is efficiently absorbed by the titanium-sapphire crystal. With the help of a resistive heater, the LBO crystal is kept at 148°C. In order to prevent unintended locking mechanisms, the Etalon is positioned inside the cavity. The Vitesse is capable of emitting pulses with a 50fs pulse width, 150 mw of power, 60 nm of bandwidth, and an 80 MHz repetition rate. The Kerr lens mode-locking technique is used to produce femtosecond pulses. The generation of femtosecond pulses involves the Kerr lens mode-locking method.

$$n = n_0 + n_2 I \tag{2.10}$$

Here, the linear and intensity-dependent refractive indices are denoted by n_0 and n_2, respectively.

Higher intensity refractive indexes would produce greater focusing action since the Gaussian beam's intensity distribution is not uniform. Kerr lensing is the term for this occurrence. Only modes with higher intensities can build up in the cavity because of the Kerr lensing effect. As a result, output laser pulses will have a wider spectral bandwidth and create pulses that last for shorter periods of time. An amplifier is used to boost the laser's intensity after the ultra-rapid femtosecond pulse is generated. There are three parts to an amplifier: a pulse stretcher, a regenerative amplifier (RGA), and a pulse compressor.

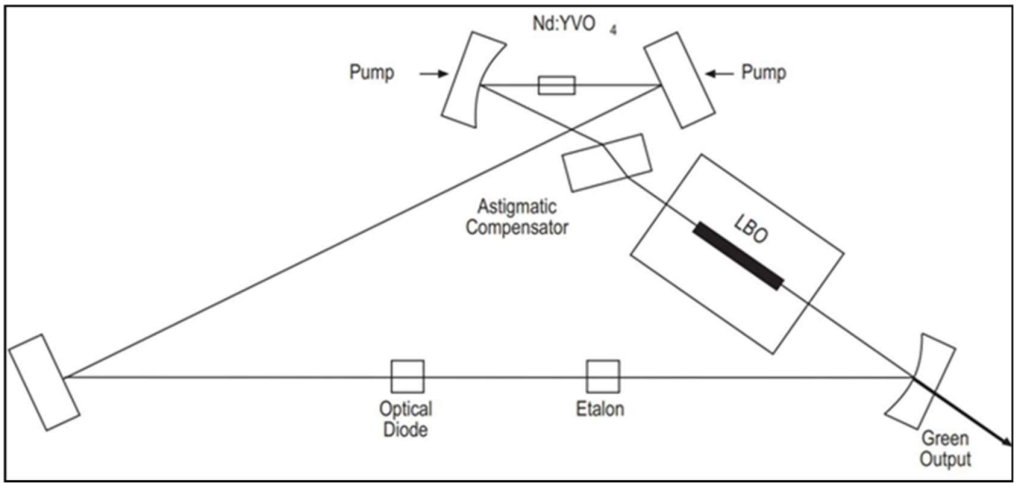

Fig.2- 11.Verdi laser head schematic (image adapted from coherent Manual)

2.3.2 (b) Pump Laser (Evolution):

It achieves twice the pulse energy of an Nd: YAG laser thanks to an upper-level lifespan of 470s, which is twice as long. However, it does so significantly more slowly. Additionally, producing a laser with high beam quality benefits from minimal thermal lensing and natural "birefringence." The most efficient pumping strategy is provided by the diode laser's narrow spectral emission, which is superior to arc lamp emissions. In addition, very little waste heat is produced when any or little of the diode light emanating from the gain medium falls outside of its absorption region. The laser pulse can be produced using the acousto-optic Q-switching approach. It offers the fundamental wavelength (1053 nm) for the 4F3/2 4 I11/2 transitions. The 1053 nm laser is propagated through an LBO crystal to double the frequency (527 nm).

2.3.2(c) Regenerative amplifier (RGA)

The Legend Elite TM platform (M/s Coherent, USA) serves as the foundation for the RGA. Compact in design, the amplifier is housed in a module with an active cooling system [13]. Excellent stability and reduced sensitivity to variations in the outside temperature are both displayed by it. The Synchronized Delay Generator (SDG) system, which synchronizes the pump laser and controls the operation of the Pockels cells for the seed laser, is a built-in component of the regenerative amplifier system. A pump beam from evolution that is focused onto the gain medium and round trips is employed to amplify the seed pulse from Vitesse in RGA.Table2- 1 lists the oscillator and amplifier laser beam's technical specifications.

Table 2.1. Lists the oscillator and amplifier laser beam's technical specifications

S. No	Parameters	Oscillator	Amplifier
1	Pulse duration	~ 100 fs	~ 100 fs
2	Rep rate	80 MHz	1 kHz
3	Beam diameter	~ 3 mm	~ 9 mm
4	Maximum energy per pulse	~ 7 nJ	~ 4 mJ
5	Polarization	Horizontal	Horizontal

2.3.2(d) Stretcher & Compressor

Within a sturdy modular shell, a single box system housing the stretcher and compressor is integrated. In RGA, the Chirped pulse amplification approach increases the energy of the oscillator pulse (7 nJ) by a factor of 10^6. This is shown in Fig.2- 12. In RGA, the oscillator's laser pulse acts as a seed and is amplified. As indicated before, RGA additionally employs Ti: Sapphire crystal as a gain medium.

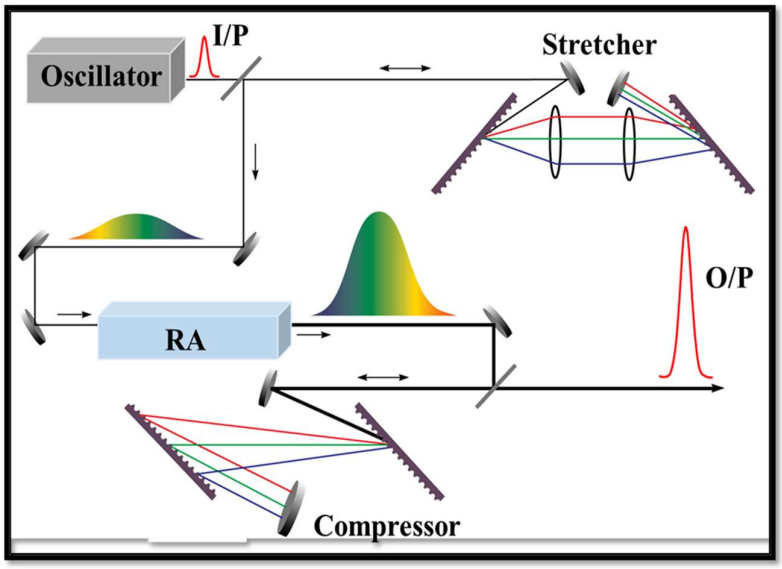

Fig.2- 12. Typical CPA method schematic [14, 15], with I/P-Input pulse and O/P-Output pulse.

Due to their high intensity and tendency to harm optical components and the gain medium during this amplification process, fs pulses have been shown to cause self-focusing phenomena. Therefore, the fs pulses must be greatly stretched to prevent damage to laser components in the cavity of the RGA (fs to ps). As a result, the laser beam's peak strength decreases by several orders, favoring the achievement of amplification without causing any harm to the laser system. When used in CPA, the

stretching compartment's grating design changes the fs pulses so that the blue components travel farther than the red components, lengthening the pulses [10, 11]. Since the peak power is reduced by 10^3 times in the current setup, the damage can be avoided. The oscillator pulses (100 fs @ 80 MHz) extend to (100 ps @ 80 MHz).

Additionally, the Pockels cell is synchronized by the RF signal produced from the oscillator's seed pulse, and the oscillator/stretcher pulses are switched to the RGA. The repetition rate of amplified pulses can also be changed between 10 and 1 kHz with the aid of the Pockels cell. The laser pulses were compressed in the compressor zone after the RGA had been amplified. When gratings are oriented so that higher frequencies must travel a shorter distance to "catch up" with lower frequencies, this is known as stretching. The compression process is the exact opposite of stretching. As a result, the pulse shrinks to its original time scales, and for the current laser system, the seed pulse of a few nJ is amplified to about 4 mJ (@ 1 kHz in RA [14].

Table2- 2: lists various Coherent laser sources utilized in experiments along with the associated specs[16–18]

Specifications	Chameleon Ultral-II (Oscillator)	Libra (Amplifier)
sPulse duration	~ 140 fs	~35 fs
Maximum Output power	4 W @ 800 nm	4 W
Repetition rate	80 MHz	1 kHz
Polarization	Horizontal	Horizontal
Beam diameter	~(1.2 ±0.2) mm	~14 mm

2.4 Details of the Terahertz Experimental setup

The primary emphasis of this section is on the Terahertz generating and detection methods employed. The thesis's primary topics include generation and detection using PCA antennas and semiconductor surface thin films for transmission mode [19–22].

2.4.1 Incoherent method of Pyro-electric detector for measuring THz power

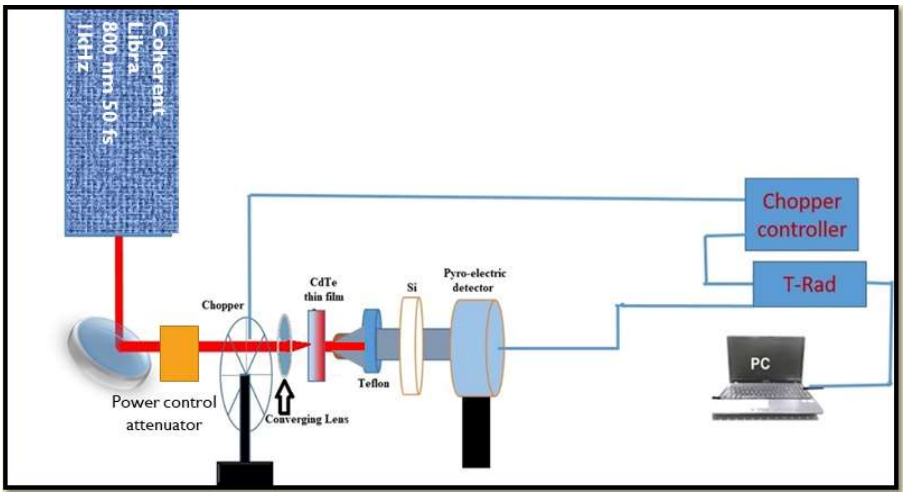

Fig.2- 13.Schematic diagram of the THz generation thin film and detection using a pyroelectric detector

The schematic of Terahertz detection using Pyroelectric detection is shown in Fig. 2 -13. The experiment was carried out utilising a Ti: sapphire laser amplifier (Model Libra, Coherent Inc. USA) utilising an 800 nm working wavelength, a pulse width of 50 femtoseconds, and a repetition rate of 1 kHz. The generated radiation and an unconverted part of 800 nm wavelength were directed to a the diverging beam of THz radiation and collimated. The produced radiation was directed toward the Pyrometer detector head using the second mirror. The unconverted part of the 800 nm wavelength transmitted through film was filtered out using Teflon and silicon plates. In order to account for changes in surface charge and spontaneous polarisation, when thermal radiation strikes the detector it causes temperature-dependent spontaneous polarisation, which generates charge. This charge then flows to electrodes attached to pyroelectric crystal. The generated THz radiation was detected using a pyrometer (Genetic made, Canada) which is connected to a preamplifier cum T-RAD-USB (lock-in) synchronized lock-in-amplifier. The pyro detector's chopping frequency was set at 22.8 Hz (Model no.SDC-500). A polarizer-based attenuator was used to regulate the incident laser's power.

2.4.2 (b) Time-Domain Spectroscopy in the THz Band for Transmission Mode

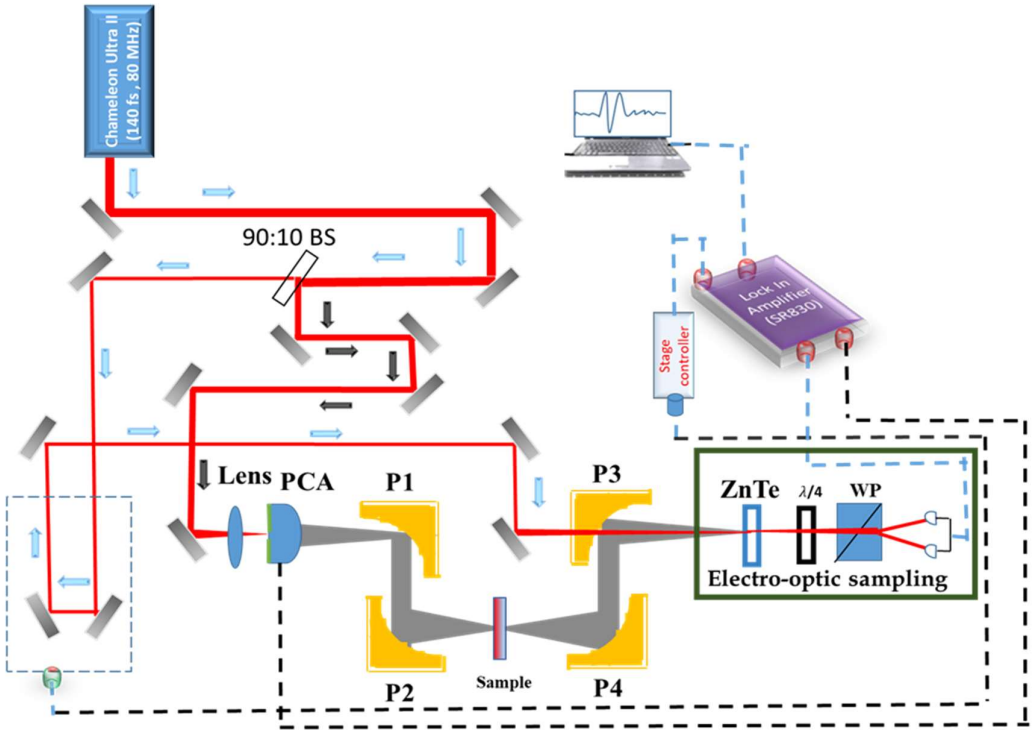

Fig.2- 14.Experimental schematic of THz time-domain spectroscopy for Transmission mode

Fig.2- 14 demonstrates the transmission mode configuration for THz time-domain spectroscopic diagrams. For this experiment, a laser source called the Coherent Chameleon Ultra-II was used. The laser beam first passed through the beam splitter (BS) on a 90:10. The reflected portion (90) of the pump beam from the beam splitter was focussed via a convex lens with a 30 cm focal length on the photoconductive Anntena (PCA). Four half-axis parabolic mirrors (P1, P2, P3, and P4) were used to collimate and concentrate THz radiation onto the ZnTe crystal detection. They were utilised to collimate and focus THz pulses generated from PCA sources. The delay stage was used to delay the transmitted component (10) (probe beams) of the laser beam from BS with regard to THz radiation. Through the half-axis parabolic mirror(P3), the focussed probe beam was permitted to hit the ZnTe detecting crystal. The antenna-generated THz is detected using an Electro-optic

sampling technique. We have to check the probe's and pump pulse's zero delays (which is transmitted through the ZnTe crystal) using the EOS technique. the balanced photodiodes, Wollaston Prism (WP), and quarter wave Plate (λ/4). An amplifier lock-in is connected to the balanced photodiodes (BPD) output (model no.SR830). The focused THz radiation on the detection crystal induces birefringence (or changes refractive index) in ZnTe crystal. The birefringent crystal causes phase retardation in the focused optical beam. The phase retarded probe beam propagates through λ/4 plate and WP. The WP splits the probe beam into two orthogonal polarization components, i.e., S and P. The two polarization components were allowed to an incident on the pair of photodiodes connected in balanced mode. The output of the balance photodiode (BPD) gives the difference between S and P polarization components in analog mode. The voltage input of the lock-in amplifier was coupled with the analogue output BPD (Model No. SR830). By changing the probe beam's delay relative to the THz pulse, the temporal profile of THz radiation was calculated.

2.4.3 THz detectors

The THz detection techniques are categorized into two types, i.e., coherent and incoherent. The basic difference between these two schemes is based on how to retrieve the information of THz radiation. The coherent system provides information about the amplitude and phase, whereas incoherent techniques offer only the THz power. The incoherent technique employs thermal detectors, which can detect THz broad spectral range. Some of the widely used incoherent detectors are bolometer, golay cells, and pyroelectric detectors [23-25]. These detectors require reference frequency to achieve high sensitivity and to surpass background noise.

2.5 Terahertz-based Optical properties:

2.5.1 Terahertz Time Domain Spectroscopy (Transmission mode)

Terahertz pulses are applied to the sample reference first, then the sample used to record the temporal characteristics. To acquire equivalent frequency domain spectra, we then execute the FFT. THz electric field E_{samp} transferred from the sample and used as E_{Ref} reference in the frequency domain represents a terahertz pulse. The characteristics of the source-detector combination as well as optical components like mirrors and lenses are included in the transmitted electric field. Additionally, the air's humidity will exhibit a prominent absorption line. In order to avoid any system parameters other than the changes

brought on by the sample to be examined, a reference is typically recorded without a sample or with an identical sample. The sample's is determined by these two fields ratio.

In order to represent the Fourier-transformed signal

$$E(\upsilon) = \int_{-\infty}^{\infty} E(t) e^{-i\upsilon t} dt \tag{2.11}$$

The signal is given by the transmission

$$H(\upsilon) = \frac{E_{Sample}(\upsilon)}{E_{\mathrm{Re}\,ferance}(\upsilon)} = T(\upsilon) e^{i\phi(\upsilon)} \tag{2.12}$$

Where $\phi(\upsilon)$ is the phase and $T(\upsilon)$ is the amplitude. The phase will be unwrapped in order to obtain the refractive index and extinction coefficient. The formula for calculating the sample's absorption coefficient (α) is given as

$$\alpha = -\frac{1}{d} \ln\left(\frac{E_{THz\text{-}Sam}(\upsilon)}{E_{THz\text{-}Ref}(\upsilon)} \right) \tag{2.13}$$

Where: ω is the THz frequency, d *is the films* Effective thickness. The sample's effective thickness is provided by

$$\alpha = -\frac{1}{d} \ln\left(\frac{E_{THz\text{-}Sam}(\upsilon)}{E_{THz\text{-}Ref}(\upsilon)} \right) \tag{2.14}$$

The material's Refractive index in the THz region is determined by

$$n(\upsilon) = 1 + \frac{c \times (\phi_s(\upsilon) - \phi_r(\upsilon))}{2\pi\upsilon d} \tag{2.15}$$

Where: $\phi_s(\upsilon)$ $\phi_r(\upsilon)$ the phase produced after applying FFT on the sample and reference is equal to the $n(\upsilon)$ frequency dependent refractive index, where c is the light's speed.

2.5.2 Spectroscopy in the terahertz time domain (Reflection mode)

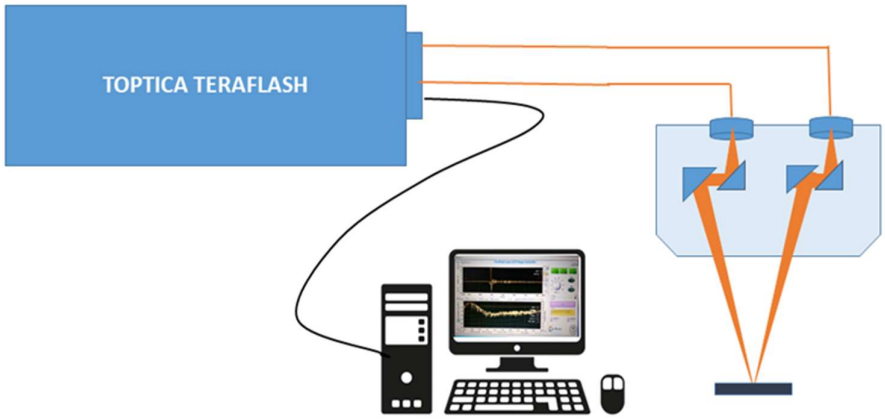

Fig.2-15: The Experimental setup used for THz time-domain spectroscopy in Reflection mode

Fig. 2 -15: shows THz time-domain spectroscopy's experimental configuration in reflection mode setup used the instrument TERAFLASH. The THz radiation in this PC is produced and detected by antennas. The femtosecond laser pulse has the following characteristics: a repetition frequency of 100 MHz, a pulse width of 50 fs, and a wavelength of 1560 nm. The power is 80 mW which is directed to the antenna using an optical fiber. InAlAs/InGaAs multilayer hetero-structure is used for the source, whereas doped InAlAs/InGaAs are used for the detector. The beam width of the output pulse is 2.5 mm. The sample is placed below with an incident angle of 8.50°. The Time Domain data was recorded using the Lab-View program.

In reflection mode, the THz signal was measured. Terahertz was first applied to the reference before being applied to the sample to record the temporal characteristics. The FFT of the time domain signal provides frequency domain spectra. The THz electric field also represents a terahertz signal in the frequency domain. E_{sam} denotes the field associated with the sample, and E_{ref} is the reference time-domain

In the reflection mode of Terahertz TDS. The real part of n(ω) R.I is given by Eqn (2.16)

$$n(\omega) = \frac{\sqrt{n^2|r|^2}}{1+|r|^2-2|r|\cos\theta} \qquad \textbf{(2.16)}$$

and Imaginary part of the refractive index k(ω) (extinction coefficient)

$$k(\omega) = \frac{-2|r|\sin\theta}{1+|r|^2-2|r|\cos\theta} \quad \textbf{(2.17)}$$

The reflection amplitude ratio is denoted by $|r|$, The phase difference between the reference and the sample is shown by the symbol θ.

The extinction coefficient k(ω) and the absorption coefficient (in cm^{-1}) are connected shown in Eqn **(2.18)**

$$\alpha(\omega)=4\pi\upsilon k(\omega)/c \quad \textbf{(2.18)}$$

2.6 References:

1.D Rajesh, C S Sunandana "Effect of etching on the optical properties of partially iodized commercial silver foil" Indian J. Phy 86(8) (2012) 681-686.A.R

2. D Rajesh, C S Sunandana, "Controlled structural and Optical properties of nanostructured Ag films reshaped by brief Iodization" Thin Solid films 524 (2012) 316-319.

3.D Rajesh, C S Sunandana "Briefly brominated Ag films: XRD, FESEM & Optical studies of surface modification" Applied Surface Science 259 (2012) 276-282.

4. C S Sunandana, D Rajesh, "Three strategies for Fabrication of I-VII Semiconductor Nano (Particles) structures" Indian J. pure & appl. Phys. 51 (2013) 149-155.

5. A. R West, 'Solid State Chemistry' John Wiley & Sons, Singapore,(2003).

6. K .L. Chopra, 'Thin Film Phenomena', McGraw Hill, New York (1969).

7. C.Kittel, 'Introduction to solid state physics' john wiley and sons,

8. R.J. Martín-Palma, A. Lakhtakia, Vapor-deposition techniques, in: Engineered Biomimicry, 2013, pp. 383–398

9. M.Mahendar, D.Rajesh, C.S Sunandan, Structral and optical properties of partially iodized Ag Thin film prepared by thermal Evopration, 2010 (MS Thesis).

10. S.M. Sze and Kwok. K. Ng, Physics of Semiconductor Devices,3rd edition, by Wiley (2003).

11.AFM", Atomic force microscopy - Wikipedia.

12. "FESEM", Guide to Electron Microscopy (healthtard.com)

13."Coherent, Operator's Manual: Libra Ultrafast Amplifier Laser System", http://lasers.coherent.com/lasers/libra-manual.

14."CPAtechnique",https://en.wikipedia.org/wiki/Chirped_pulse_amplification

15. D. Strickland, and G. Mourou, "Compression of amplified chirped optical pulses", Optics communications, 55, 1985.

16.S. S. Dhillon, M. S. Vitiello, E. H. Linfield, A. G. Davies, M. C. Hoffmann, J. Booske, C. Paoloni, M. Gensch, P. Weightman, G. P. Williams, E. Castro-Camus, D. R. S. Cumming, F. Simoens, I. Escorcia-Carranza, J. Grant, S. Lucyszyn, M. Kuwata-Gonokami, K. Konishi, M. Koch, C. A. Schmuttenmaer, T. L. Cocker, R. Huber, A. G. Markelz, Z. D. Taylor, V. P. Wallace, J. Axel Zeitler, J. Sibik, T. M. Korter, B. Ellison, S. Rea, P. Goldsmith, K. B. Cooper, R. Appleby, D. Pardo, P. G. Huggard, V. Krozer, H. Shams, M. Fice, C. Renaud, A. Seeds, A. Stöhr, M. Naftaly, N. Ridler, R. Clarke, J. E. Cunningham, and M. B. Johnston, "The 2017 terahertz science and technology roadmap," J. Phys. D. Appl. Phys. (2017).

17. S. Du, K. Yoshida, Y. Zhang, I. Hamada, and K. Hirakawa, "Terahertz dynamics of electron–vibron coupling in single molecules with tunable electrostatic potential," Nat. Photonics (2018).

18. C. Bosshard, "Third-Order Nonlinear Optics in Polar Materials," in (2000).

19. P. R. Smith, D. H. Auston, and M. C. Nuss, "Subpicosecond photoconducting Dipole Antennas," IEEE J. Quantum Electron. (1988).

20. P. J. Hale, J. Madeo, C. Chin, S. S. Dhillon, J. Mangeney, J. Tignon, and K. M. Dani, "20 THz broadband generation using semi-insulating GaAs interdigitated photoconductive antennas," Opt. Express (2014).

21. X. C. Zhang and J. Xu, "Chapter 2 - Generation and detection of terahertz waves," in Introduction to THz Wave Photonics (2010).

22. M. Hoffmann, "Novel Techniques in THz-Time-Domain-Spectroscopy A comprehensive study of technical improvements to THz-TDS," (2006).

23. B.I. Greene, J.F. Federici, D.R. Dykaar, R.R. Jones, P.H. Bucksbaum, Appl. Phys. Lett. 59, 893 (1991).

24. N. Daghestani, S. Persheyev, M. Cataluna, G. Ross, M. Rose, Semicond. Sci. Technol. 26, 075015 (2011).

25. F. Turkoglu, H. Koseoglu, Y. Demirhan, L. Ozyuzer, S. Preu, S. Malzer, Y. Simsek, P. Müller, T. Yamamoto, K. Kadowaki, Supercond. Sci. Technol. 25, 125004 (2012).

This page is intentionally left blank

Chapter 3: Elaboration of thermal annealing of the structure and optical properties of CdTe thin films for efficient terahertz generation

Abstract:

In this chapter, we have discussed the process of thin-film preparation on a glass substrate using the evaporation technique under vacuum (at 10^{-5} mbar pressure) and investigated their X-ray diffraction (XRD) and UV/Vis/NIR spectrophotometer, respectively, are used to measure structural and optical properties. The as-deposited films were annealed at 200, 300, and 400°C temperatures, respectively for the period of 30 min. Some of the important structural parameters such as grain size, dislocations density, and macro strain of thin films were also investigated. The absorbance and transmission data were recorded between 400–900 nm wavelength range which also reveals the effect of annealing in terms of shift in the bandgap between 1.35 to 1.45 eV. Whereas the XRD data confirms the significant effect of temperature on the change of structural properties which include crystallinity and preferential orientation. Finally, these films were subjected to 800 nm wavelength of 50fs pulses obtained from Ti: sapphire amplifier at a 1kHz repetition rate for evaluating their potential as a THz generator. The incident power of the laser was focused and tuned between 150-350 mW range and generated THz signals was recorded using calibrated Pyroelectric detector at 22.5 Hz frequency. The intensity of the generated signal was increased from 254.8 nW/cm² to 108.2 nW/cm² reported at 200°C annealed film. The highest efficiency of the generated THz signal was of the order of 3.41E-5% at 180mW incident laser power. We have also explained the effect of carrier concentration and phase transition with respect to temperatures for the efficient generation of the THz signal.

3.1 Introduction:

Cadmium telluride (CdTe) is one of the most prominent polycrystalline materials used for making thin-film solar cell devices because of its important physical properties. It can be prepared with high conductivity in both n and p-type forms. CdTe is a member of the II-VI periodic group and an optically active chalcogenide semiconductor material with immense applications in optoelectronics, photonics, and bio-labeling applications. Far from the past two decades, the terahertz generation and detection technology field have gotten much attention due to its potential applications in the field of homeland security, defense, spectroscopy, and semiconductor industries. Since it possesses very low energy and has deep penetration ability from the organic and packing materials including cloths and semiconductors etc. Therefore, it is preferred over X-rays due to its non-ionizing nature [1-3].

The fabrication of the thin-film process also plays an important role in deciding the final cost of the device. Though the conventional vacuum technique leads to produce a better-quality low-cost alternative to the material science researchers. The doped CdTe is available both in n and p-type semiconductors. Presently, different preparation techniques such as thermal evaporation, electrodeposition, spin coating, and chemical bath deposition are commonly used for synthesizing the high-quality nanoparticles, thin films, or even large-area devices. However, the thermal evaporation technique is often preferred because it offers large possibilities to modify the deposition conditions. Numerous techniques, including the use of photoconductive switches, semiconductor surfaces, and optical rectification (OR) in the nonlinear crystal, can be used to produce THz pulses with a broad frequency range [4-6]. An EO sampling-based approach called coherent detection. which is widely used for detecting time-domain spectra [7-8]. In this technique, the effect of generated THz radiation is realized in the nonlinear crystal such as ZnTe which changes the polarization state of the transmitted optical pulse. T-rays can be successfully generated from various types of optical and metallic materials available in the form of crystals, wafers, and thin films, etc. ZnTe, GaAs, CdTe, BNA, and DAST are some popular inorganic semiconductors and organic nonlinear crystals. These materials are used due to owing to their higher nonlinear coefficients and good transmission in optical and THz domains along with high or moderate damage threshold [9-11]. CdTe thin films are widely used in photovoltaic, sensors, diodes, rectifiers, and detectors, as it is a direct bandgap

semiconductors with a high atomic number and electron density. However, the generation of powerful THz through a simple experimental arrangement is still a challenging task and needs a rigorous investigation of new materials in the form of film or crystals [12-15].

CdTe is a direct bandgap, high-performing, high mobility, and extremely high diffusion coefficient low-cost semiconductor. The pure CdTe has a direct electronic bandgap of Eg= 1.5 eV at room temperature. The direct bandgap stands for the difference between the highest occupied electron state of the v_b-valence band to the lowest unoccupied electron state of the c_b-conduction band. The lowest energy at which a photon can be absorbed or emitted, however, is represented by the optical energy bandgap. It varies between 1.37-1.54 eV [16-18]. The diffusion, resistivity, and mobility properties of CdTe orientation also depend on its annealing temperature. The annealing process also improves the transmission and surface properties of the semiconductor.

In the present study, we have evaluated the performance of CdTe thin films grown by evaporation technique and annealed between 200-400^{o}C (between 30 to 90 minutes duration) for efficient THz generation using a femtosecond laser. Since the process of photoexcitation from the surface of the semiconductor surface was used for THz generation, which was attributed to the transient surface surge current under the influence of ultra-short optical pulses and directly related to the structural and optical properties of the films [19]. We have attempted to demonstrate the process of post-annealing of CdTe films modified the structure and the optical band gaps, which helped to generate the short-lifetime surface charge current under the influence of femtosecond laser pulses. However, THz generation mechanism form CdTe films after annealing open two channels of generation mechanisms i.e.(i) Photo-dember effect (ii) Electric field-induced Optical rectification process.

When the photoexcited electron-hole pairs take place near a semiconductor surface, these generated charge carriers diffuse away into the bulk. Generally, the mobility of these charge carriers is different, for example, the effective mass of electrons is much smaller than the holes and they move faster than the other. The excess energy of photoexcitation is transferred to the electron. Now two interesting physical phenomena simultaneously occur due to the diffusion and charge carriers' flexibility (i) the spatial separation of charge carriers creates a field known as the screening effect. The field is also known as the photo dember field. (ii) The large mobility and kinetic energy of electrons result in a large

diffusion transient current. This transient current is associated with an electric field (E_{THz})which falls in the terahertz domain. Also, when the surface depletion field of the semiconductor is significantly strong, this contributes to the THz emission together with the PD effect. The Physics of THz generation in CdTe film becomes more interesting due to its centrosymmetry nature and surface depletion field.

THz radiation emitted from the photo-excited semiconductor surface by a dipole that is induced either due to a fast transient photocurrent or by the nonlinear polarization of the materials. Also, due to symmetry of CdTe, the second-order nonlinearity or optical susceptibility tensor $\chi(2)$ becomes zero While the third-order optical susceptibility value,$\chi(3)$ is of the range of ~ 2.45 $x10^{-15}$ (m/W) [20-21]. Therefore, under the influence of DC field 'F' which is produced due to the separation of charge carriers in CdTe film is responsible for the Electric field-induced optical rectification (EFIOR) process and produces a second-order time derivative of polarization waves which is responsible for THz generation and shown in equation no (3.5).

Table 3- 1:Comprises some of the important properties of CdTe crystal [30].

Properties of material	Symbol	Value	THz Region
Chemical forms	CdTe		
Molecular weight	W	240	
Crystal Structure		Cubic (1 1 1)	
Lattice Constant	A	6.482 A°	
Dielectric Constant		18.2	
Hole Mobility	μ_h	65 $cm^2/V.s$	
Electron Mobility	μ_e	700 $cm^2/V.s$	
Carrier Concentration	P	6 x 10^{16} cm^{-3}	
Carrier Mobility	μ	1064 $cm^2/V.s$	
Density	D	5.85 g/cm^3	
Melting Point	M.P	1092°C	
Ref. Index	n	2.67	2.85
Band gap	E_g	1.5 eV (Room Temp)	
Nature of a bandgap		Direct optical band gap	
Absorption Coefficient	α	>10^5 /cm	
Thermal expansion coefficient		5.9 x 10^{-6} /k	

3.2 Experimental Procedure:

Thin Cadmium Telluride films were prepared by a thermal evaporation method using vacuum evaporation (HINDHIVAC Vacuum coating unit, Model No: 12A4U), in a high vacuum (10^{-6} Torr) on glass substrates. The solid form of Cadmium (Cd) and Tellurium (Te) with purity (99.999 %) was used as source material. Glass substrates were cleaned with a cleaning solution and rinsed in distilled water then pure alcohol in an ultrasonic cleaner. The deposition rate was 0.1 nm /min, and the films' thickness was fixed at 50 nm. These samples were annealed at 200°C for 30 min, 300°C for 60 min, and 400°C for 90 minutes and subjected to the XRD, UV-Visible spectrophotometer (Model Optima SP-3000 plus) for their structural and optical characterizations. Finally, these samples were subjected to a femtosecond laser for THz generation. We have evaluated the potential Hz terms of the efficiency of generation efficient THz radiation using 800 nm wavelength pulses of 50 fs duration at 1 kHz repetition rate obtained from Ti: Sapphire laser amplifier.

3.3 Results and Discussion:

There are three sections in this paragraph. XRD data analysis is covered in the first section., while the second section discusses the optical characterization of the CdTe films. Finally, the third part comprises a discussion on the mechanism of THz generation and the impact of annealing on the effectiveness of the signal produced.

3.3.1 X-Ray Diffraction:

The structural properties of the films were investigated by the XRD technique. The important structural parameter utilizing Scherrer's equation (3.1), for instance, the average grain size (D) of thin films was estimated.[22] along with the dislocation density, and microstrain.

$$D = k\lambda/\beta\cos(\theta) \qquad (3.1)$$

Where λ denotes wavelength ($\lambda = 1.5406$ A°) β (in radian) refers to Full Width at Half Maxima (FWHM) obtained from the XRD spectra at fact, k symbolizes the shape factor, which is=0.94 and θ (in degree) is the diffraction angle which shows the of orientation (111) arises (obtained from

show the XRD spectra of different types of CdTe films. The value of θ is the diffraction angle and obtained by dividing the valve of 2θ by 2), δ=1/D2 represents the dislocation density and $\boldsymbol{\varepsilon = \beta/4tan\theta}$ stand for microstrain. Table 3 -2, comprises all the calculated values of the different temperature-annealed CdTe films.

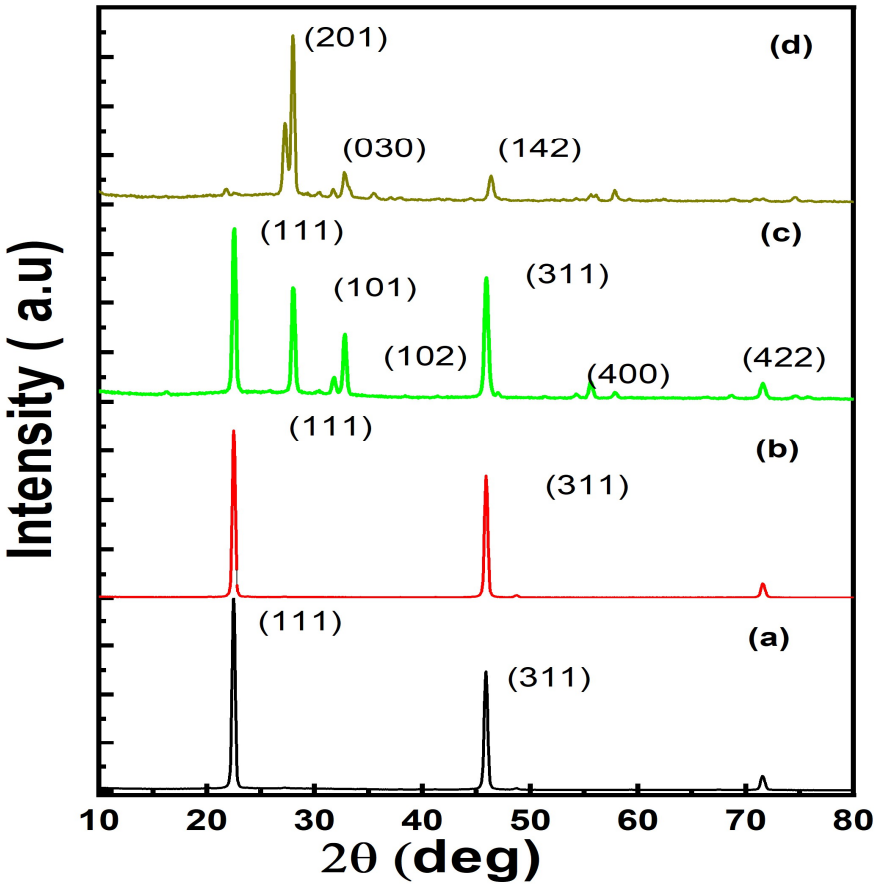

Fig.3- 1. XRD pattern of the deposited CdTe thin film a) As-deposited b) 200°C c) 300°C d) 400°C

XRD analysis was performed using a Philips X' pert pro diffractometer with Cu-Kα excitation wavelength of 1.54 Å. Fig.3 -1:(a) and (b) show the X-ray diffraction patterns of as-deposited and annealed at 200°C for 30 minutes. The CdTe films were cubic Zinc blende structures and the main diffraction peak is located at 2θ = 23.47° which corresponds to the preferred orientation along (111) plane. There are some weak reflections from the (311) and (422) planes. After annealing at 200°C for 30 minutes, the intensity of (111) peak gets decreases is accompanied by an enhancement in (311) and (422) peaks. The observed decrease in the intensity may be due to the change in the stoichiometry of the film. These peaks correspond to the JCPDS (15-0770) data of cubic CdTe. However, in all the cases the intensities of the (311), (422) peaks are extremely low

as compared to the (111) peak, which indicates the preferential orientation of the crystallites in the (111) direction perpendicular to the substrate [23]. An estimation of these parameters was carried out and shown in Table 3- 2. It has been noticed that the dislocation densities are reduced for CdTe thin-film while they are thermally annealed and indicates the sign of the release of microstrains. Following this effect, the grain size of those films is also increased. Fig.3- 1(c) shows the XRD pattern of CdTe film annealed at 300oC for durations of 60 minutes. The corresponding peak at 2θ =23.49° belongs to the (111) plane of cubic and hexagonal phase are overlapped. Hexagonal peaks correspond to (101), (102), and (400). This represents that increase in the randomness of the film which is also reflected by a decrease in the intensity of (111) and the formation of other peaks at (101) (102) and (400), respectively, along with a decrease in average grain size at 300^{o}C, Fig.3 -1:(d) shows the XRD pattern of CdTe film annealed at 400^{o}C for durations of 90 min. These peaks correspond to the JCPDS (055-0530) data of the monoclinic structure of the CdTe film. The process of annealing from 200 to 400^{o}C temperature changes the intensity of the (111) peak and diminishing of the peak's values represents at 2θ =21.83°,28.01°, 32.37^{o},35.62^{o},46.40^{o} and 57.96^{o}. The annealing temperature at 400^{o}C treatment could be attributed to the possibilities of oxidation and intensity of XRD peaks decrease and indicates the deterioration of the crystallinity.

Table 3- 2:The grain size, micro-strain, and dislocation density of CdTe thin films

CdTe Thin Film	Grain size D (nm)	Micro-strain $\varepsilon x10^{-3}$	Dislocation density $\delta x\ 10^{-3}(nm^{-2})$	Bandgap (eV)
As deposited	23.7	7.47	1.76	1.35
Annealed at 200^{o}C	24.3	7.29	1.68	1.33
Annealed at 300^{o}C	22.2	6.44	2.02	1.31
Annealed at 400^{o}C	18.2	8.07	1.77	1.45

3.3.2 Characterization of Optical Properties:

The optical transmittance and absorbance properties of CdTe films of 50 nm thickness on glass substrates were measured by a UV-Visible spectrophotometer. Fig.3- 2.(b) shows the absorption spectra of the as-deposited films which show minimum absorption but broad between 470 to 540 nm raise it is attributed to the free carrier and Increasing the Annealed temperature at 200°C shows the high absorption but the same region appears in the broad peak. It is a clear-cut indication of a shift in the optical band gap as well as the surface quality of the films. Annealed at 300 and 400°C temperature shows an exponential drop in absorption after crossing 400 nm. Fig.3- 2(a) shows the transmission behaviors of the CdTe films. It also reveals that CdTe films as-deposited have very low transmission i.e., 7% only while annealing at 200°C increases the level up to 15%, at 300°C it almost becomes 25% and

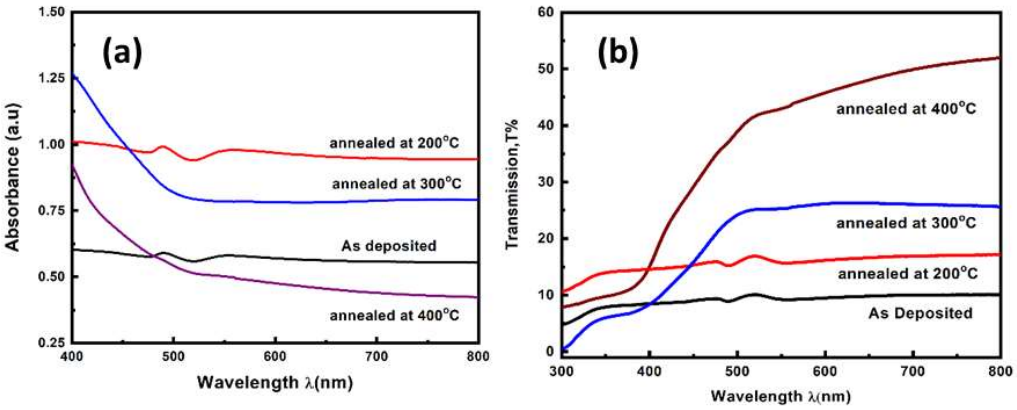

Fig.3- 2. a) Transmission and b) Absorbance wavelength of CdTe thin film

Tauc has proposed a mathematical equation to present the relationship between the optical energy gap and the energy of the incident photon [24]:

$$(\alpha h\upsilon)^2 \propto (h\upsilon - Eg)^n \qquad \textbf{(3.2)}$$

Where hα is the optical absorption coefficient, A is a constant, hυ is the energy of the incident photon, Eg is the optical band gap and n is an index which could take different values according to the electronic transition.

The characteristics response of $(\alpha h\upsilon)^2$ versus (hυ) were plotted for evaluating the bandgap (Eg) of the CdTe thin films by extrapolating the linear portion near the onset of

absorption edge to the energy axis as shown in Fig.3- 3:(a, b, c, and d), respectively. Fig.3–3 (a) shows the bandgap of the as-grown film of 1.35 eV, which corresponds to the infrared region and is attributed to the electronic transition between the valence and conduction bands of the CdTe film. Fig.3- 3(b) shows the decrease in bandgap and shift towards the infrared region to annealing temperature at 200°C. It is due to a rise in grain size that resulted in the improvement of crystallinity and attributed to the more realignment in orientation and strong interaction between film and substrate that also enhances the optical property of the film [25-26]. Further, Fig. 3 – 3(c) shows the bandgap of film annealed at 300°C. It is noticed the bandgap decreases and shows a slight shift toward the infrared region with rise in annealing temperature at 300°C. It is attributed to a grain size reduction that minimizes structural imperfection. However, Fig. 3- 3(d) shows the increase in the bandgap of film annealed at 400°C

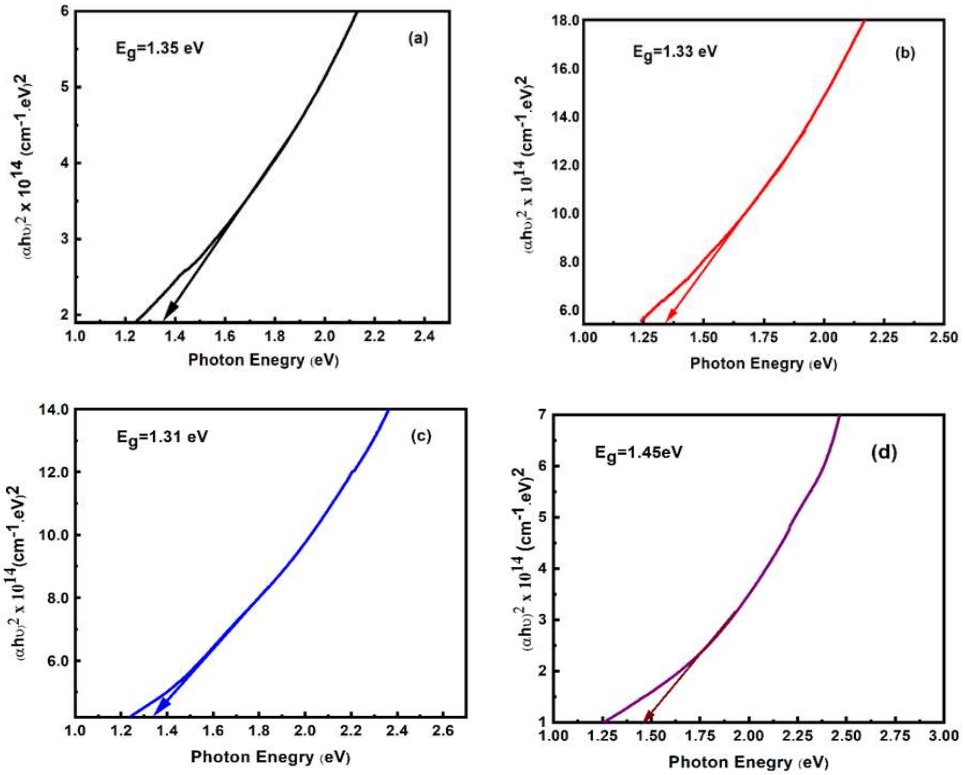

Fig.3- 3.$(\alpha h\upsilon)^2$ Vs Photon Energy for CdTe thin films annealed at a different temperature (a) As-deposited (b) 200°C (c) 300°C (d) 400°C.

3.4 Terahertz generation mechanisms and efficiency:

The CdTe film with orientations (111) and (211) has a similar bandgap but show distinct polarization properties. These surfaces exhibit stable surface alignment. In addition, they possess larger balanced charge densities of ~$7.3x10^{10}$ e/cm^2 and $1.1x10^{11}$ e/cm^2, respectively. The charge density for (111) has diffusion coefficients (D) 14,460 $cm^2.s^{-1}$. The hall mobility for bulk CdTe single crystals of (111) and (211) orientations are 658 cm^2/V.S and 316 cm^2/V.S, respectively [27-28]. The effect of nonlinear absorption of femtosecond pulses on the refractive index and THz generation of CdTe crystal is already been shown by us [29]. However, the process of THz generation can be explained using the following equations:

$$E_{THz} = S/c^2 L \int_0^{\infty} \left(\frac{\partial J}{\partial t} + \frac{\partial 2P}{\partial t}\right) dz \quad \text{----------(3.3)}$$

Where S= fluence of incident laser; c =speed of light and L= length

Photo-dember Effect: The first terms of the bracat represents the transient current density which is due to electron and holes and is given the by following equations (3.4-3.6):

$$E_{THz} \propto \frac{\partial J_n}{\partial t} \propto \mu(\mathrm{T}) \frac{d\Delta n}{dx} \quad \text{------(3.4)}$$

$$J_p \propto eD_e \frac{d\Delta n}{dx} \quad \text{------(3.5)}$$

$$J_n \propto eD_e \frac{d\Delta n}{dx} \quad \text{------(3.6)}$$

$$J = Jn + Jp \quad \text{-------(3.7)}$$

Electric Field-Induced Optical Rectification (EFIOR): The second terms of the bracat of Eq. (3.3) represent the second derivatives of polarized waves produced due to EFIOR and given by:

$$Po = \chi 2\, E\, E^* + \chi 3\, EE^*F \quad \text{------(3.8)}$$

$$P_0 = \chi^3(0; -\omega, \omega)\left|E_\omega\right|^2 \quad \text{--------(3.9)}$$

$$P_i = \chi^3(0;-\omega,\omega)\,\mathrm{E}_j\,E_k^* + \chi^3(0;\omega,-\omega,0)\,\mathrm{E}_j\,E_k^* F_l \quad \text{---(3.10)}$$

$$\chi^2(0;-\omega,\omega) = \chi^3(0;0,-\omega,\omega)\,\mathrm{F} \quad \text{------(3.11)}$$

The first term χ2 and χ3 are the second and third-order nonlinear susceptibilities ω and E is the frequency and the amplitude of the optical field. The third-order term in equation (3.10) contains the built-in surface electric field 'F' and also describes the (EFIOR) effect.

In the case of CdTe, the value of χ2 becomes zero due to centrosymmetric, therefore, THz generation is contributed by the third-order nonlinear term χ3. Equations (3.9, 3.10, and 3.11) clearly show the contribution from χ3 in optical rectification and EFIOR effects. The equation (3.11) clearly explains the OR effect due to second-order χ2 where two frequencies –ω and ω produce a DC field which is associated with THz wave generation and equivalent to third-order nonlinearity χ3 multiplied by F as shown in Eq.No.(3.10). Also, the first term of equation (3.11) shows the OR due to third-order χ3 which is very weak. It is attributed to the value of χ3 that is of the order of 10^{-15} V/m influenced by the surface electric field 'F' as shown in second terms the THz generation becomes equivalent to second-order based OR process.

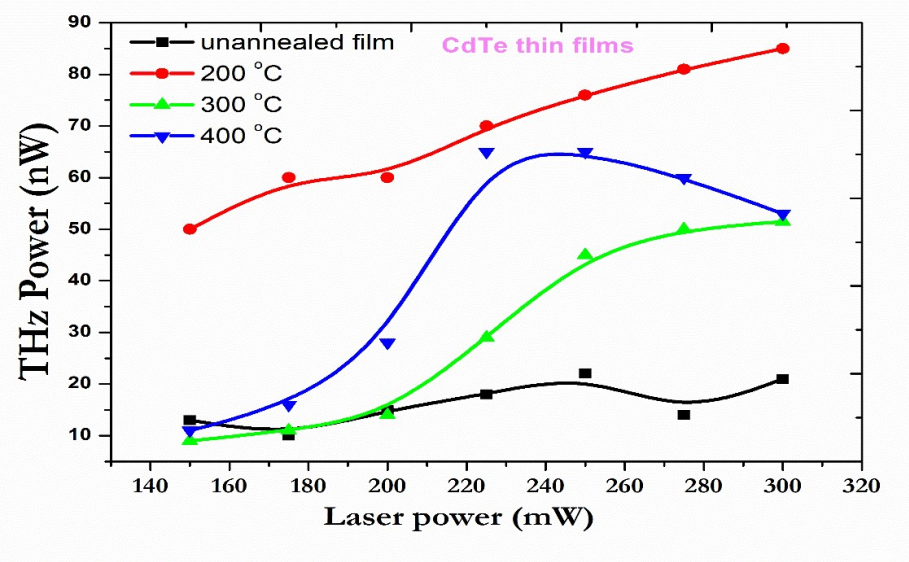

Fig.3- 4. Depicts the variation of intensity of THz radiation with incident power at different annealed temperatures

Fig.3- 4.Shows the curve between incident laser power vs the strength of the generated THz radiation in nW. It is interesting to note that the

maximum generated signal from the as-grown film is 20 nW while film annealed at 200^{o}C can enhance the strength of the generated signal to the order of 88 nW which is almost 4.4 times of the as-grown signal. The corresponding efficiency of the generated signal efficiency is of the order of 2.93 x10^{-5} %. This is even comparable with the efficiency of the many nonlinear crystals such as BNA crystal grown from ethanol: methanol solution. The nature of the curve shows the possibility of further enhancement in the THz signal. But a THz signal at 400^{o}C is lower than the 200^{o}C annealed films. It confirms two important aspects of the temperature (i) modification of the crystalline structure (ii) change in the optical absorption and bandgap properties of CdTe films. Also, direct demonstration of THz signal from CdTe film under the measurable limit is attributed to the introduction of nonlinear absorption mechanisms in CdTe films. This is a clear-cut demonstration of surface phenomena known as the surface surge current effect. Since the contribution is due to optical rectification, the effect is more dominant in transmission mode, therefore, the possibility of the OR effect is quite weak. It also shows the future potential of CdTe film as compared to other types of ferroelectric metallic films like Ni and other materials.

In addition, the observed optical energy band gap is located at approximately 1.5 eV [OLD SOLAR PAER] which indicates the shift of Fermi energy level and also influenced the process of THz generation due to ultrafast transition. The increase in carrier concentration with respect to the temperature of annealed CdTe films resulted in the enhancement of THz intensity. Fig. 3- 4. The intensity of the generated signal was increased from 254.8 nW/cm^{2} to 1082.8 nW/cm^{2} at 200^{o}C which is almost 3.7 times higher than the room temperature grown CdTe.

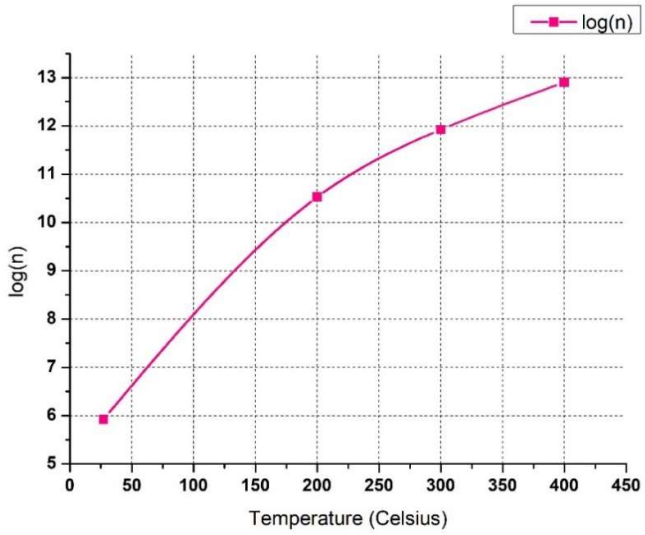

Fig.3- 5.Shows the log (carrier concentration) vs temperature

.

The carrier concentration was increased from $8x10^5$ to $8.0x10^{12}$ when the annealed temperature is increased from 300 K to 673 K. This indicates that carrier lifetime is getting decreased and more possibility of intra-band transitions.

The carrier concentrations are calculated using the standard equation. Which is given below:

$$n_i^2 = N_c N_v e^{\frac{-E_g}{k_B T}} \quad \textbf{(3.14)}$$

The intensity of the output THz radiation is increased in incident power. The drastic increase in the output power when the thin film is annealed at 200°C is mainly due to increase in carrier concentration without any distortions in the film. The decrease in intensity after 200°C is due to phase transitions from cubic to triclinic.

Fig.3-5.Shows the increase in carrier concentration with respect to temperature. The curve shows exponential growth. This can be explained using (Eq. No: 3.14) The graph also shows a saturation behavior at 400°C temperature

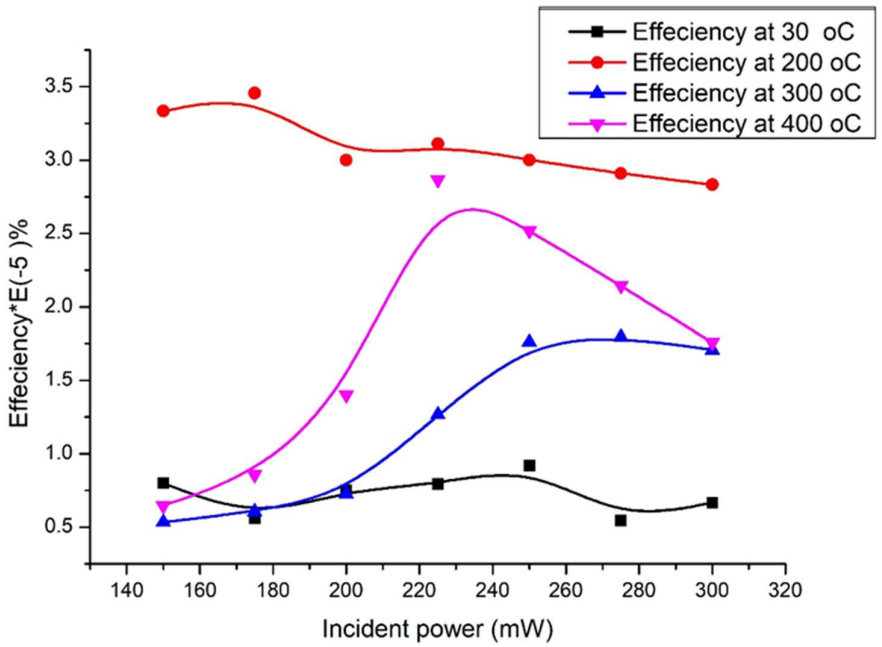

Fig.3- 6.Shows the variation of efficiency of the generated THz radiation with respect to the incident laser power at different annealed temperatures.

It is also to be shown in Fig.3- 6. that the efficiency of the generated THz signal is decreasing with respect to an increase in the incident laser power below the temperature of 200^{o}C and showing a gaussian behavior above 200^{o}C. The decrease in efficiency is mainly caused due to

formation of plasmons. The formation of plasmonic states affected the refractive index of the medium and responsible for reducing the transmittance of the thin film. The phase transition above 200^{o}C is also attributed to anomaly behavior of the efficiency of the thin film. It is also due to a change of transmission behavior i.e., a drop in the transmission due to change in the temperature is caused by high laser power density.

We have shown the role of symmetry in generating THz involving the photo-dember effect in the CdTe thin films annealed at different temperatures. The phase change after 200^{o}C from cubical to triclinic is losing the centrosymmetric making the contribution of $\chi 3$ less. This in turn reduces the power of the recorded THz signal.

Table 3- 3:Brief work related to THz generation carried out the CdTe crystal and thin film

S. No	Type of Materials/deposition	Thickness	Laser system	THz	Application	References
1	CdTe (110) crystal	1 mm	Ytterbium laser	1 THz	Optoelectronics devices	X. Ropagnol .et.al.*(31)
2	CdTe Crystal	2 mm	Ti:Sapphire laser/413-473 K	-	Optoelectronics devices	Archana et.al*(29)
3	CdTe/electrochemically	10-20 nm	200 to 500°C	-	Solar cell	Chu et al *(12)
4	CdPTe/PVD	300-500 nm	100 -200°C	-	Optoelectronics devices	Segui.y.et. al *(13)
5	Cd1-xMnxTe/PVD	250 nm	100 - 200°C	-	Solar cell	Kusmorskie .et.al*(15)

3.5 Conclusion:

We have successfully demonstrated the contribution of the combined PD and EFIOR effects to the efficient creation of THz radiation from the annealing of CdTe films at various temperatures. Also, we investigated the effects of annealing temperature on the structural and optical properties of CdTe thin films deposited on glass substrates using the thermal evaporation technique. From the XRD analysis and the cubic phase of the (111) direction perpendicular to the substrate surface became more dominant as the annealing temperature increased. The grain size increases with an annealing temperature upto 200°C, which reduces with further increase in temperature small changes along with structural properties of the bandgap and enhances the optical property of the thin film. The bandgap is rising, and grain size decrease at 400°C annealing treatment could be attributed to the electron confinement to the nano-scale range. The intensity of the THz radiation is increased by 1.7 times with an increase in incident power at as-deposited temperature, and at 200°C The THz signal's intensity shows Gaussian-like behavior for temperature above 200°C, with an increase in incident power. The change in crystal structure after 200°C reduced the intensity of THz radiation compared to the lesser temperatures. The efficiency of the CdTe thin film is increased by 4.31 times when annealed at 200°C than at room temperature. Above the temperature of 200°C, efficiency

is decreased. At all temperatures, the efficiency of generation of THz radiation is reduced with an increase in incident power. The highest conversion efficiency of the generated THz signal is ~ 3.11×10^{-5} %. that can even be compared with the efficiency of the BNA crystal grown from an ethanol methanol solution.

3.6 References:

1. Tonouchi M (2007) Cutting-edge terahertz technology.Nat. Photonics 1: 97–105. doi:10.1038/2007.3

2. Funk D J, Calgaro F, Averitt R D, Asaki M L T, And Taylor A J (2004) Thz Transmission Spectroscopy And Imaging: Application To The Energetic Materials Pbx 9501 And Pbx 9502 Appl. Spectrosc. 58, 428-431. doi:10.1366/000370204773580275.

3. Zeitler J A, Kogermann K, Rantanen, Rades J, Taday P F, Pepper M, Aaltonen J, and Strachan C J (2007) Drug hydrate systems and dehydration processes studied by terahertz pulsed spectroscopy. Int. J. Pharm. 334(1-2) :78-84. doi:10.1016/2006.10.027

4. Auston D H, Cheung K P, and Smith P R(1984) Picosecond photoconducting Hertzian dipoles. Appl.Phys. Lett. 45:284–286. doi:10.1063/1.95174

5. Ch. Fattinger and D. Grischkowsky (1989) Terahertz beams. Appl. Phys. Lett.54, 490–492. doi:10.1063/1.100958

6. X.-C. Zhang, B. B. Hu, J. T. Darrow, and D. H. Auston(1990) Generation of femtosecond electromagnetic pulses from semiconductor surfaces. Appl. Phys. Lett. 56, 1011–1013. doi:10.1063/1.102601

7. Q. Wu and X.-C. Zhang(1995) Free-space electro-optic sampling of terahertz beams. Appl. Phys. Lett. 67, 3523–3525. doi:10.1063/1.114909

8. P. UhdJepsen, C. Winnewisser, M. Schall, V. Schyja, S. R. Keiding, and H. Helm (1996) Detection of THz pulses by phase retardation in lithium tantalite. Phys. Rev. E 53, R3052. doi:10.1103/PhysRevE.53.R3052

9. G. Damarala, M. Venkatesh, and A.K. Chaudhary Temperature-Dependent terahertz spectroscopy and refractive index measurements of aqua-soluble and plastic explosives. Applied Optics, 29, 8743 -8750. doi:10.1364/AO.57.008743

10.A. G. Davies, A. D. Burnett, W. Fan, E. H. Linfield, and J. E. Cunningham(2008) Terahertz spectroscopy of explosives and drugs. Mater. Today, 11, 18–26. doi:10.1016/S1369-7021(08)70016-6

11. M. Venkatesh, K.S. Rao, T.S. Abhilash, S.P. Tewari, A.K. Chaudhary, (2014) Optical characterization of GaAs photoconductive antennas for efficient generation and detection of Terahertz radiation Opt. Mater.,36,596-601. doi:10.1016/j.optmat.2013.10.021

12. Makoto Takahashi, Kohei Uosaki, Hideaki Kita, Yoshikazu Suzuki (1986)Effect of heat treatment on the composition and semiconductivity of electrochemically deposited CdTe films J.Appl. Phys. 58(11): 4292-4295. doi:10.1063/1.335514

13.Y. Segui, F. Carrere, A. Bui (1982) Thin Solid Films. Vol.92, PP, 303–310.

14.T.S. Moss 1957 Optical Properties of Semiconductors. Butterworths, London.

15. S.A. Gad, M.Boshta, A.M. Abo El-Soud, Y.A. El-Gendy(2010) Effect of the annealing temperature on the structure and optical properties of Cd1−x MnxTe thin films. Physica B: Condensed Matter, Vol.405, P 4664-4667. doi:10.1016/j.physb.2010.08.057.

16. Krishna C. Mandal, Sung Hoon Kang, Michael Choi, Jian Chen, Xi-Cheng Zhang, James M. Schleicher, and M. James (2008) III-VI chalcogenide semiconductor crystals for broadband tunable THz sources and sensors IEEE J.Sel. Top. Quantum Electron. 14, 284–288. doi: 10.1109/JSTQE.2007.912767

17.R. F. Brebrick and R. Fang (1996) CdTe I: solidus curve and composition temperature-tellurium partial pressure data for Te-rich CdTe(s) from optical density measurements J. Phys. Chem. Solids 57, 451–460.doi:10.1016/0022-3697(95)00251-0

18. G. Fonthal, L. T. Mejia, J. I. M. Hurtado, H. A. Calderon, and J. G. M.Alvarez (2000) Temperature dependence of the bandgap energy of crystalline CdTe J. Phys. Chem. Solids 61, 579–583.doi:10.1016/S0022-3697(99)00254-1

19.Shun Lien Chuang (1992) Optical Rectification at semiconductor surfaces, Phys. Rev. Lett.68,102-105.doi: 10.1103/PhysRevLett.68.102.

20. N.H. Al-Hardan, K.T. Rasoul, S.A. Hussain (2010)The Effect of Annealing Time on The Structural and Electrical Properties of CdTe Thin Films. journal of al-qadisiyah for pure science,Vol.15 Pg:98-108.

21.Vitalij L. Malevich, Ram¯unas Adomavi˘cius, Arunas Krotkus, (2007) THz emission from semiconductor surfaces, C. R. Physique. DOI:10.1016/j.crhy.2007.09.014.

22.EricLifshin(1999), X-ray Characterization of Materials, Wiley-VCH, NY, 37.

23.B.Qi, D. Kim, D.L. Williamson, J.U. Trefny(1996) Effects of post deposition heat-treatment on morphology and microstructure of CdTe grown by electrodeposition, J. Electrochem. Soc. 143, 517.

24.S. M. Alnaimi and M. N. Al. Dileamy (2007) Determination of the Optical Constant of Cadmium Stannate Film, International Journal of Pure and Applied Physics, Vol.3(1), p. 30.

25.S. Deivanayaki, P; Jayamurugan, R. Mariappan, V. Ponnuswamy (2010) OPTICAL AND STRUCTURAL CHARACTERIZATION OF CdTe THIN FILMS BY CHEMICAL BATH DEPOSITION TECHNIQUE Chalcogenide. Letters 7-3159-163 (2010).

26. J. J. Pankove(1971) Optical Processes in Semiconductors, Prentice-Hall, Englewood Cliffs.

27. A M El-Zohry, B.S.Saheen, V.M. Burlakov, J. Yin, M.N. Hedhili, S.Shikin, B.Ooi, O.S.Bakr and O.F. Mohammed (2018) Extraordinay Carrier diffusion on CdTe

surfaces uncovered by 4D electron microscopy, Chem 5, 706-718.doi: 10.1016/j.chempr.2018.12.02028.

28. L.A.Kosyachenko (2006) Problems of efficiency of photoelectric conversion in Thin-Film CdS/CdTe solar cells, Semiconductors 40 (6),710-727.doi:10.1134/S1063782606060182Z.

29.Archana Kumari, A. K. Chaudhary, and M. Venkatesh(2020) Linear and nonlinear temperature-dependent transmission/absorption characteristics of cadmium telluride crystal for terahertz generation. Applied Optics, Vol. 59, No. 11,3417.doi: 10.1364/AO.366208.

30. Bibin John, S. Varadharajaperumal, Comprehensive Review on CdTe crystals: Growth, Properties, and Photovoltaic Application, Electr Power Energy Syst. 23 May 2022 10.5152/tepes.2022.22016.

31. X. Ropagnol,1,2 M. Matoba,3 J. E. Nkeck,2 F. Blanchard, Efficient terahertz generation and detection in cadmium telluride using ultrafast ytterbium laser, Appl. Phys. Lett. 117, 181101 (2020); doi: 10.1063/5.0024112.

Chapter 4: Studies on Structural and Electrical Properties of CdTe, Te, and Cd Deposited on GaAs Substrate for THz Domain.

Abstract:

This chapter deals with the systematic study on the role of GaAs wafer act as an active substrate for the growth and optical properties of 3N and 5N Te, Cd, and CdTe, films in THz domain. An indigenously designed THz spectrometer tunable between 0.1- 2.5 THz range was employed for the optical characterization of deposited thin film samples. The 800 nm wavelength 140 femtosecond pulses obtained from Ti: sapphire femtosecond laser at 80 MHz repetition rate were used as a pumping source. Time-domain THz spectroscopy in transmission mode confirmed the role of interaction of free charge carriers of newly formed crystallographic structures of GaAs and other semiconductor films under the influence of applied THz field that which resulted in the enhancement of the charge carrier densities, conductivity of the CdTe, and other elemental films. Additionally, it had an impact on optical characteristics like scattering in the terahertz range, refractive index, absorption coefficients, and dielectric constants. Further, the X-ray diffraction (XRD) also confirms the variation in crystallographic properties in terms of average crystallite size, lattice constant, microstrain, dislocation densities, etc., during the growth process. This is also confirmed by the I-V characteristics graphs of these films in terms of enhancement of current charge density (j). Moreover, it is inferred that the modification of the optical and dielectric properties is attributed to the close band gaps of GaAs and CdTe, which is of the order of 1.43 and 1.54 eV, respectively. Finally, we have made an attempt to ascertain the conductivity, optical impedance surface roughness (g), and ϱ values along with reflection coefficient for both T.E. and T.M. modes of improvised semiconductor structures for the first time.

4.1 Introduction:

Designing new efficient optical sources in the far-infrared region in form of ultrafast switches, sensors, quantum computers, missiles control in defense and efficient solar devices, etc., requires rapid development of GaAs-based semiconductor technology. On the other hand, thin-film devices on passive substrates like glass or Si helped develop new materials for different types of applications such as anti-reflecting and hard layer coatings on optics and machine tools, hard disc insulators conductors' films, etc. [1]. The tailor-made GaAs-based heterojunction devices possess many advantages over a passive substrate, such as high (i) electron mobility, (ii) drift velocity, (iii) stable Schottky barrier height at room temperature, (iv) Thermally stability, and the ability to form a variety of new devices. In addition, GaAs-based carbon nanotube enhances the photovoltaic (P.V.) properties of the thin film and is used to make high-efficiency stable solar cells [2-3].

THz spectroscopy is essential for examining the optical and dielectric characteristics of new, highly effective photovoltaic devices made using thin-film technology. Junyi Nan et al. reported the use of terahertz spectroscopy for understanding the role of photoelectron emission from nanoporous gold films (N.P.G.) deposited on GaAs substrate. In addition, they have also confirmed the acceleration of charge carriers under the influence of femtosecond laser pulses on N.P.G. films [4]. Xiaojun Wu et al. reported the emission of THz radiation between 0-2.5 Terahertz range from a semi-insulating GaAs octadecanthionl-passive surface (1 0 0). Also, they have reported the role of inhomogeneity on the surface plasmons effect of GaAs surface coated with rough Au nanofilms [5-6]. Michael Schall and Peter Uhd Jepsen reported the mechanisms of terahertz generation from GaAs, the process of THz generation was attributed to photoexcited transient current, which was verified using terahertz time-domain transmission spectroscopy [7].

CdTe is II-VI polycrystalline compound with a zinc blend crystal structure and possesses a direct bandgap of 1.44 eV [8]. Because of its high atomic number and electron density. It is one of the most promising alternatives for electronic applications, sensors, diodes, Photovoltaic (PV) rectifiers, detectors [9-10], and Laser [11]. The structure of CdTe thin films were carried out by many authors [12-17]. The CdTe is one of the most It has a high absorption coefficient (10^4 cm^{-1}). It is important to grow high-quality CdTe

films that can be of the different substrates such as grown on Si, Ge, and GaAs substrates [18].

But Fourier transforms infrared spectroscopy & time-domain THz spectroscopy (T.D.S.) are the most common techniques used to retrieve spectral features in this range. Rapid development in the ultrafast laser system, nonlinear optics (N.L.O.), and materials science have helped develop compact-sized terahertz sources. THz technology has found potential applications in spectroscopy, imaging & sensing. Due to the distinctive molecular vibrational features of many organic compounds and explosive materials, Terahertz Time-domain Spectroscopy (T.D.S.) has been shown to be exceptional in defining and detecting these substances. For the investigation of explosives, THz waves' low photon energy is often preferred to x-rays or gamma rays. It is penetrating through dielectric materials that reveal that the highly reflected metal surface strongly interacts with the polar molecule to identify the hidden objects.

The surface and electronic states of III-V compound semiconductors are primarily responsible for their optical and dielectric characteristics. Both physical and chemical techniques can be used to modify semiconductor surfaces. It can be applied as a potential path for device functional improvement and efficient access to molecule sensing based on tracking the semiconductor's physical properties affected by the agent molecules. Several experimental approaches, including surface photovoltaic spectroscopy, photoluminescence spectroscopy, and X-ray photoelectron spectroscopy, can be used to probe and monitor the surface states for semiconductors, etc. Femtosecond's laser-based Terahertz (THz) A sensitive and contactless method for the optical evaluation of thin films has also been developed using terahertz spectroscopy. Investigating the optical and dielectric characteristics of photovoltaic (P.V.), Solar cell applications has been made possible recently because of the Terahertz-TDS technique in transmission geometry mode. This is a desirable alternative because large area GaAs wafers with excellent structural perfection are easily accessible at a reasonable price. THz pulses' bandwidth can be produced utilizing a variety of pulses, specifically by using photoconductive switches, [19-20] semiconductor surface [21], and OR (optical rectification) in nonlinear optical crystal. Electro-optic (EO) sampling is a method that is often utilized for their coherent detection. [22]. The method is based on the interaction of a THz wave and an optical pulse in nonlinear materials. T-rays can be successfully generated from various types of optical and metallic materials available in the form of crystals, wafers, and thin films. Some

popular inorganic semiconductors and nonlinear organic crystals, such as ZnTe, GaAs, CdTe, DAST, BIBO, etc., are being used due to their higher nonlinear coefficients and good transmission in optical and THz domains along with high or moderate damage threshold [23-25].

GaAs wafers with excellent structural perfection are easily accessible at a reasonable price because of the huge area. Therefore, in the present work, we have evaluated the I-V response of CdTe, 5N and 3N Te, and Cd films deposited on (111) GaAs substrates. In addition, the generated THz signal is attributed to the transient surface surge current under the influence of ultra-short optical pulses and is directly related to the structural phase and Nonlinear optical properties in the terahertz domain, including the dielectric constant, refractive index, and absorption coefficient. We also believe that the CdTe, pure and Raw Te, Cd deposited on GaAs substrate, these films have surface orientation perpendicular to the (1 1 1) GaAs substrate which is responsible for the increase of the terahertz signal and the conductivity, optical impedance, g value, ϱ value & reflection coefficient for both T.E. and T.M. mode. The present study's surface roughness assessment is another crucial component that indicated Mie scattering losses and a commensurate decline in the signal's power. The non-contact measurement of surface roughness scattering characteristics and optical impedance of building materials, textiles, thin films, etc. using THz radiation [26-29], has been described by Mittleman et al.

4.2 Experimental details:

The GaAs substrate of 2 μm thickness was used for the deposition of Te (5N), Te (5N- high purity elements), Cd, and CdTe film using a PVD method in a vacuum at ambient temperature (at 10^{-5} millibar pressure). These films were prepared by a vacuum thermal evaporation technique using the HINDHIVAC vacuum coating unit, Model No: 12A4U. The GaAs substrate was cleaned using distilled water and pure alcohol solution using an ultrasonic cleaner in the first step. The zone refining approach was used to produce materials that are high purity (99.999%) of the metal's cadmium and tellurium. The composition mixture of Cd and Te in the ratio of 1:1 was subjected to the molten tube. The evacuated tube was then placed inside the furnace in the next step. The furnace temperature was gradually raised between 500 -1000°C range. During the entire coating period, the molten crucible boat was used to shake and maintain the uniformity of the

sample mixture evacuated at a pressure of 10^{-5} millibar. A digital thickness monitored the thickness of these films during the entire coating process. The thickness of the films lies between 200 and 650 nm range.

4.3 X-Ray Diffraction (XRD):

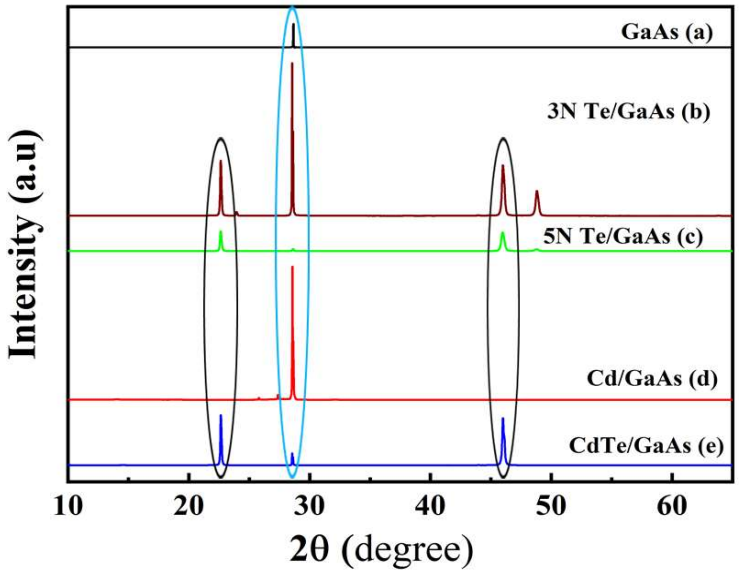

Fig.4- 1(a), (b), (c), (d), and (e) shows the XRD diffraction pattern of GaAs (substrate), 3N Te/ GaAs, 5N Te/ GaAs, Cd/ GaAs, and CdTe/GaAs films.

XRD analysis was performed using a Philips X' pert pro diffractometer with Cu-Kα excitation wavelength of 1.54 Å. Fig.4- 1 (a) and (e) show the patterns of X-ray diffraction of CdTe/GaAs films and GaAs Substrate were cubic Zinc blende structures, and the prominent diffraction peak at 2θ values of 28.64°, 22.62°, 28.65°, and 46.62° which correspond to (111), (200), and (311), planes and cubic phase of CdTe films JCPDS (15-0770). The XRD peak of GaAs single-crystal substrate has the corresponding peak at 2θ=28.64° showing the preferential orientation along with a (111) cubic Phase of all remaining samples showing a GaAs peak occurring at 2θ=28.64°. Because primary diffraction lines of cubic CdTe film are grown on (111) GaAs substrate are close to each other. The microstructure of the substrate surface may play an important role in determining whether (111) CdTe grow on (111) GaAs substrates crystalline had a cubic structure highly strong orientation with (1 1 1). The XRD pattern of 3N Te and 5N Te grown on (111) GaAs substrate indicates that the structure is a hexagonal phase (JCPDS 96-151-2547). Fig.4- 1(b) and (c) show the pattern of X-ray diffraction of three main

diffraction patterns at 22.82°,45.69°and 48.82°, respectively. Which correspond to (100) (003) and (200) (111) peaks have high-intensity peaks of pure Te film on (111) GaAs substrate, which indicates a preferential orientation of the crystallites in the (111) direction c-axis perpendicular to the (111) GaAs Substrate and the cubic and hexagonal phase respectively and 3N Te deposited on (111) GaAs substrate which is corresponding to (100), (003), and (200) peaks observed in the intensity of the GaAs peak extremely low due to the change in stoichiometry and purity of materials. Fig.4- 1(d) shows the x-ray diffraction pattern of Cd deposited on (111) GaAs substrate see the intensity GaAs peaks is corresponding to 2θ =28.58° are very high-intensity peaks observed, and other cadmium peaks intensity are significantly less, which indicates the strong orientation of the crystallites in the (111) cubic phase.

Using Scherrer's formula, the average crystallite size of the film sample was determined. [30],

$$D = k\lambda/\beta\cos(\theta) \quad (4.1)$$

Where λ denotes wavelength (**λ= 1.5406 A°)** β (in radian) refers to Full Width at Half Maxima (FWHM) obtained from the XRD spectra at fact, k symbolizes the shape factor, which is=0.94, and θ (in degree) is the diffraction angle. These results indicate the crystalline phase formation and δ=1/D2 is dislocation density, and ε= β/4tanθ is a macro strain. Applying all these parameters to Eq. (4.1). **Error! Reference source not found.** can be achieved.

Table 4- 1.The average crystalline size, micro-strain, and dislocation density of these films

Film Name	*2θ (degree)*	*Micro-strain ξx10^{-3}*	*Dislocation density δx 10^{-3}(nm^{-2})*	*Average Crystalline Size*	*Miller indices*
GaAs	*28.6*	*4.58*	**2.5**	*1.9 µm*	*(1 1 1)*
Te/GaAs (3N)	*22.6*	*1.46*	**4.25**	*281 nm*	*(1 1 1)*
	28.6	*1.78*	**3.81**		*(0 0 3)*
	45.9	*6.00*	**14.10**		*(2 0 0)*
	48.7	*8.61*	**24.93**		*(1 1 1)*
Te/GaAs (5N)	*22.6*	*1.21*	**2.94**	*381 nm*	*(1 0 0)*
	28.5	*3.05*	**11.25**		*(1 1 1)*
	46.0	*4.84*	**9.16**		*(0 0 3)*
	48.7	*5.80*	**11.3**		*(2 0 0)*
	25.8	*1.28*	**24.8**		*(1 0 0)*

Cd/GaAs	***27.3***	***1.36***	**24.7**	***611 nm***	***(0 0 2)***
	28.5	***1.42***	**24.6**		***(1 1 1)***
CdTe/GaAs	***22.6***	***1.11***	**24.8**	***550 nm***	***(1 1 1)***
	28.5	***1.37***	**22.7**		***(1 1 1)***
	46.0	***4.32***	**7.37**		***(3 1 1)***

4.4 THz Time-domain Spectroscopy:

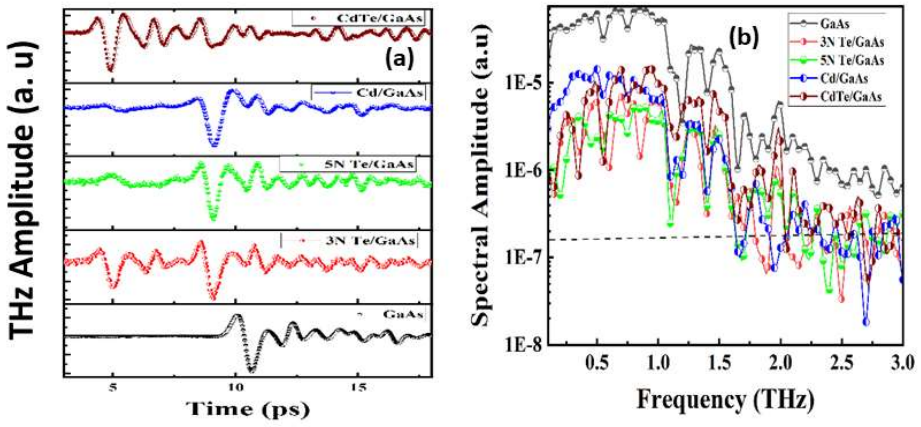

Fig.4- 2.(a) Temporal and (b) Spectral profile of 3N Te/GaAs, 5N Te/GaAs, Cd/GaAs, and CdTe /GaAs.

We have employed an indigenously designed THz system for capturing the test sample's time and frequency domain spectra. The low temperature (LT)- GaAs a THz source, a stripe antenna built of GaAs was utilized, and the combination of a Wollaston prism, $\lambda/4$ plate a ZnTe detection crystal, and two photodiodes in an electro-optic configuration served as the detector. A repetition rate of 80 MHz laser oscillator made of Ti; Sapphire. produced pulses with an 800 nm wavelength and 140 fs duration as the system's pump [17]. The incident laser beam was split into two portions with 90:10 ratios; the higher portion was allowed to the incident on the photoconductive LT-GaAs antenna for the producing of THz radiation, and the second portion was directed to the ZnTe crystal placed in to regulate the delay between the pump and probe laser beams. Auto-correlation was used to account for the differences in the path lengths of the pump and probe. Measuring the photocurrent produced by a balanced photodiode allowed for the mapping of the THz waveform. The lock-in amplifier, which was timed to an 11.5 kHz function generator and used to trigger the photoconductive antenna, received the output of the balanced photodiode. The signal-to-noise ratio is improved as a result. An application for data acquisition that was created with Lab View software was used to record the

experimental data. The samples were subjected between the two parabolic mirrors for the record transmission-based time-domain spectra.

4.5 Results and Discussion:

There are five sections in this section. (i)The first section deals with the time and frequency domain THz spectra of given samples, while (ii) the second section comprises the optical and dielectric parameters such as R.I., Abs. Coeff, conductivity, etc.(iii)This section deals with the FESEM-based surface imaging and roughness measurements of films. (iv) While Section four covers the measurements of optical impedance and reflectivity coefficients, and finally, (v) section 5 deals with the I-V characteristic of these films using the four-probe technique (KEITHLEY-4200SCS).

4.5.1 Optical and dielectric characterization of thin films:

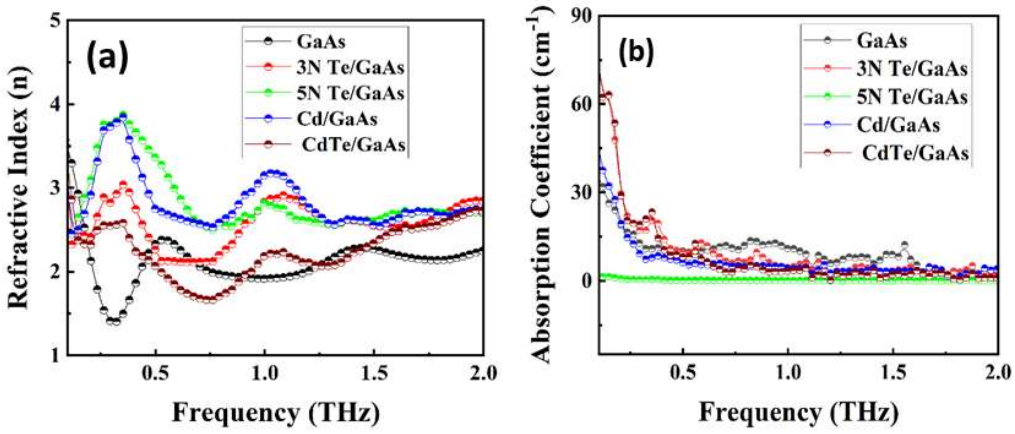

Fig.4- 3.(a) Refractive Index and (b) Absorption Coefficient of 3N & 5N Te Cd, and CdTe films deposited on GaAs substrate

The optical thickness of the nanofilms was of the order of 520 μm. The measured values of the refractive index and absorption coefficients are shown in Fig.4- 3 (a and b), respectively. Fabry-Perot effects due to multiple reflections of these thin nanofilms deposited on GaAs substrate have been taken into consideration. Therefore, the spectral profile was recorded for the long temporal scale. We have analyzed the transmission data to correct these films' refractive index and absorption coefficient measurements. The refractive indices curves show abrupt variation at 0.25 and 1.0 THz frequency ranges. 5N Te and Cd films show the highest variation, whereas 5N GaAs and CdTe films show small

variations between the 0.5 to 2.0 THz range. Whereas 5N Te film shows the lowest absorption coefficients in the entire THz region.

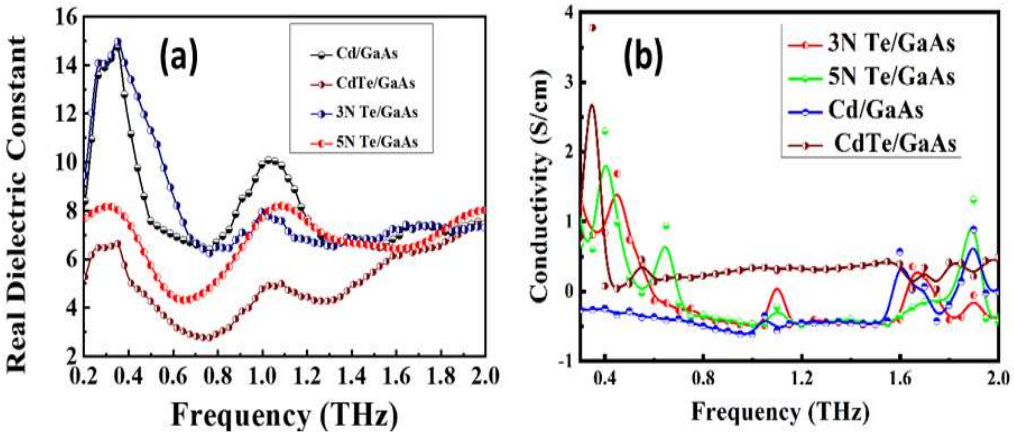

Fig.4- 4. (a) Dielectric Constant and (b) Conductivity of Te, Cd, and CdTe films deposited on GaAs substrate

Fig. 4- 4 (a and b) Display the tangent loss and dielectric constants of these films with respect to THz frequency. The conductivity of Cd, 5N and 3N Te show negative values whereas CdTe films show positive values in the entire terahertz range. It is interesting to note that the dielectric constant of GaAs substrate reaches to a maximum value of ~16 (at 0.75 THz), which is attributed to the 100 cubic phase boundary. Similarly, other thin films also show the maximum value at 1.1 THz also attributed to 100 cubic phases.

4.5.2 Field emission Scanning Electron Microscopy:

Fig.4-5.(a)Display the FESEM image of 3N Te, 5N Te, Cd, and CdTe films deposited on GaAs substrate, (b) 3D simulation of the surface image of these films which are deposited on GaAs substrate (c) Display that 2D surface image of these films using a profilometer. FESEM is used to investigate the surface morphology, particle size, particle shape, imperfections, and topology of thin films, monocrystalline powder, bulk materials, and their element compositions on a micron scale. The fractured surface confirms the presence of the fatigue crack mechanism.

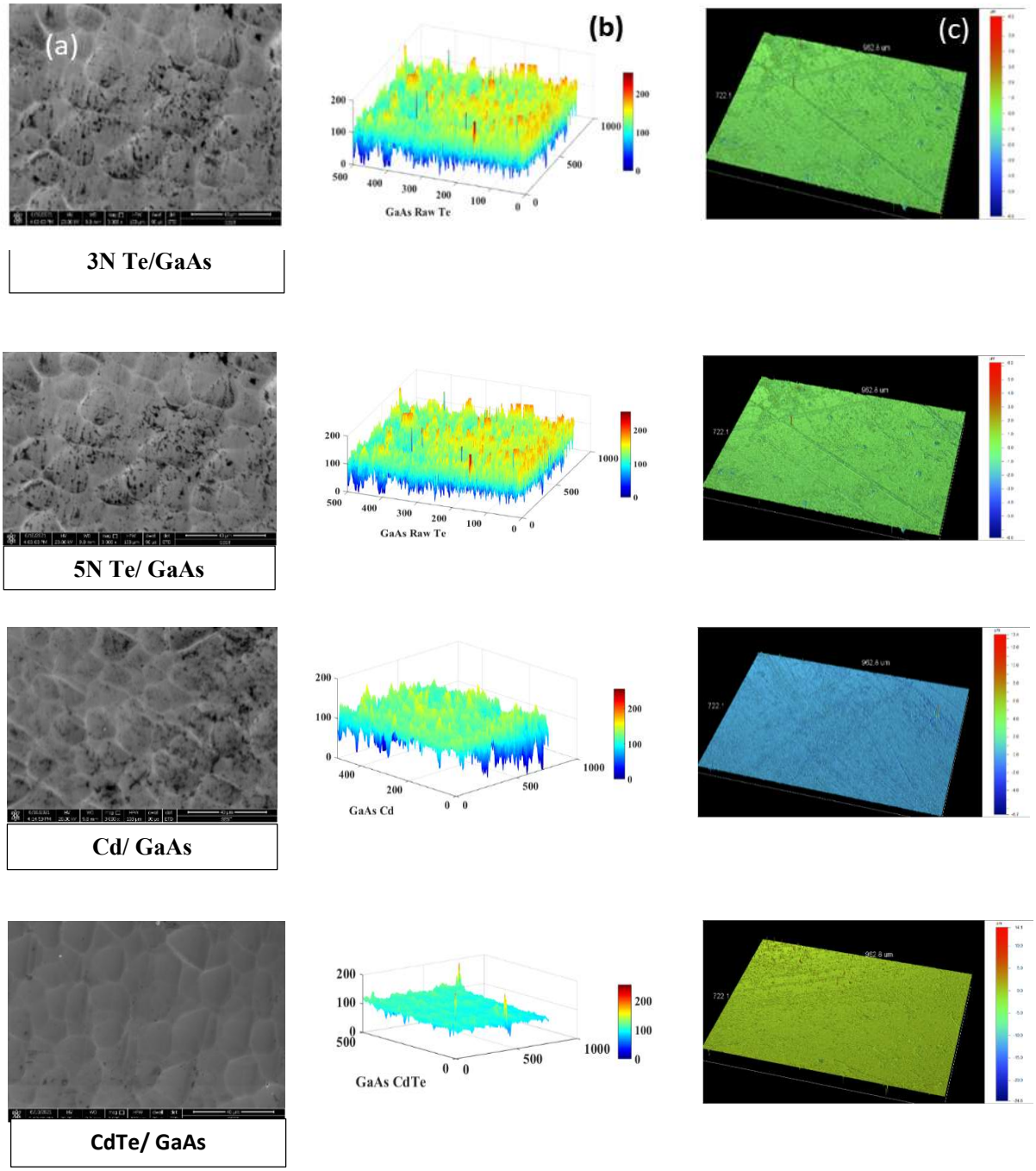

Fig.4- 5.(a) FESM image (b) 3D Simulation surface (c) 2D Surface image of Cd, 5N and 3N Te, and CdTe films deposited on GaAs substrate.

4.5.3 Determination of Optical Impedance and Reflection Coefficient:

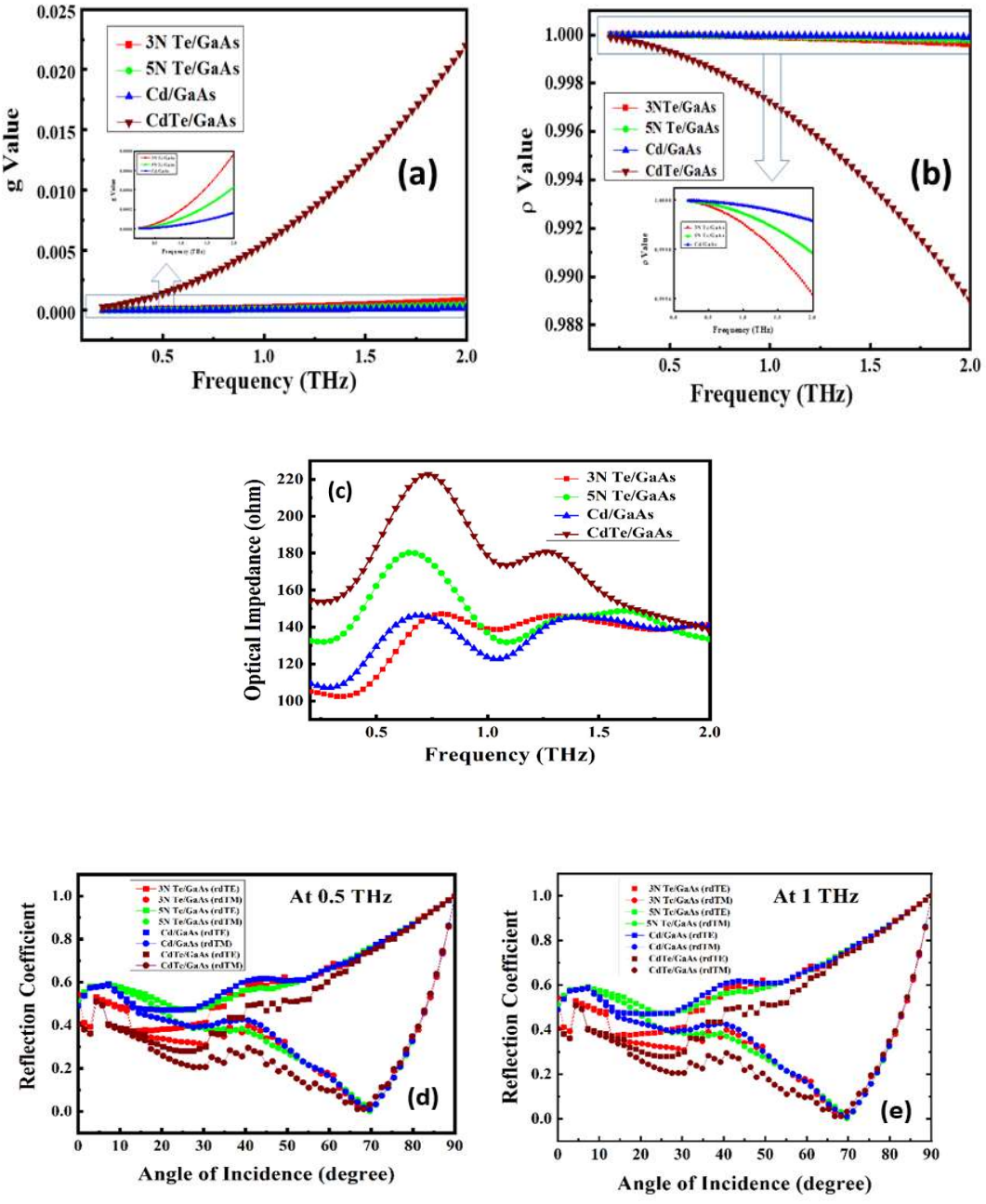

Fig.4- 6.(a) g Value (b) ϱ Value (c) Optical Impedance (d) reflection coefficient of 3N & 5N Te, Cd, and CdTe films deposited on GaAs substrate at 0.5 THz both T.E. and T.M. mode (e) reflection coefficient of these films at 1THz both T.E. and T.M. mode.

Fig.4- 6 (a) shows that the g value of 5N & 3N Te, Cd, and CdTe films deposited on the GaAs substrate sample increases up to 2.0 THz and is determined by utilizing the Rayleigh roughness factor. The values of the roughness factor for Te, Cd, and CdTe films show a gradual decrease up to 2.0 THz. Surface roughness influences the pulse spectra that are reflected. By resolving the Maxwell boundary value issue and adding the experimental surface roughness values, the effect of the roughness on the determination of the refractive index of these thin films was examined for the case of 250 angles of incidence. It enables us to calculate the optical impedance and surface scattering effect of Te, Cd, and CdTe films deposited on GaAs substrate. These problems were solved by numerical based on integral or differential equations which are complex in nature. Due to the availability of refractive index, we have utilized the analytical approximations approach (R.I) and these films' absorption and surface roughness data. This work follows the Kirchhoff theory applicable to scattering from rough surfaces. It is ascertained by multiplying the reflection coefficient of both T.E. and T.M. mode and the Rayleigh roughness factor (ϱ). According to the Kirchhoff theory of scattering, a locally smooth surface is free from multiple scattering and shadowing issues, which means the surface shouldn't have any sharp edges or corners. Additionally, the profile of the surface height distribution will only produce the best results if it is Gaussian in character. Determine the surface roughness by computing the Rayleigh factor. The exponent factor 'σ', which stands for the measured value of the standard deviation of the surface height of the thin films, also has a significant impact on the modified reflection coefficients evaluated in terms of the Rayleigh roughness factors. This allows us to calculate the roughness factor. Here, the value of "g" at the 0.2-2.0 THz regime is less than 1.0, defining the surface roughness. The value of the surface roughness factor 'ϱ' which varies from sample to sample, can be used to calculate the corresponding impedance and modified reflection coefficient of the T.E. and T.M. modes as well as calculate the actual loss caused by scattering in that direction.

4.6 I-V Characterization:

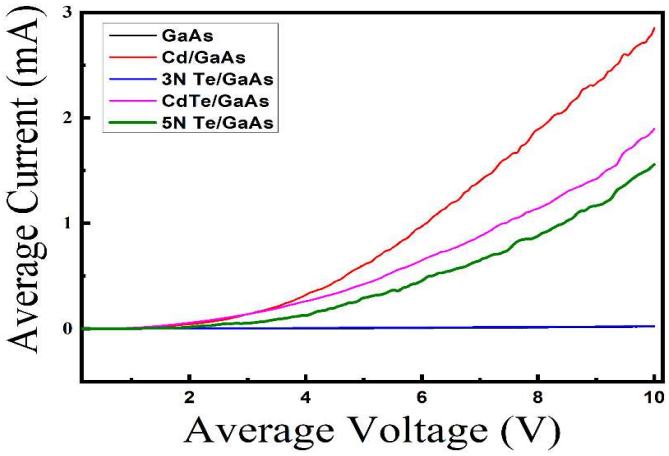

Fig.4- 7 I-V characterization of CdTe/GaAs, 3N Te/GaAs, 5N Te/GaAs, Cd/GaAs, and GaAs

Fig.4- 7, observed good rectification of these films at room temperature. In the voltage range examined up to 10 V, the forward characteristic departs from a straightforward exponential behavior dependence. The I-V curve of measurements interesting results to show that the maximum current in this region of these films is Cd/GaAs, 3N Te/ GaAs, and CdTe/GaAs order of the range is 1.25 $x10^{-3}$ to $3x10^{-3}$ A while other films are 3N Te, and GaAs current is the order of micrometer range which is almost 100 times as compared to 5N Te, Cd and CdTe/GaAs films. The exponential results show that the I-V curve in forwarding bias condition whereas the current in this region these films is GaAs and 3N & 5N Te, Cd/GaAs, CdTe/GaAs, almost constant at 0.2, 0.5, 1, 1.5, and 2.5 V behavior of non-ohmic region and the current increases exponential and depends on the depletion region of the CdTe and other films. It is clear-cut that the indication of 3N Te deposited on GaAs substrate is current in the order of micrometer range because of the impurity defects states in the 3N Te /GaAs films compared to 5N Te/GaAs films. An explanation for the forward current in this ohmic area involves a tunneling mechanism whereby electrons from GaAs recombine with holes caught by the gap states in CdTe. According to this observation, the current in these films Cd/GaAs, 5N Te/GaAs, and CdTe is caused by the space charge current. A result of the ohmic contact's ohmic injection of holes and electrons from GaAs, which are then absorbed by the electrons, this area charges current.

Ohmic Conduction behavior of films

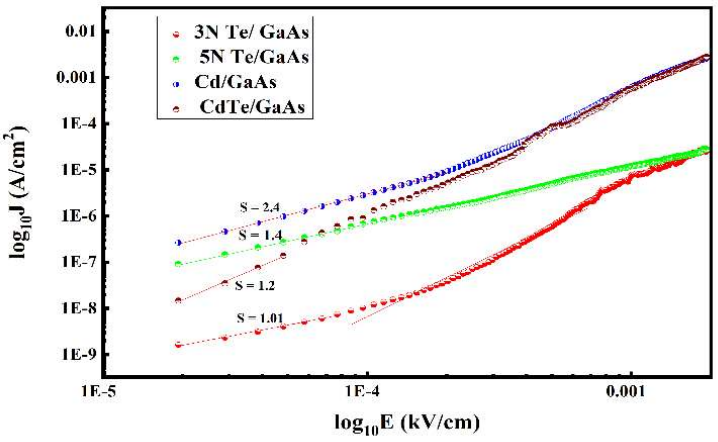

Fig.4- 8 log10 J vs. log10E graph Cd, Te, and CdTe films deposited on GaAs substrate

Fig.4- 8. Shows the Ohmic behavior of 3N Te, 5N Te, and CdTe deposited films on the GaAs semiconducting substrate at 1.5 x10^{-5} kV/cm to 10^{-4} kV/cm regime. Only GaAs with Cd shows the non-Ohmic behavior.

4.7 Hall effects measurements:

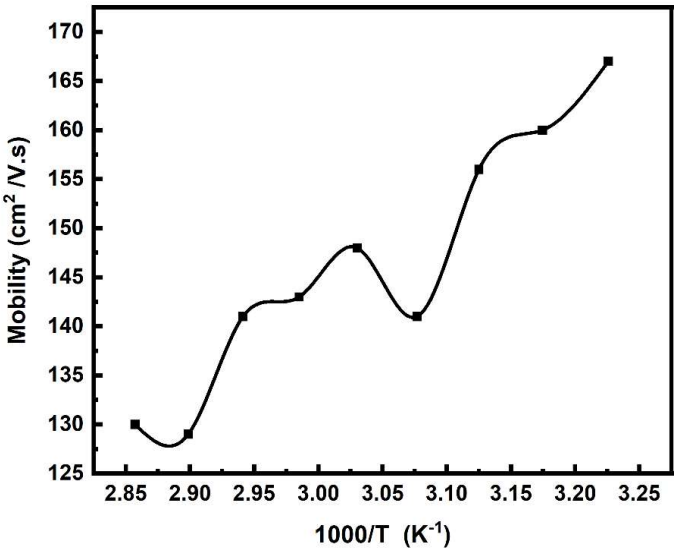

Fig.4- 9 Mobility as a function of temperature graph CdTe on GaAs Substrate

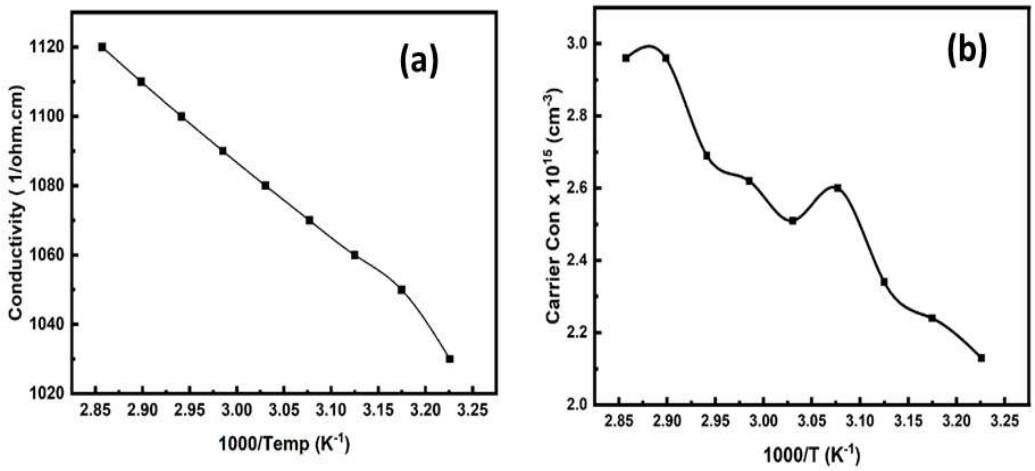

Fig.4- 10. a) Conductivity & b) Carrier concentration as a function of temperature graph CdTe on GaAs Substrate

To study the electrical properties and evaluate the influence of CdTe deposited on GaAs substrate film. It's crucial to be aware of the density of contaminants that are electrically active. The first one examines how the Hall constant varies with temperature, while the second examines how the Hall mobility relates to the scattering mechanism. In the type of electrical conductivity of the prepared films and the different carrier concentrations, mobility, and conductivity in relation to temperature, the film thickness of average grain size. As shown in Fig.4-11, the film has an electrical conductivity of P-type. Fig.4 -9. shows that the increase in the current passing through the film causes an increase in the induced voltage for the specified thicknesses in the presence of an ordinary magnetic field. Table.4 -2, shows variations in carrier concentration, mobility, conductivity, and thickness of the prepared films. It is clear from Fig.4- 11, that the carrier concentration increases with increasing electron density, and a collision of lattice atom's mobility decreases, influenced by scattering from longitudinal optical phonons. It can also be observed that there is an apparent increase in conductivity values with increasing film thickness, as shown in Table.4 -2. The main causes of this variation in the electrical conductivity values are thought to be two distinct contributions: the film's increased doping concentration and the annealing of the film, as shown in Table.4- 2. It is clear that the conductivity slightly increases for doping of CdTe film and abruptly increases for large thicknesses ranging from 200 to 550 nm. We believed that such a difference in the film's conductivity could be associated mainly with the change of carrier concentration, as shown in Fig.4- 11. These results agree with those obtained.

Table 4- 2.Comparison of the measured electrical parameters for different deposition growth techniques of prepared films [31-32].

Thin Film	Temp (K)	Hall Mobility μ ($Cm^2/V.s$)	Conductivity $\sigma_{d.c}$ (1/ohm.cm)	Carrier Con (Cm^{-3}) x 10^{15}	Thickness	Growth Technique
CdTe/GaAs	310	165	1031	2.13	550 nm	Thermal Evaporation
	315	158	1045	2.24		
	320	155	1058	2.34		
	325	154	1072	2.6		
	330	142	1081	2.51		
	335	140	1092	2.62		
	340	139	1100	2.69		
	345	133	1110	2.96		
	350	128	1118	2.96		
GaAs	300	7600	-	0.20	4.3 μm	MBE
		5400	-	0.45	10 μm	VPE
		7300	-	0.14	10 μm	VPE
		7100	-	1.2	4 μm	OMVPE
		6300	-	2.3	4	OMVPE
GaAs	77	36000	-	1.6	4.3	MBE
		85500	-	0.35	10	VPE
		130000	-	0.09	10	VPE
		42000	-	1.0	4	OMVPE
		33000	-	1.6	4	OMVPE

4.8 Conclusion:

In the present work, we have successfully calculated the Transmission of THz radiation and investigated the structural and nonlinear optical of 3N & 5N Te, Cd, and CdTe films were deposited on GaAs substrates using PVD thickness 200 to 620 nm. From the XRD analysis, We also confirm that the CdTe, 5N, and 3N Te, Cd deposited on GaAs substrate, these films have surface orientation perpendicular to the (111) GaAs substrate which is responsible for the increase of the terahertz signal and the conductivity, optical impedance, g value, ϱ value & reflection coefficient for both T.E. and T.M. mode and resulting in optical rectification and photo carriers generated due to excitation of laser pulses accelerated free charges resulting in an electric field opposite to the transient current surge mechanism, the emits THz pulses. The surface morphology in the presence of the fracture surface and fatigue crack process is utilizing a field emission scanning electron microscope, examined (FESEM).

4.9 References:

1. G. Helsch, J. Deubener, Compatibility of anti-reflective coatings on glass for solar applications with photocatalytic properties, Solar Energy 86 (2012) 831–836.
2. Tejas A. Shastry, Mark C. Hersam, Carbon Nanotubes in Thin-Film Solar Cells, Adv. Eng. Mater. 7 (2016) 1-15 . DOI: 10.1002/aenm.201601205
3. 8. Daniel D. Tune, Benjamin S. Flavel, Ralph Krupke, and Joseph G. Shapter, Carbon NanotubeSilicon Solar Cells, Adv.Energy Mater.,2(2012)1043-105. DOI: 10.1002/aenm.201200249.
4. Junyi Nan, Min Li, Ling Zhang, Shuai Yuan, Boqu He and Heping Zeng, Terahertz & Photoelectron Emission from Nanoporous Gold Films on Semiconductor, Nanomaterials, 9 (2019) 1-8. DOI.org/10.3390/nano9030419
5. Xiaojun Wu, Xinlong Xu, Xinchao Lu, Li Wang, Terahertz emission from semi-insulating GaAs with an octadecanthiol-passivated surface, Appl.Surf.Sc. 279 (2013) 92–96. http://dx.doi.org/10.1016/j.apsusc.2013.04.040
6. 11. Xiaojun Wu, Baogang Quan, Xinlong Xu, Fangrong Hu, Xinchao Lu, Changzhi Gu, Li Wang, Effect of inhomogeneity and plasmons on terahertz radiation from GaAs (1 0 0) surface coated with rough Au film, Appl. Surf. Sc.285(2013)853–857. http://dx.doi.org/10.1016/j.apsusc.2013.09.001
7. Michael Schall and Peter Uhd Jepsen, Photoexcited GaAs surfaces studied by transient terahertz time-domain spectroscopy, Opt. Lett. 25 (2000) 13-15.
8. Taki, M. Structural and optical properties of Cadmium Telluride CdxTe1-x thin film by evaporating technique, Int.J. of Appl.of Inn. in Engg. & Manag. 2 (2013) 413–417.
9. C. Scheiber and J. Chambran, Nucl. Inst. Meth.Phys. Res. A322 (1994) 604~1994.
10. J.Brittand C. Ferekides, Appl.Phys.Lett.62(1993)2851-2852. https://doi.org/10.1063/1.109629
11. R. K. Ahrenkil, B. M. Keyes, D. L. Levi, K. Emery, T. L. Chu, and S. Chu, Appl. Phys. Lett.64, (1994) 2879 -2881. https://doi.org/10.1063/1.111402.
12. B.J.Wu, L.H. Kuo, J.M. DePuydt, G.M. Haugen, M.A.Haase, L.Salamanca- Riba, Growth and characterization of II-VI blue light- emitting diodes using short-period superlattices.Appl.Phys.Lett.68(1996), 379-381. https://doi.org/10.1063/1.116691.
13. A.K. Papikyan, V.A.Gevorgyan,N.R.Mangasaryan, P.P Gladyshev, Characterization of vacuum flash evaporated CdTe thin films for solar cell application. Journal of Physics: Conference Series, 2018 945, 012013. https://doi.org/10.1088/1742-6596/945/1/012013.
14. M.H.Ehsani, H. Rezagholipour Dizaji, S. Azizi, S.F.Ghavami Mirmahalle, F. Hosseini Siyanaki, Optical and structural properties of cadmium telluride films grown by glancing angledeposition.Phys.Scr.88(2013),02560291-7).https://doi.org/10.1088/0031-8949/88/02/025602. 20. C.Huimin, G.Fuqiang, Z. Baohua, Properties of CdTe nanocrystalline thin films were grown on different substrates by low temperature sputtering.
15. J. of Semi. 30(2009) 053001 (1-4) https://doi.org/10.1088/1674-4926/30/5/053001.

16. M. Venkatesh and A. K. Chaudhary, "Generation of THz radiation from Low temperature Gallium Arsenide (LT-GaAs) photoconductive (PC) antennas using tunable femtosecond oscillator," in 12th International Conference on Fiber Optics and Photonics (2014), p. S5A.33.
17. K. S. Rao, A. K. Chaudhary, M. Venkatesh, K. Thirupugalmani, and S. Brahadeeswaran, "DAST crystal based terahertz generation and recording of time resolved photoacoustic spectra of N2O gas at 0.5 and 1.5 THz bands," Curr. Appl. Phys. 16 (2016) 777–783 .
18. M. Venkatesh, K. Thirupugalmani, K. S. Rao, S. Brahadeeswaran, and A. K. Chaudhary, "Generation of efficient THz radiation by optical rectification in DAST crystal using tunable femtosecond laser pulses," Indian J. Phys. 91 (2017) 319–326.
19. C.Ghorui, A.M.Rudra, U.Chatterjee, A.K.Chaudhary, Efficient second harmonic and terahertz generation from Single BiB3O6 (BIBO) Crystal using nanosecond and femtosecond lasers, Appl. Opt., 60 (2021)5643-5651.DOI:10.1364/AO.424241.
20. S.Lalitha,S.Z.Karazhanov,P.Ravindran,S.Senthilarasu,R.Sathyamoorthy,J.Janabergenov, Electronic structure, structural and optical properties of thermally evaporated CdTe thin films.PhysicB:CondensedMatter,387(2007),227-238,(2007). https://doi.org/10.1016/j.physb.2006.04.008.
21. M.Mahendar, A.K.Chaudhary, D.Ganesh, V.Gupta, Evaluation of Cadmium telluride (CdTe) thin films grown at different annealing temperatures for efficient terahertz generation.Workshop on Recent Advances in Photonics(WRAP),2019, DOI:10.1109/WRAP47485.2019.9013662.
22. . M.H.Matt, N.C. Shivappa, R. Patel, S.Jeetendra, Thickness Dependent Optical Parameters of Vacuum Evaporated Cadmium Telluride Thin Films. Inter. J. of Renew. Ener. & Biofuels 2014 (2014)1-8. https://doi.org/10.5171/2014.791671.
23. A.A.Alnajjar, F.Y.Al-Shaikley, M.F.A.Alias, Optical Properties and photoconductivity of Undoped and n-doped CdTe thin films. Journal of Electron Devices, 16 (2012), 1306 - 1314.
24. W. Lei, R.J. Gu, J. Antoszewski, J. Dell, G. Neusser, M. Sieger, B. Mizaikoff, L. Faraone, M.B.E. Growth of Mid-wave Infrared HgCdTe Layers on GaSb Alternative Substrates, J. Electron. Mater. 44 (2015) 3180–3187. https://doi.org/10.1007/s11664-015-3876-4. Jens Neu, Kevin P. Regan, John R. Swierk, and Charles A. Schmuttenmaer, Applicability of the thin-film approximation in terahertz photoconductivity measurements, Appl. Phys. Lett.113 (2018), 233901-4. https://doi.org/10.1063/1.5052232.
25. Jens Neu, Kevin P. Regan, John R. Swierk, and Charles A. Schmuttenmaer, Applicability of the thin-film approximation in terahertz photoconductivity measurements, Appl. Phys. Lett.113 (2018), 233901-4. https://doi.org/10.1063/1.5052232.
26. Dominik Bänninger and Hannes Flühler, Modeling light scattering at soil surfaces, IEEE Transactions on Geoscience and Remote Sensing, 42(2004) 1462-1471.
27. Radoslaw Piesiewicz, Christian Jansen, Daniel Mittleman, Thomas Kleine-Ostmann, Martin Koch, and Thomas Kürner, IEEE Transactions on Antennas and Propagation, 55(2007) 3002-3009 .
28. L. Tsang, J. A. Kong, K. H. Ding, and C. O. Ao ,Scattering of Electromagnetic Waves, Vol. 2: Numerical Simulations, Wiley Interscience, 2001, 705 pages. New York: Wiley.

29. R. Piesiewicz, T. Kleine-Ostmann, N. Krumbholz, D. Mittleman, M. Koch, and T. Kürner, "Terahertz characterisation of building materials" IEE Electron.Lett. 41(2005), 1002– 1004.
30. Eric Lifshin, X-ray Characterization of Materials,1999, Wiley-VCH, NY, 37.
31. S. M. Sze, Physics o/Semiconductor Devices (Wiley, New York, 1981).
32. E. H. Putley, Contemp. Phys.16, 101 (1975)

Chapter 5: Temperature-Dependent Annealing Effect on Structural, Morphological, Optical, and Electrical Properties of TeO_2 Films for Efficient Terahertz Generation

Abstract:

In this chapter, we have discussed this temperature-dependent annealing on structure, morphology, optical, and electron properties of tellurium dioxide thin film prepared on a glass substrate using the evaporation technique under a vacuum (at 10^{-5} mbar pressure). The as-deposited TeO_2 films were annealed at 400 and 450ºC for 30 minutes. TeO_2 thin film of 120 nm thickness as a function of temperature. The structural properties were investigated by X-ray diffraction (XRD). The optical properties were determined, which are transmittance, absorbance, and the energy band gap. These films have a direct allowed transition with optical energy of 3.66, 3.64, and 3.54 eV at different annealing temperatures. The electrical properties of this film are determined using Hall measurements such as conductivity and Hall coefficient. The Hall effect measurement results show that the TeO2 Thin-film is a p-type semiconductor, and carrier concentration and Hall mobility strongly depend on the effect of temperature at 310 to 355 K. The surface roughness and film morphology were analyzed by AFM. The optical parameters of this film were determined by the refractive index and absorption coefficient in the terahertz domain. Finally, these films were subjected to 800 nm wavelength of 50 fs pulsed obtained from Ti: sapphire amplifier at 1kHz repetition rate. The incident power of the laser beam was focused and tuned between 65-115 mW range, and generated THz signals were recorded using a calibrated Pyroelectric detector at 22.5 Hz frequency. The highest power of the THz signal was 210nW for 450oC annealed film with respect to the incident power of 115mW..

5.1 Introduction:

A crucial substance because of its intriguing physical and chemical characteristics is tellurium dioxide (TeO_2) [1-2]. Tellurium dioxide is material in amorphous and crystalline forms and finds device application in active optical devices. Tellurium dioxide thin films can be made using several of methods, including the sol-gel method, thermal evaporation or magnetron sputtering, and chemical vapor deposition. [3-5]. TeO2 has P-type electrical conductivity with a 3.75 eV energy gap [6-8]. Tellurium oxide and for optical switching devices, including optical transistors, optical amplifiers, and ultrafast switching devices, TeO_2-based glass is potential active material. Their high linear and non-linear refractive indices are excellent for transmitting infrared and visible light [9-10]. TeO_2's characteristics allow for a variety of useful applications in the fields of optics, electronics, and optoelectronics. [11-12]. The three well-known variations of crystalline TeO2 at this time are - α-TeO_2, β-TeO_2, and γ-TeO_2 [13-16]. According to reports, the temperature-induced crystallization of TeO_2 glass causes the γ-TeO_2 phase to form as the initial crystalline structure [17]. Few attempts have been made to create the TeO_2 thin film utilizing a variety of processes, including sputtering, thermal evaporation, sol-gel, etc. Thin films always have an advantage over their bulk counterpart [18-22].

Generally, THz radiation is generated using Photoconductive switches (PCS), non-linear crystal-based Optical rectification (OR), and Difference frequency mixing (DFM) [23-24]. TeO_2 is a fantastic option for monolithic integration in optical sources and linear and non-linear functionality in photonics without incurring non-linear absorption loss. It has made a name for itself as a host medium for different rare-earth ions as a source, providing chances for amplifiers and lasers at a variety of wavelengths [25-27]. TeO_2 Waveguides have been the subject of numerous attempts, but the manufacture of integrated tellurium oxide has proven difficult during the past 20 years. Using ion exchange and femtosecond laser writing, for instance [28]. For the first time, third-harmonic generation (THG) was successfully demonstrated in an integrated TeO_2 platform with signal strengths of tens of nanowatts (nW). [29].

This is mainly focused on study of optical, electrical, and phase properties of TeO_2 as a function of temperature. The phase part involves finding the state of TeO_2 at different temperature ranges. Secondly, the electrical properties include hall effect parameters, conductivity, and carrier concentration. The optical characteristics, including the

refractive index and reflectivity of TeO_2 as functions of frequency and temperature, are discussed last. The experiment was done at a low temperature for electrical properties. The non-linear optical and phase experimentation was done at the temperature starting from room temperature to 400, and 450^{o}C. X-ray Diffraction (XRD), Atomic Force Microscopy, and electrical characteristics were used to characterize the material.

5.2 Experimental details:

The PVD technique was used for depositing thin films of tellurium oxide. The target material, 5N-purity of tellurium dioxide (TeO_2) powder, was used as the source material. The Tellurium dioxide powder was synthesized to deposit onto the glass substrate was cleaned using distilled water and pure alcohol solution using an ultrasonic cleaner in the first step. These films were prepared by a vacuum thermal evaporation technique using the HINDHIVAC vacuum coating unit, Model No: 12A4U, under 10^{-5} millibar pressure. After that, the furnace's temperature was gradually raised from room temperature to 200°C while the evacuated tube was within. By running a current through the boat, the coil was gradually heated till the substance reached the samples. The deposited rate was 120 nm (0.2 ± 3 . 0) nm/s evap, and observed during the time of coating by using a digital thickness monitor for the sample preparation. These samples were annealed for 30 minutes at different temperatures (400 and 450^{o}C). These samples were subjected to THz generation using a femtosecond laser. We have evaluated the potential of the efficiency of generated THz radiation of (111) TeO_2 films were measured using 800 nm wavelength pulses of 50 fs duration at 1 kHz repetition rate obtained from Ti: Sapphire laser amplifier.

5.3 Results and Discussion:

There are three parts to this section. The first section covers the analysis of XRD data, while the second part discusses the discussion of the evaluation of TeO_2 films for terahertz generation and efficiency. Finally, the third part comprises the terahertz-based optical properties of the TeO_2 films at different annealed temperatures like 400, and 450^{o}C and hall effect measurements of the effect of annealing films and morphology investigated by the atomic force microscope.

5.3.1 X-Ray Diffraction:

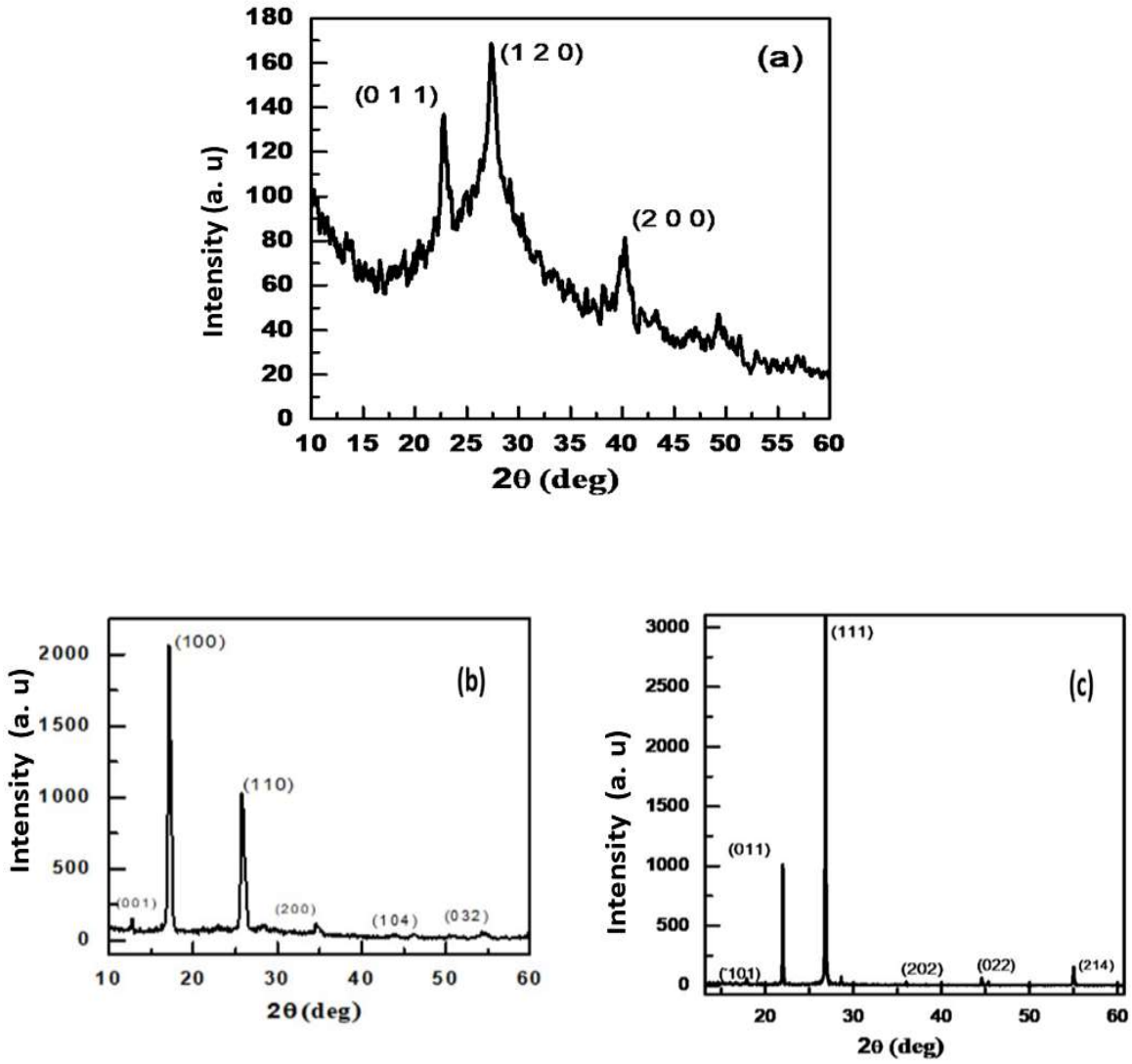

Fig.5- 1.XRD pattern of tellurium dioxide thin film (a) As-deposited (b) Annealed at 400°C (e) Annealed at 450°C.

XRD analysis was performed using a Philips X' pert pro diffractometer with Cu-Kα excitation wavelength of 1.54 Å. Its structure and identify the components and phases in the present work. The X-ray diffraction pattern of thermal evaporation of TeO_2 thin film is shown in respectively whereas Fig.5- 1**Error! Reference source not found.**(a). The pattern of X-ray diffraction as-deposited TeO_2 films from the figure shows was in the orthorhombic phase, and the main diffraction peaks are located at 2θ = 22.7°, 27.4°, and 40.1°, respectively corresponding to the preferred orientation along (011), (120), and (200)

planes and these peaks match with the JCPDS (76-0680) data of orthorhombic TeO_2 phase, respectively.Fig.5- 1(b) shows the X-ray diffraction pattern of TeO_2 film annealed at 400°C for 30 minutes. The corresponding peak at $2\theta=17.29^{o}$ belongs to JCPDS (71-0508) to the monoclinic structure (100) plane. Fig.5- 1(c) shows the X-ray diffraction pattern of TeO_2 films annealed at 450°C. The Corresponding peaks at $2\theta=27.39^{o}$ belong to JCPDS (65-2825) data and high-intensity peaks indication for the tetragonal

structure, which corresponds to the preferred orientation along (011) (111) planes.

The average grain size of the sample of the film was measured using Scherrer's formula [30],

$$D= k\lambda/\beta Cos(\theta) \qquad (5.1)$$

Where λ denotes wavelength ($\lambda= 1.5406$ A°) β (in radian) refers to Full Width at Half Maxima (FWHM) obtained from the XRD spectra at fact, k symbolizes the shape factor, which is=0.94, and θ (in degree) is the diffraction angle. These results indicate the crystalline phase formation and $\delta=1/D^2$ is dislocation density, and $\varepsilon= \beta/4\tan\theta$ is a macro strain. Applying all these parameters to Eq. (5.1). Table.5- 1 Comprises all important crystallin data of variation of TeO_2 films.

Table 5- 1: **The grain size, micro-strain, and dislocation density of TeO_2 for as-deposited and annealed at different temperatures from 400, and 450 °C for 30 min.**

TeO_2 Thin Film	Grain size D (nm)	Micro-strain $\varepsilon x10^{-3}$	dislocation density δ x 10^{-3} (nm^{-2})	Plane of Orientation (hkl)
As-deposited	15.0	11.71	4.44	(011)
	13.6	10.73	5.38	(120)
	35.2	2.86	0.80	(200)
Annealed at 400°C	36.3	8.63	0.75	(001)
	17.0	13.64	3.42	(100)
	14.5	10.71	4.72	(110)
	14.3	8.15	4.86	(200)
Annealed at 450°C	62.2	2.92	0.25	(011)
	54.4	2.74	0.33	(111)
	42.6	1.75	0.54	(214)

5.3.2 Optical Properties:

The optical transmittance and absorbance properties of TeO_2 films of 120 nm thickness on glass substrates were measured by a UV-Visible spectrophotometer. demonstrates the as-deposited material's absorption spectrum. films, from the graphs, clearly show the significantly fewer absorption ranges of TeO_2 film. The annealed temperature at 400°C shows moderate absorption spectra and an exponential drop in absorption after crossing 400 nm, and annealed at 450°C shows high absorption spectra from the graphs, clearly showing the broad absorption peak at 460 to 550 nm. It is a clear-cut indication of a shift, showing an annealing temperature of 450°C, the optical band gap, and the surface quality of the films. Fig.5- 2 (b) shows the transmission behaviors of the TeO_2 films. It also reveals that TeO_2 films as-deposited have deficient transmission, i.e., 1 % only while increases in annealing temperature at 400°C exponential increase transmittance 5 to 30%, the Annealed temperature at 450°C shows the nearly 60% of the transmission.

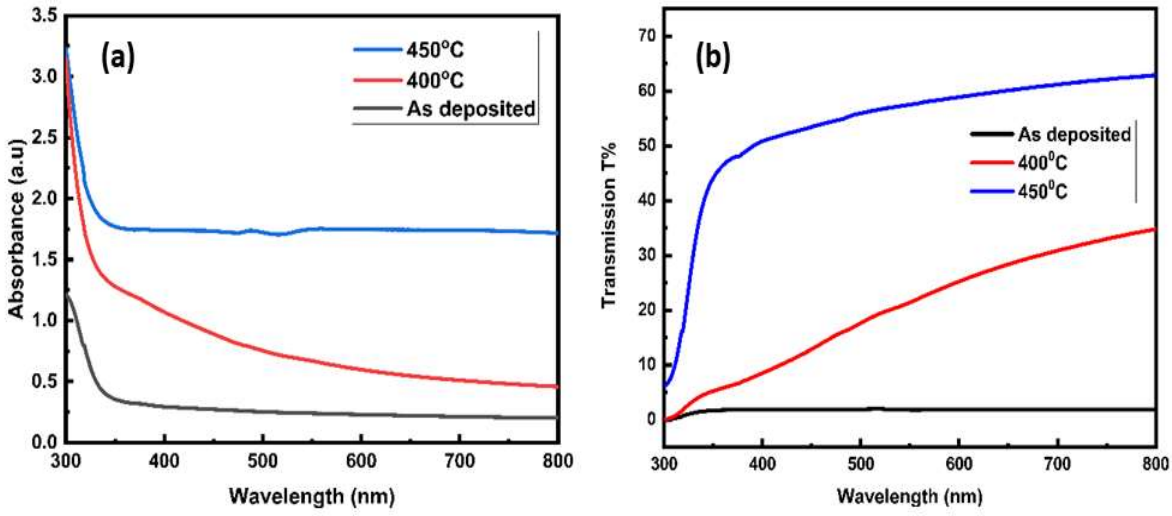

Fig.5- 2.(a)Absorbance, and 2(b). Transmittance vs Wavelength of TeO_2 films

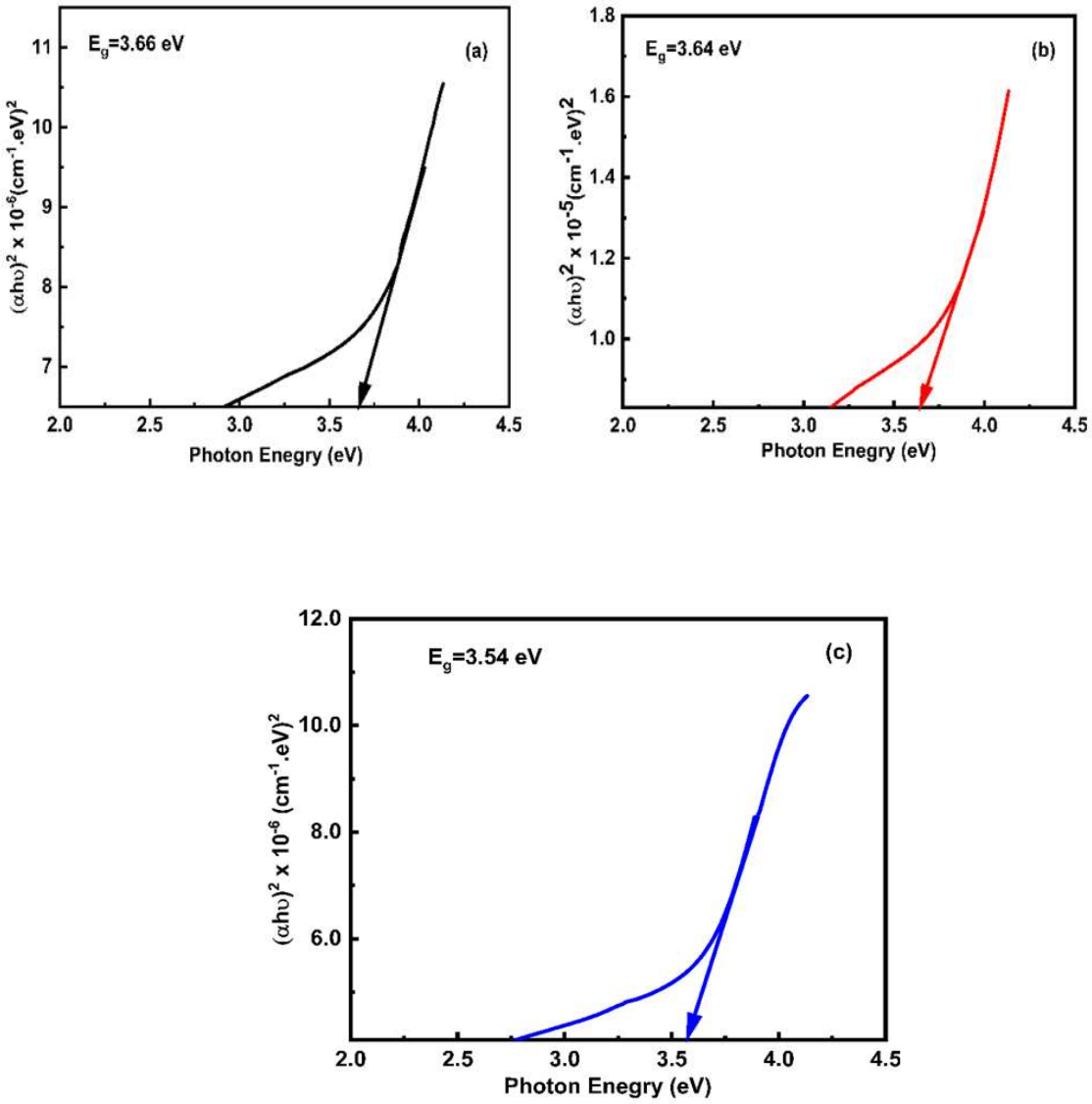

Fig.5- 3.$(\alpha h\upsilon)^2$ Vs Photon Energy for TeO_2 films annealed at different temperature (a) As- deposited (b) 400°C (c) 450°C.

Tauc has proposed a mathematical equation to present the relationship between the optical energy gap and the energy of the incident photon[31]:

$$(\alpha h\upsilon)^2 \propto A(h\upsilon - Eg)^n \qquad (5.2)$$

Where $\alpha h\upsilon$ is the optical absorption coefficient, A is a constant, $h\upsilon$ is the energy of the incident photon, Eg is the optical band gap, and n is an index that could take different values according to the electronic transition. The characteristics of $(\alpha h\upsilon)^2$

Vs. (hυ) were plotted for evaluating the bandgap (Eg) of the TeO_2 films as depicted in Fig. 5 -3:(a), (b), and (c) shows the value of Eg as-deposited films is 3.66 eV, and the annealing temperature of the TeO_2 film at 400 and 450^{o}C is showing a 3.64 and 3.54 eV. As the annealing temperature rises, it can be seen that the value of the photo energy gap reduces. This might be because the minimization of structural perfection is the cause.

5.3.3 Atomic Force Microscopy:

AFM is a useful method for examining the surface roughness and morphology of thin films. Figure AFM micrographs of Fig.5- 4.(a) Heat treatment was performed on the as-deposited material at 400 and 450°C. These micrographs' brightness reveals the variety in surface morphology's depth. The spherical shape of a particle is visible on the surface of the as-deposited TeO_2, indicating that the layer is homogeneous as a result of the creation of smaller grains. Fig.5- 4.(c) Another observation is that TeO_2 that has been annealed at various temperatures exhibits a triangle shape at 450°C. Due to the expansion of the grain size, the films' roughness reduces as the annealing temperature increase.

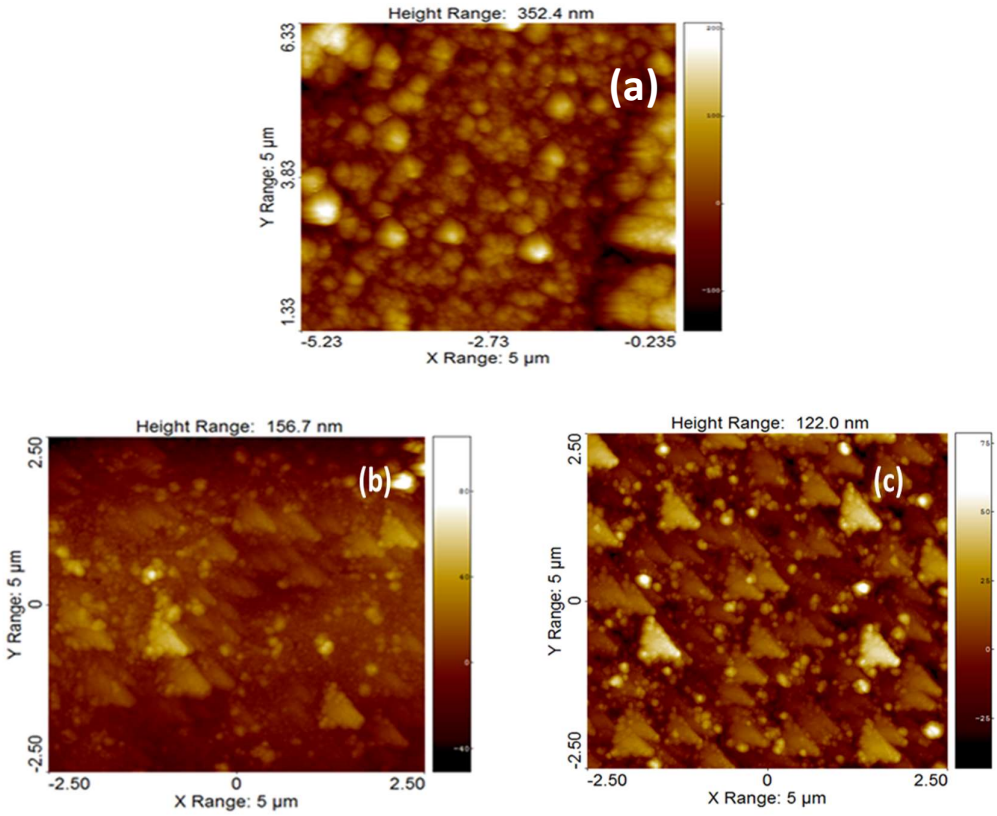

Fig.5- 4.Typical AFM images of (a) as-deposited; and heat-treated at (b) 400°C and (c) 450 °C. These layers have been annealed for 30 min in atmospheric conditions.

5.3.4 Hall effect Measurements:

The tellurium dioxide thin film surface was created with ohmic connections, and electrical measurements were carried out in a standard environment. One method for characterizing the conductivity mechanism, which takes into account the materials' mobility and carrier concentration, is the Hall Effect measurement. When measuring current and voltage using a D.C power supply PE1540 and a digital electrometer Keithley 616. The variation of conductivity ('σ') as a function of temperature is given by the "Arrhenius" Eqn. (5.3)[32].

$$\sigma = A \exp(-E_a/kT) \quad (5.3)$$

Where "k" stands for the Boltzmann constant, "A" stands for the pre-exponential factor, "Ea" stands for the activation energy, and "T" stands for the temperature in Kelvin.

By analyzing the slope of the Arrhenius plot of (ln(σ) vs (1000/T), one may determine the activation energy.

Ea = -slope x k, where Ea is the activation energy (Slope being negative, activation energy is positive)

By studying the Hall effect, we can identify semiconductors i.e. the type of 'n' or 'p'-type and concentration of electric charge carrier concentration of TeO_2 thin film between room to 300^o K temperature a constant magnetic field (B), on the film, applied perpendicularly for a generation of the Hall magnetic field given by Eqn. (5.4) using this we can determine the value of the Hall coefficient (R_H) where:

$$R_H = (V_H * I)/(t * B) \quad (5.4)$$

Further, the values of R_H were used to measure the charge carrier concentration using the given Eqn (5.5).

$$n = A/|R_H|e \quad (5.5)$$

The charge of an electron, e, is determined by assuming that the Hall factor A is unity.From the Eqn (5.5), the Hall mobility (μ_H) can be measured at room temperature

$$\mu_H = |R_H| \sigma \quad (5.6)$$

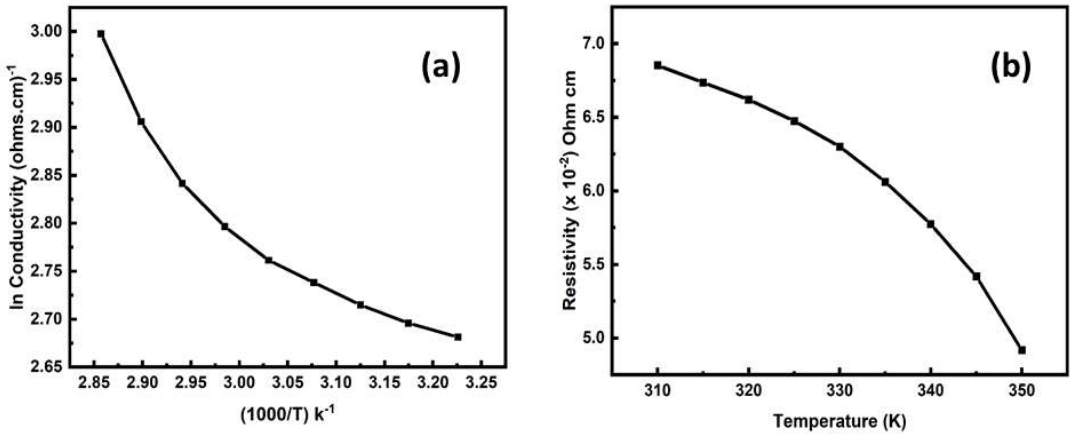

Fig.5- 5. a) Variation in Conductivity and b) Resistivity as a function of the temperature of tellurium dioxide (TeO_2) thin film

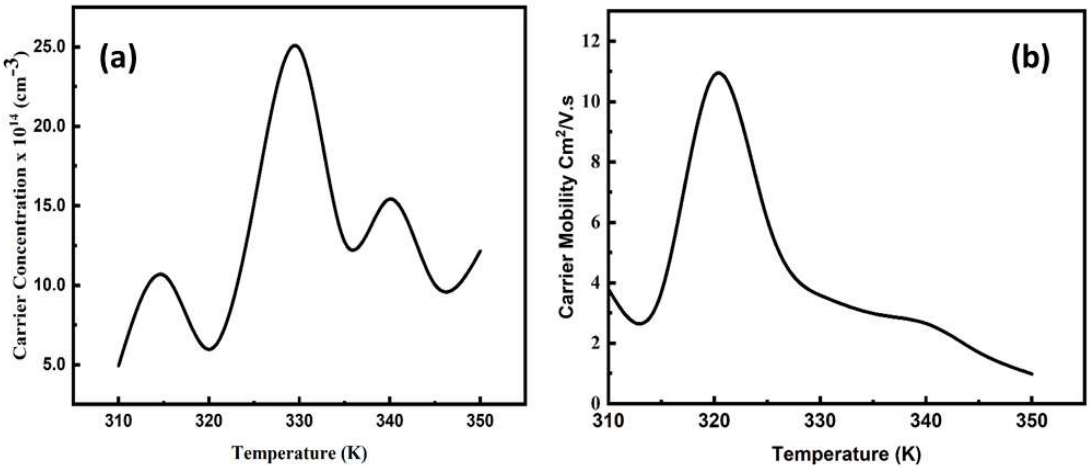

Fig.5- 6.a) Carrier Concentration and b) Carrier Mobility as a function of the Temperature of Tellurium dioxide (TeO_2) thin films

At various annealing temperatures (310 to 355 K), the Hall effect measurements are a mandate that uses thermoelectric power to determine the kind of carriers and confirm the nature of charge carriersTeO_2 thin films made by thermal evaporation and deposited on substrates at room temperature are subjected to heat treatment under vacuum, and it is found that the R_H is negative, indicating that the prepared films are (p-type), with the exception of when the film is annealed at 310 to 355 K temperature. We can observe that

the carrier concentration -n_H, which falls with increasing temperature from 2.52 × 10^{14} cm^{-3} at 330 K to 1.0 × 10^{14} cm^{-3} at 350 K., increases with decreasing temperature as a result of the effect of annealing temperature on R_H for TeO_2 thin film. In contrast, the Hall mobility (H) rises as the annealing temperature falls, from 1.1x10^1 $cm^2/V{\cdot}sec$ at 320 K to 1.5x10^o $cm^2/V{\cdot}sec$ shown in Fig.5- 8.

5.4 Time Domain Spectroscopy:

In reflection mode, the THz signal was measured. Terahertz was first applied to the reference before being applied to the sample to record the temporal characteristics. The FFT of the time domain signal provides frequency domain spectra. The THz electric field also represents a terahertz signal in the frequency domain. E_{sam} denotes the field associated with the sample, and E_{ref} is the reference time-domain

In the reflection mode of Terahertz TDS. The real part of n(ω) R.I is given by Eqn (5.6)

$$n(\omega) = \frac{\sqrt{n^2}|r|^2}{1+|r|^2-2|r|\cos\theta} \quad \textbf{(5.6)}$$

and Imaginary part of the refractive index k(ω) (extinction coefficient)

$$k(\omega) = \frac{-2|r|\sin\theta}{1+|r|^2-2|r|\cos\theta} \quad \textbf{(5.7)}$$

The reflection amplitude ratio is denoted by $|r|$, The phase difference between the reference and the sample is shown by the symbol θ.

The extinction coefficient k(ω) and the absorption coefficient (in cm^{-1}) are connected shown in Eqn (5.8)

$$\alpha(\omega)=4\pi\upsilon k(\omega)/c \quad \textbf{(5.8)}$$

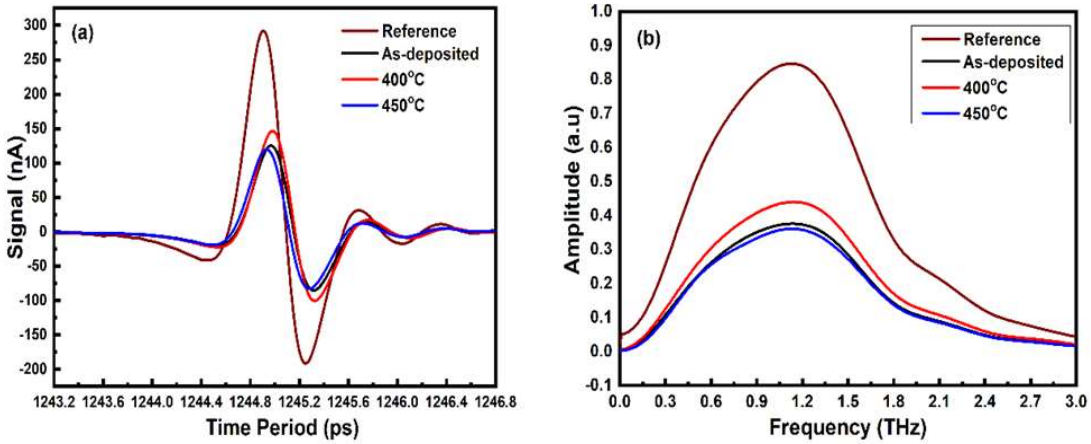

Fig.5- 7.Graphs the TeO_2 thin film annealed at 400 and 450oC a) THz temporal profiles b) frequency domain

Fig.5- 7 we can see that the amplitude spectrum of the signal at 350°C is lesser than the signal generated by the as-deposited thin film. From the XRD observation, we can see that the intensity of the orthorhombic structure is increased this also confirms that a perfect orthorhombic structure can act as a good transmitter of THz radiation as well as a generation. The signal at 400°C has the amplitude of all others. XRD analysis shows that it possesses the monoclinic structure with multiple symmetries.

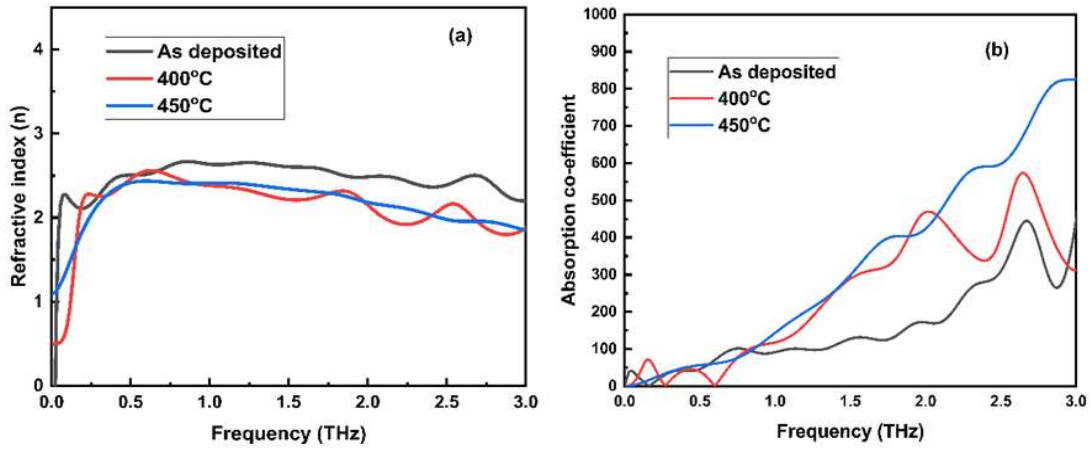

Fig.5- 8. Graphs the TeO_2 thin film annealed at 400 and 450°C a) Refractive index (n) (b) absorption coefficient

Refractive index and absorption coefficients were measured and displayed as optical characteristics in Fig.5- 8(a). The refractive index of the as-deposited film was measured

and found to vary from 2 and 2.5 between the 0.2 to 3 THz range. Annealing temperatures at 400 and 450°C showed the refractive index varies from 0.5 and 2.5 from 0.5 to 3 THz, nearly closer to the refractive index of Annealed temperatures. It is noticed that these films have a different refractive index in the Terahertz region, showing some characteristics variations of these films are 0.5, 1.7, and 2.6 THz frequency ranges. The measured absorption coefficients in as-deposited films show in Fig.5-8(b). some interesting and helps explain the film's physical properties from the UV-Visible spectrophotometer Fig.5- 2(a). It is noticed that less transmittance spectrum, almost 1%, acts as a reflector. However, at Annealing temperature 400°C, the absorption spectrum increase shows multiple peaks detected because the monoclinic structure has multiple defects for THz frequencies. The exponential growth in absorption coefficient at 450°C shows can act as a good transmitter of THz radiation as well as a generation, whereas, at the lower frequency, the value of the absorption coefficient of the film is less compared to that of other films. It is noticed that the tetragonal structure of the film shows multiple absorption peaks at the 1.6 and 2.2 THz frequencies range. It is also observed that the smoothness of the curves of refractive index is high at as 450°C and at the as-deposited temperature which is proving a single phase whereas, the variation at 400°C indicates multiple phases

5.5 Evaluation of TeO_2 film for Terahertz generation and efficiency

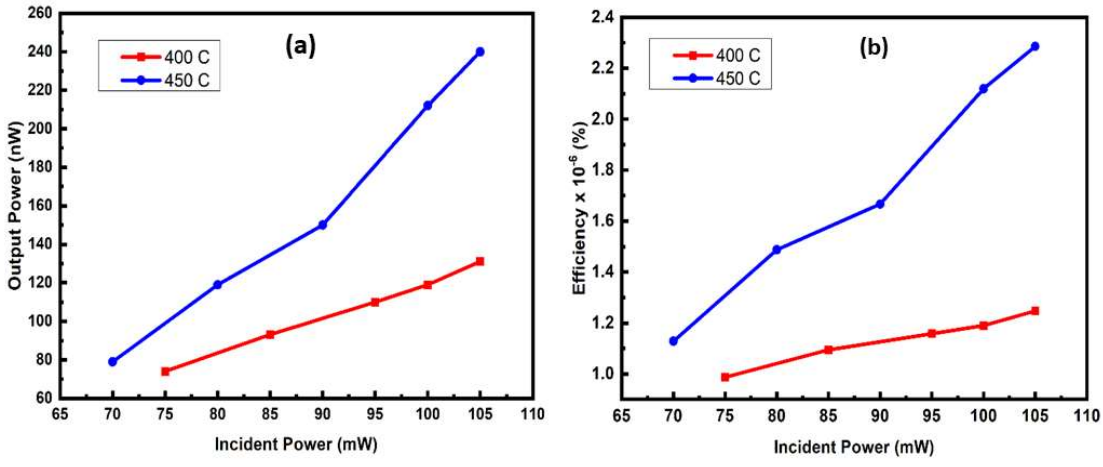

Fig.5- 9. Shows the TeO_2 thin film the curve between incident a) laser power Vs THz Output power (nW), and b) Incident Power Vs Efficiency of the generated THz radiation in nW.

As shown the Fig.5- 9, It is interesting to note that the maximum generated signal from the annealed at 400°C film is 115 nW while film annealed at 450°C has shown enhancement in the strength of the generated signal to the order of 240 nW, which is almost 2.2 times the 400°C film's signal. From Fig.5-12, the corresponding efficiency of the generated signal efficiency is of the order of 2.3 x10^{-6} %. The nature of the curve shows the possibility of further enhancement in the THz signal. But a THz signal at 400°C is lower than the 450°C annealed films. It confirms two crucial aspects of the temperature (i) modification of the crystalline phase changes the as-deposited film shows an orthorhombic crystalline phase and annealed at 400°C shows a monoclinic and 450°C shows a Tetragonal crystalline phase (ii) change in the optical parameters of TeO_2 films in the terahertz domain and AFM results show morphology in the presence of the triangle shape of 400°C and 450°C. In these films, the generation of THz radiation is mainly caused due to photo-Dember effect and radiation produced by accelerated charge carriers due to the liberations and subsequent acceleration of electrons from the metal by a strong electric field in proximity to the metal surface [27-28]. Since the contribution is due to optical rectification, the effect is more dominant in transmission mode.

Table 5- 2. Comparison of the THz generation efficiency of crystals DAST, BNA, LAP, and thin films *[33]*.

S.NO	Name of the sample	Space group (Point Group)	$n_{optical}$ (800nm)	n_{THz}	Conversion Efficiency (η)
1	BNA	$Pna2_1$ ($mm2$)	1.66	~1.65	26. 1$x10^{-4}$
2	DAST	P1	2.07	~2.2	16. 1 x 10^{-4}
3	LAP	P21	1.51	~1.52	6.2 x 10^{-4}
4	CdTe	-	-	-	2.3 x 10^{-4}
5	TeO_2	-	-	~2.2	2.6 x 10^{-4}

5.6 Conclusion:

In the present work, we successfully have the Terahertz generation of THz radiation and investigated the structural and optical properties in the THz domain of Tellurium dioxide were deposited on glass substrates using a PVD technique thickness of 120 nm. From the XRD analysis, we also believe that these films have a surface orientation (110) and phase change which is responsible for the generation of the terahertz signal for 400 and 450^{o}C resulting in optical rectification and photo carriers generated due to excitation of laser pulses accelerated free charges resulting in an electric field-induced photo carrier transient current surge mechanism, the emits THz pulses. The highest power of the THz signal was 210 nW for 450^{o}C annealed film to incident power of 115 mW. TeO_2 thin-film measurements of the Hall effect reveal that the annealing temperature has a significant impact on the film's (p-type) structure, carrier concentration, and Hall mobility. The derived values for dc are in accordance with Arrhenius's behavior with an activation energy of 0.0651 eV. For TeO_2 thin films, the annealing temperature has an impact on the Hall coefficient such that R_H rises with falling temperature and the carrier concentration- n_H, falls with rising temperature. from "2.52×10^{14} cm^{-3} at 330 K to 1.0×10^{14} cm^{-3} at 350 K". Atomic Force Microscopy results shows morphology in the presence of the triangle shape of 400^{o}C and 450^{o}C.

5.7 References:

1. N. Dewan, K. Sreenivas, V. Gupta, Properties of crystalline γ-TeO2 thin film, J. Cryst. Growth 305 (2007) 237–241. https://doi.org/10.1016/j.jcrysgro.2007.03.054

2. H. Kong, J-B. Yeo, H-Y. Lee, A Study on the properties of tellurium-oxide thin films based on the variable sputtering gas ratio, Journal of the Korean Phys. Soc. 66 (2015) 1744-1749. https://doi.org/10.3938/jkps.66.1744

3. H-Y. Wei, J. Lin, W-H. Huang, Z-B. Feng, D-W. Li, Preparation of TeO2 based thin films by nonhydrolytic sol–gel process, Mat. Sci. Eng. B 164 (2009) 51–59. https://doi.org/10.1016/j.mseb.2009.07.001

4. A. Lecomte, F. Bamière, S. Coste, P. Thomas, J.C. Champarnaud-Mesjard, Sol –gel processing of TeO2 thin films from citric acid stabilised tellurium isopropoxide precursor, J. Eur. Ceram. Soc. 27 (2007) 1151–1158. https://doi.org/10.1016/j.jeurceramsoc.2006.05.029.

5. N. Lakshminarayan, M. Radhakrishnan, C. Balasubramanian, J. Mater Sci 21 (1986) 246-250. https://doi.org/10.1007/BF01144728.

6. P. K. Gupta, P. P. Sharma, A. Sharma, Z. H. Khan, P. R. Solanki, Electrochemical and antimicrobial activity of tellurium oxide nanoparticles, Mat. Sci. Eng. B 211 (2016) 166–172. https://doi.org/10.1016/j.mseb.2016.07.002

7. W.A. Dutton, W. Cgarles Cooper, The oxides and oxy acids of tellurium, Chem. Rev. 66 (1966) 657–675. https://doi:10.1021/cr60244a003.

8. R. Nayak, V. Gupta, A.L. Dawar, K. Sreenivas, Optical waveguiding in amorphous tellurium oxide thin films, Thin Solid Films 445 (2003) 118–126. https://doi.org/10.1016/S0040-6090(03)01284-7.

9. Properties of tellurite glasses doped Dy 3+ and Eu 3+ for the UV and blue converted WLEDs, J. Non-Cryst. Solids 457 (2017) 1-8.

10. A. K. Yakhkind,J. Am. Ceram. Soc.49,670 (1966).

11. H. Takebe, S. Fujino, and K. Morinaga,J. Am. Ceram. Soc. 77, 2455 (1994).

12. P. K. Gupta, P. P. Sharma, A. Sharma, Z. H. Khan, P. R. Solanki, Electrochemical and antimicrobial activity of tellurium oxide nanoparticles, Mat. Sci. Eng. B 211 (2016) 166–172. https://doi.org/10.1016/j.mseb.2016.07.002

13. O. Noguera, T. Merle-Mejean, A.P. Mirgorodsky, M.B. Smirov, P. Thomas, J.-C. Chamarnaud-Mesjard, J. Non-Cryst. Solids 330 (2003) 50.

14. P.A. Thomas, J. Phys. C 21 (1988) 4611

15.V.H. Beyer, Z. Kristallogr. 124 (1967) 228

16. S. Blanchandin, P. Marchet, P. Thomas, J.-C. Champarnaud-Mesjard, B. Frit, J. Mater. Chem. 9 (1999) 1785.

17. N. Dewan, K. Sreenivas, R.S. Katiyar, V. Gupta, J. Appl. Phys. 101 (2007) 84910.

18. I. Podolesheva, V. Platikanova, I. Konstantinov, M. Rosler, J. Vac.Sci. Technol. A 12 (2) (1994) 393.

19.M.F. Al-Kuhaili, S.M.A. Durrani, E.E. Khawaja, J. Shirokoff, J. Phys. D: Appl. Phys. 35 (2002) 910.

20.F.D. Amore, M.D. Giulio, S.M. Pietralunga, A. Zappettini, L. Nasi, V. Rigato, M. Martinelli, J. Appl. Phys. 94 (2003) 1654.

21. D. Di Giulio, A. Zappettini, L. Nasi, S.M. Pietralunga, Cryst. Res. Technol. 40 (2005) 1023.

22. S.N.B. Hodgson, L. Weng, J. Sol–Gel Sci. Technol. 18 (2000) 145.

23. J.R. Middendrof. and E.R. Brown, THz generation using Extrinsic photo conductivity at 1550 nm Optic express Vol. 20, Issue 15, pp 16504-16509(2012).

24. klass Wynee John J.Carey , An integrated desctription of terahertz generation through optical retification, optical communictaions, Vol. 256,isssues 4-6, 400-413, (2005).

25. J Hu, L Yang - Springer Handbook of Glass, 2019,

26. A.Jha, S. Shaoxiong, L.H.Huang, and P.Joshi "Spectroscopic properties of rare metal ion doped tellurium oxide glasses and fibres," J.Opt. 33, 157-170 (2004).

27. S. Shen, A. Jha, X.Liu and M. Naftaly "Tellurite glasses for broadband amplifiers and integrated optics", J.Am. Ceram. Soc.85, 1391-1395 (2002).

28. S. J. Madden and K. T. Vu, "Very low less reactively ion etched Tellurium Dioxide planar rib waveguides for linear and non-linear optics," Opt. Express 17, 17645-17651 (2009).

29. Neetesh Singh, Hamidu M. Mbonde, Henry C. Frankis, Franz X. Kartner' Nonlinear Silicon Photonics on CMOS-compatible tellurium oxide" Photonics research Article. 1904 Vol. 8, No. 12.

30. S.M. Sze and Kwok. K. Ng, Physics of Semi-conductor devices,3rd edition, by Wiley (2003).

31. S. M. Alnaimi and M. N. Al. Dileamy (2007) Determination of the Optical Constant of Cadmium Stannate Film, International Journal of Pure and Applied Physics, Vol.3(1), p. 30.

32. Sudha L.K, Sukumar Roy, and K. Uma Rao, (2014) Evaluation of Activation Energy (Ea) Profiles of Nanostructured Alumina Polycarbonate Composite Insulation Materials International Journal of Materials, Mechanics and Manufacturing. 2: 96-100.

33. Ganesh Damarla, A. K. Chaudhary "Efficient Terahertz (THz) generation from some indigenously grown organic nonlinear crystals and designing of bandpass filters for spectroscopy of high energy materials" Ph.D. Thesis.

This page is intentionally left blank

Chapter 6: Applications of Terahertz Spectroscopy in Biomolecules

Abstract:

In this chapter, we have discussed the terahertz time-domain spectroscopy-based study of ribo- and deoxyribonucleosides constituting RNA and DNA in the aqueous solution. They play pivotal roles in the biological information cascade and functioning of the cell. The specified molecules' collective low-frequency vibrational modes are examined using terahertz spectroscopy. THz fingerprint spectra of DNA and RNA molecules are isolated from the cells which could provide crucial information about the basic constituents and conformations. These modes may provide information about the biomolecule fingerprint in the THz domain. In addition, We also determined the optical characteristics of these molecules in the 0.1-2.0 THz spectral range, including their refractive index, absorption, and extinction coefficients.

6.1 Introduction:

The recent development of THz technology has paved the way for its applications in the fields of medicine and biology [1-3]. One of the key areas for liquid vibrational spectroscopy and low-frequency dielectric relaxation, including H_2O, CH_3OH, C_2H_6O, and C_3H_8O is the spectrum range between 0.1 and 10 THz (3.3 to 333 cm^{-1}), etc.[4-5]. When used with density functional theory, THz-Time domain Spectroscopy (DFT) [6-12], is used to research amino acids [13-18] and peptides [19-20] drugs, and explosives [21-23]. THz spectroscopy-based data analysis and characterization of molecules can enable us to investigate and interpret complex biochemical processes and be useful as a tool for molecular and cellular medical diagnosis.

The low-frequency vibration modes of the massive atomic groups present in the molecule give rise to the optical characteristics of macromolecules in the THz spectrum range. Due to their collective nature, these vibrational modes are sensitive to the intermolecular structure and enable the investigation of conformational states. The low-frequency vibrational modes play vital roles in biochemical reactions. Numerous groups have reported on the specificity of the THz spectra to different conformers and isomers of the compounds under study. Additionally, environmental factors and mutations may have an impact on the THz absorption bands.

THz spectroscopy's use in the investigation of nucleobases, which are nitrogen-containing biological compounds remains limited. Their conjugates with ribose or deoxyribose sugar are known as ribo or deoxyribonucleoside, which can be phosphorylated to form corresponding nucleotides that polymerize to form RNA or DNA, respectively. Adenine-A, Guanine-G, Thymine-T, Cytosine -C, and Uracil-U are the five nitrogenous bases that make up the biological system (U). They form corresponding nucleosides Adenosine, Guanosine, Thymidine, Cytidine, and Uridine. Deoxynucleotides polymerize to form deoxyribonucleic acid (DNA) and ribonucleotides form ribonucleic acid (RNA). A, T, G, and C are present in both DNA and RNA, as are A, U, G, and C. Nucleic acid molecules serve as genetic material in biological organisms. While THz techniques have been used on hybridized DNA molecules in the past, few of them have addressed the binding states [24]. When Brucherseifer and Nagel et al. used a DNA sample's far-infrared absorption

and index of refraction to determine its hybridization state, they brought attention to the significance of the refractive index of DNA molecules [25-26].

Chemical modification of these nitrogenous bases can modify the nature of information flow and thereby change the functional status of the cell. These modifications are highly regulated through a dedicated set of enzymes. These modifications have been reported in several diseases like diabetes, cardiovascular disease, neurodegenerative disease, cancers, etc. Several studies have also shown their prognostic and diagnostic values. Therefore, direct monitoring of the nucleobases and their chemical modification holds tremendous interest in the field of biochemistry. The commercially available authentic standards for modified bases, nucleosides, and nucleotides will be analyzed for orthogonal signatures, sensitivity, and dynamic range in an aqueous solution. Pure RNA and DNA-modified and unmodified oligos will be used to check the ability to identify/quantify modifications from intact oligos.

6.2 Experimental details:

Terahertz time-domain spectroscopy (THz-TDS) experiment was carried out in reflection geometry by using the self-reference method [6]. The THz-time domain system used an optical fiber-connected femtosecond laser and InGaAs/InAlAs photoconductive antennas for Terahertz generation and detection (TeraFlash-Toptica photonics, Germany). The average output power of the femtosecond fiber-coupled laser, which had a 1.5 m central wavelength and a repetition rate of 100 MHz, was 80 mW. The purest form of every molecule was bought from Sigma-Aldrich (Germany) and used without further purification or recrystallization. To create a consistent sample mixture in aqueous media, 5 ml of distilled water was combined with a 10 mg molecular powder from and sonicated for 15 minutes. A quartz plate of 2 mm thickness was used as the reference material, and the reference signal was measured. The liquid sample was deposited on the quartz plate, and time-domain spectra were recorded, as shown in Fig 1. The liquid sample's complex refractive index is given by the formula ($\tilde{n} = n + ik$) and was calculated using the Eqn (6.1) as given below. The Refractive index (n) is represented by the real component, and the extinction coefficient (k) is represented by the imaginary part.

6.3 Results and Discussion:

6.3.1 Terahertz Time-domain spectroscopy:

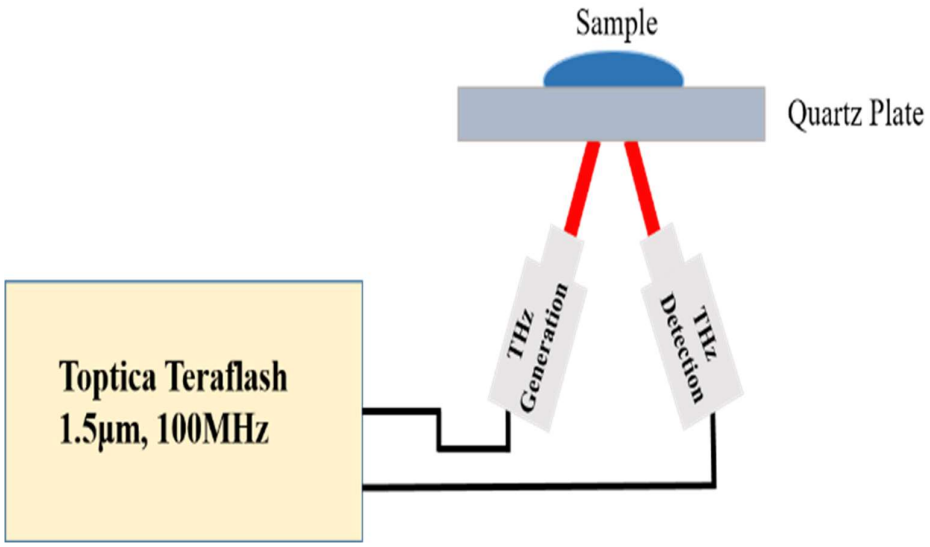

Fig. 6- 1. Schematic of an experimental setup for Terahertz Spectroscopy

The reflection mode was used to measure the THz signal. First, the reference was subjected to terahertz followed by the biomolecules sample to record the temporal profiles. Signal in the time domain using FFT provides frequency domain spectra. Terahertz signal in the frequency domain is also represented by the THz electric field "E_{sam}" represents the field associated with the biomolecules sample and "E_{ref}" is the reference time-domain

The spectral and temporal responses of the THz time domain reflection mode are depicted in Fig.6- 1. In the reflection mode of Terahertz Time-domain Spectroscopy.

$$\tilde{n}(\omega) = \frac{\sqrt{n_q^2(1-\hat{r}_{qs})^2 + 4\hat{r}_{qs}\sin\theta^2}}{1+\hat{r}_{qs}} \quad (6.1)$$

Where "θ" is the angle of incidence of THz radiation, "r_{qs}" is the reflectance from the quartz-sample contact, and "n_q" is the refractive index of quartz.

The relationship between the extinction coefficient k(ω) and the absorption coefficient α(ω) (cm^{-1}) shown in Eqn **(6.2).**

$$\alpha(\omega)=4\pi\upsilon k(\omega)/c \quad (6.2)$$

If the frequency in the THz range is "υ" and "c" is the velocity of light.

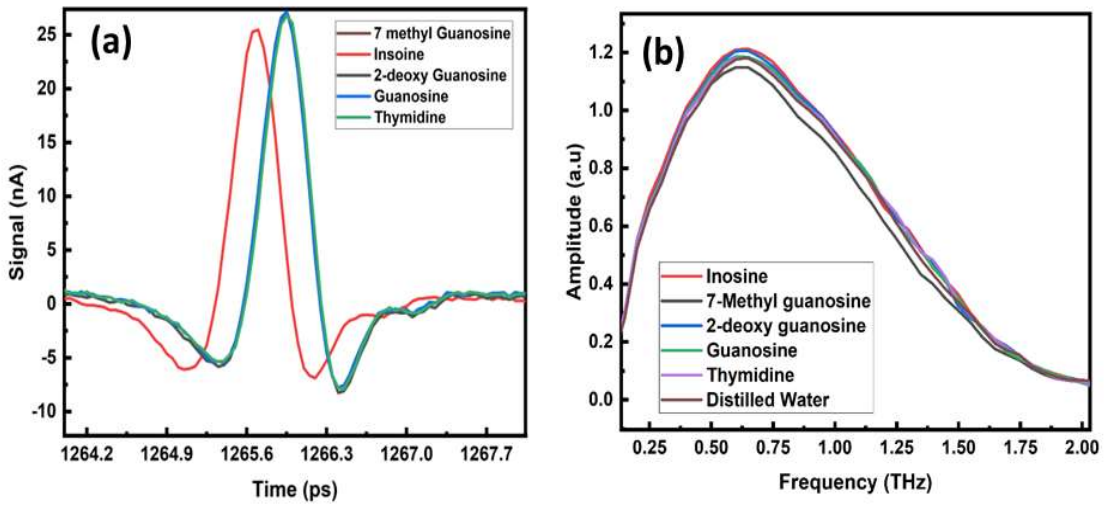

Fig.6- 1.a) Time-domain and b) frequency domain spectra of the aqueous solution of ribo and deoxyribonucleosides molecules

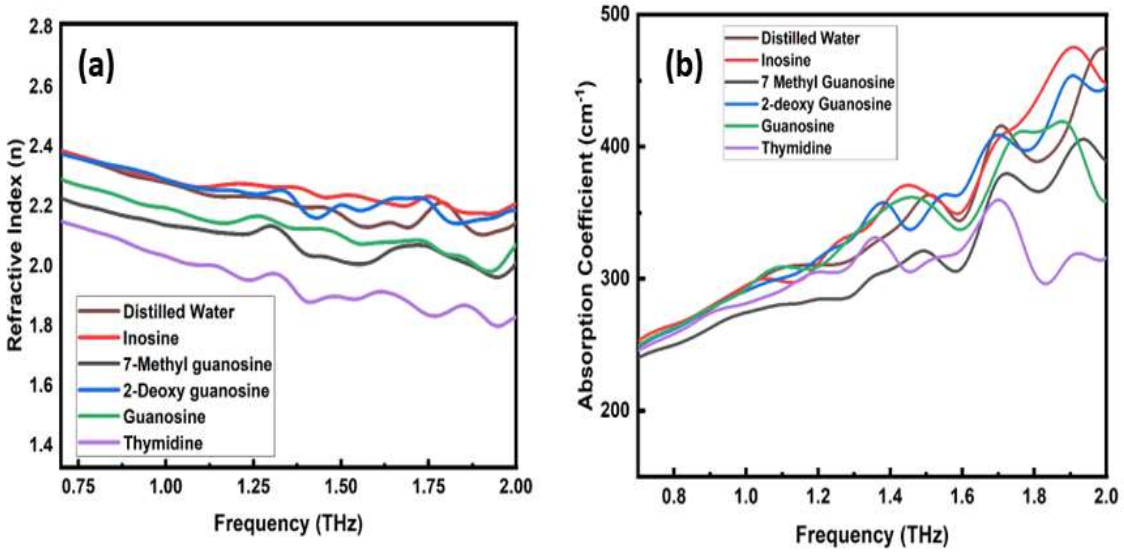

Fig.6- 2.a) THz refractive index and b) Absorption Coefficient of ribo and deoxyribonucleosides molecules

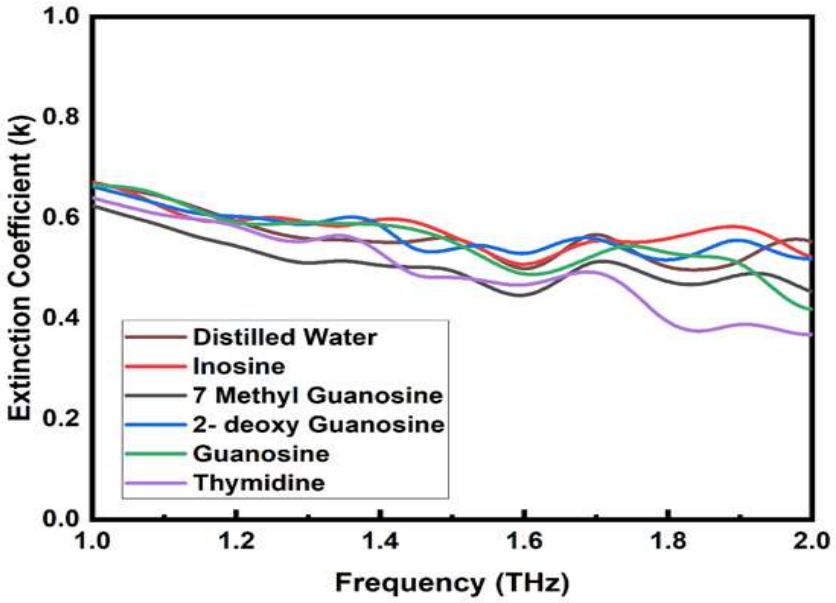

Fig.6- 3.THz Extinction coefficient of ribo and deoxyribonucleosides molecules

6.4 Conclusion:

In the present work we successfully identification of Nucleotides polymerized to form Deoxyribonucleic acid (DNA) or Ribonucleic acid (RNA) that can exist as a single base molecule structure has been demonstrated via THz-TDS. The following conclusions can be made in light of our findings and research. Due to their typically low and featureless absorption in the THz band, quartz is suited as a window material for aqueous solutions observed value is 1.5 to 2.0 THz range and the refractive index also changes with respect to the extinction coefficient. THz-frequency domain and the very limited volume of the liquid sample biomolecules in this experiment significant benefits, especially as a probe for molecular dynamics, including the behaviour of DNA and RNA. experimental work remains to be undertaken if useful information on Nucleic acid molecules serves as genetic material in biological organisms from which the information flows through RNA.

6.5 References:

1. J. T. Kindt and C. A. Schmuttenmaer, J. Phys. Chem. 100, 10373 (1996).

2. B. Reinhard, K. M. Schmitt, V. Wollrab, J. Neu, R. Beigang, and M. Rahm, Appl. Phys. Lett. 100, 221101 (2012).

3. R. M. Dreizler and E. K. U. Gross, Density Functional Theory an Approach to the Quantum Many-Body Problem (Springer, 1990). 13M. Orio, D. A. Pantazis, and F. Neese, Photosynth. Res. 102, 443 (2009).

4. T. M. Korter, R. Balu, M. B. Campbell, M. C. Beard, S. K. Gregurick, and E. J. Heilweil, Chem. Phys. Lett. 418, 65 (2006).

5. D. G. Allis, A. M. Fedor, T. M. Korter, J. E. Bjarnason, and E. R. Brown, Chem. Phys. Lett. 440, 203 (2007).

6. M. D. King, W. D. Buchanan, and T. M. Korter, Anal. Chem. 83, 3786 (2011).

7. D. G. Allis, D. A. Prokhorova, and T. M. Korter, J. Phys. Chem. A 110, 1951 (2006).

8. M. D. King, P. M. Hakey, and T. M. Korter, J. Phys. Chem. A 114, 2945 (2010).

9. B. Yu, F. Zeng, Y. Yang, Q. Xing, A. Chechin, X. Xin, I. Zeylikovich, and R. R. Alfano, Biophys. J. 86, 1649 (2004).

10. J. Neu, C. T. Nemes, K. P. Regan, M. R. Williams, and C. A. Schmuttenmaer, Phys. Chem. Chem. Phys. 20, 276 (2018).

11. J. Neu, H. Nikonow, and C. A. Schmuttenmaer, J. Phys. Chem. A 122, 5978–5982 (2018).

12. M. R. C. Williams, A. B. True, A. F. Izmaylov, T. A. French, K. Schroeck, and C. A. Schmuttenmaer, Phys. Chem. Chem. Phys. 13, 11719 (2011).

13. M. R. C. Williams, D. J. Aschaffenburg, B. K. Ofori-Okai, and C. A. Schmuttenmaer, J. Phys. Chem. B 117, 10444 (2013).

14. M. Yamaguchi, K. Yamamoto, M. Tani, and M. Hangyo, in 2005 Joint 30th International Conference on Infrared and Millimeter Waves and 13th International Conference on Terahertz Electronics (IEEE, 2005), Vol. 2, pp. 477–478.

15. M. Yamaguchi, K. Yamamoto, M. Tani, and M. Hangyo, in Infrared and Millimeter Waves, Conference Digest of the 2004 Joint 29th International Conference on 2004 and 12th International Conference on Terahertz Electronics, 2004 (IEEE, 2004), pp. 779–780.

16. M. Lu, J. Shen, N. Li, Y. Zhang, C. Zhang, L. Liang, and X. Xu, J. Appl. Phys. 100, 103104 (2006).

17. M. C. Kemp, in 2007 Joint 32nd International Conference on Infrared and Millimeter Waves and the 15th International Conference on Terahertz Electronics (IEEE, 2007), pp. 647–648.

18. F. Ellrich, G. Torosyan, S. Wohnsiedler, S. Bachtler, A. Hachimi, J. Jonuscheit, R. Beigang, F. Platte, K. Nalpantidis, T. Sprenger, and D. Hübsch, in 2012 37th International Conference on Infrared, Millimeter, and Terahertz Waves (IEEE, 2012), pp. 1–2.

19. J. F. Federici, B. Schulkin, F. Huang, D. Gary, R. Barat, F. Oliveira, and D. Zimdars, Semicond. Sci. Technol. 20, S266 (2005).

20. J. F. Federici, B. Schulkin, F. Huang, D. Gary, R. Barat, F. Oliveira, and D. Zimdars, Semicond. Sci. Technol. 20, S266 (2005).

21. J. Wang, "From DNA biosensors to gene chips," Nucleic Acids Res. 28(16), 3011–3016 (2000).

22. M. Chee et al., "Accessing genetic information with high-density DNA arrays," Science 274(5287), 610–614 (1996).

23. H. Ozaki and L. W. Mclaughlin, "The estimation of distances between specific backbone-labeled sites in DNA using fluorescence resonance energy-transfer," Nucleic Acids Res. 20(19), 5205–5214 (1992).

24. Z. Zhu and A. S. Waggoner, "Molecular mechanism controlling the incorporation of fluorescent nucleotides into DNA by PCR," Cytometry 28(3), 206–211 (1997).

25. M. L. Larramendy, W. El-Rifai, and S. Knuutila, "Comparison of fluorescein isothiocyanate- and Texas red-conjugated nucleotides for direct labeling in comparative genomic hybridization," Cytometry 31(3), 174–179 (1998).

26. A. Rahman, B. Stanley, and A. K. Rahman, "Ultrasensitive label-free detection and quantitation of DNA hybridization via terahertz spectrometry," Proc. SPIE 7568, 756810 (2010).

Chapter 7: Conclusions and Future Plan

In this present work, we have made an attempt to demonstrate the art of developing semiconductor (CdTe) and semi-metallic (TeO_2) films on a glass substrate and investigated the effects of annealing temperature on the structural and optical properties. Finally, these films were employed as a source for efficient THz generation. From the XRD analysis, it is intended that the cubic phase of (111) direction perpendicular to the substrate surface becomes more effective with respect to the rise of annealing temperature. The average grain size of the CdTe increases with respect to an annealing temperature upto 200^{o}C. It also decreases the bandgap and enhances the optical properties of the thin film. Finally, the grain size starts decreasing after annealing treatment at 400^{o}C. This could be attributed to the electron confinement to the nano-scale range. The intensity of the THz radiation was increased upto 1.7 times with an increase in the incident power after annealing the film at 200^{o}C. It was observed that the change in crystal structure above 200^{o}C reduces the strength of THz radiation. The efficiency of the CdTe thin film is increased by 4.31 times when annealed at 200^{o}C an compared to the room temperature. This might be due to changes of irradiative phonon and plasmonic states, carrier concentration, mobility, and bandgap of the thin film.

We estimated the transmission of THz radiation and investigated the structural and nonlinear optical properties of 3N & 5N Te, Cd, and CdTe films deposited on GaAs substrates using a physical vapor deposition (PVD) thickness 200 to 620 nm. From the XRD analysis, We also confirm the CdTe, 5N, and 3N Te, Cd deposited on the GaAs substrate, these films have surface orientation perpendicular to the (111) GaAs substrate which is responsible for enhancement of the terahertz signal and the conductivity, optical impedance, g value, ϱ value & reflection coefficient for both T.E. and T.M. mode and resulting in optical rectification and photo carriers generated due to excitation of laser pulses accelerated free charges resulting in an electric field opposite to the transient current surge mechanism, the emits THz pulses. To study the surface morphology, researchers employ a field emission scanning electron microscope (FESEM), in the presence of the fracture surface and fatigue crack mechanism.

The Terahertz generation of THz radiation and investigated the structural and optical properties in the THz domain of Tellurium dioxide were deposited on glass substrates using a PVD thickness of 120 nm. From the XRD analysis, we also believe that these films have a surface orientation (110) and phase change which is responsible for the generation of the terahertz signal for 400 and 450^{o}C resulting in optical rectification and photo carriers generated due to excitation of laser pulses accelerated free charges resulting in an electric field-induced photo carrier transient current surge mechanism, the emits THz pulses. The highest power of the THz signal was 210 nW for 450^{o}C annealed film to incident power of 115 mW. The hall effect measurement results of TeO_2 thin film show that the film was (p-type), the carrier concentration, and Hall mobility is strongly dependent on the annealing temperature. The effect of annealing temperature on Hall coefficient for TeO_2 thin film such that R_H increases with respect to drop of temperature, we can also observe that the carrier concentration (n_H) decreases with respect of increase temperature from 2.5 x 10^{14} cm^{-3} at 330 K to 1.0 x $10^{14}cm^{-3}$ at 350 K. Atomic Force Microscopy results shows morphology in the presence of the triangle shape of 400^{o}C and 450^{o}C.

We have successfully identified the Nucleotides polymerizes to form Deoxyribonucleic acid (DNA) or Ribonucleic acid (RNA) with only sole base molecules which were shown by THz-TDS. The following conclusion can be drawn from our findings and analysis can be drawn the quartz is suitable as a window material for aqueous solutions due to its low absorbance in the THz region between 1.5 to 2.0 THz range and the refractive index also changes with the respect to extinction coefficient. Specifically, as a probe for molecular dynamics, including the behavior of DNA and RNA, the Biomolecules used in this experiment were sampled from a liquid using a terahertz frequency domain and a comparatively small volume. will give significant benefits. If helpful knowledge is available, experimental work must still be done on Nucleic acid molecules serves as genetic material in biological organisms from which the information flows through RNA and proteins via the processes of transcription and translation.

7.1 Future plan:

For the following potential applications in the future, the research done for this thesis can be expanded:

- Annealing is an important process which can be applied to many other semi-metallic and semiconductor films for improving their structural and optical properties which can be employed for making low-cost THz sources.
- We have experimentally demonstrated the enhancement of conductive current in I-V Characteristics of the order of 10^{-3} Amp as compared to pure GaAs i.e 10^{-6} Amp. The role of Active substrate for enhancement of the carrier concentration and conductivity which can be explored for making THz-based sensors. Therefore, it can be used for making gas sensors, and biomolecules (proteins).
- These semiconductor films can be deposited on Teflon/Si prism for making a THz-based SPR sensor the detection of explosive, toxic chemicals, viruses, biomolecules,etc.
- The THz-based photoacoustic cell can be designed which will be pumped with optical pulses.
- Annealing of the sample shows the phase transition from alpha to gamma phase of tellurium oxide. This indicates that annealing can play a significant role in semiconductor and semi-metallic TeO_2 films.
- Teo_2 films can be used in acoustic optics and THz-based photoacoustic devices.
- The THz spectroscopy can help to plan the study the current cell line such as cancer cell line, and health cell line then analysis is mostly based on some staining/tagging directed against specific markers. Tag-free cell type analysis can find important applications in the diagnostics of diseases, including cancer as well as other hematological and degenerative diseases (ex vivo/in vitro) using a terahertz (THz) time-domain spectroscopy.
- We also demonstrated the use of terahertz spectroscopy of the nucleotides in terahertz fingerprint spectra which is related to the DNA and modified RNA. This Visibility of molecules-related experiments opens a new channel for studying the health cell line, cancer tissues, DNA and RNA molecules confocal optical microscopy imaging and terahertz imaging able to relieve many unknown features of cancer cells and tissues.

Therefore, based on the above-mentioned studies the following future work can be planned.

Publications

- **M. Mahendar**, A. K. Chaudhary, Ganesh Darmala, Vinay Gupta," Evaluation of cadmium telluride (CdTe) thin films grown at different annealing temperatures for efficient terahertz generation" Workshop on Recent Advances in Photonics (WRAP), Guwahati, 2019, DOI:10.1109/WRAPP47485.2019.9013662**.**

- **M. Mahendar,** R, N Vamsi Krishna & A. K. Chaudhary, Femto Seconds Laser-Based Efficient THz Generation from Different Temperature annealed CdTe Thin films and Effects of carrier Concentration and Phase transition on Efficiency of Generation" submitted to the Indian Journal of Pure & Applied Physics (IJPAP) Vol.60, (2022) **(Chapter 3).**

- **M. Mahendar**, P. Naveen Kumar, A.K. Chaudhary, SK. Ramiz Islam SoumenKanti Manna "Study of nucleotides using Terahertz Time Domain Spectroscopy", in URSI-RCRS (2022). **(Accepted).**

- **M. Mahendar,** R, N Vamsi Krishna & A. K. Chaudhary, "Effect of Annealing Temperature on Structural, Morphological, and Nonlinear Optical Properties of TeO_2 films used for Efficient THz Generation", **(Communicated).**

- **M. Mahendar,** Chandan Ghorui, & A.K. Chaudhary," Evaluation of terahertz (THz) based optical, dielectric, current density, conductivity and scattering, properties of Cd, Te, and CdTe films deposited on the GaAs substrate for device applications, (2022). **(Communicated).**

Indian Journal of Pure & Applied Physics
Vol. 60, May 2022, pp. 401-406

Femto Seconds Laser Based Efficient THz Generation from Different Temperature Annealed CdTe Thin Films and Effects of Carrier Concentration and Phase Transition on Efficiency of Generation

M Mahendar, R N Vamsi Krishna & A K Chaudhary*
Advanced Center for Research in High Energy Materials, University of Hyderabad, Hyderabad-500 046, India

Received 16 February 2022; accepted 19 April 2022

The paper reports the thermal evaporation based growth process of CdTe thin films on glass substrates. These films were annealed between room temperature to 200, 300 and 400 °C, respectively. The XRD characterization of these films revealed the change in crystalline phase from cubic to triclinic above 200 °C. Finally, these films were subjected to 800 nm wavelength of 35fs pulsed obtained from Ti: sapphire amplifier at 1kHz repetition rate. The incident power of the laser was focused and tuned between 150-350 mW range and generated THz signals were recorded using calibrated Pyroelectric detector at 22.5 Hz frequency. The highest power of the THz signal was 80nW for 200 °C annealed film with respect to incident power of 300mW. The highest efficiency of THz signal was of the order of 3.11E-5%. We have also explained the effect of carrier concentration and phase transition with respect to different annealed temperature for efficient generation of THz signal.

Keywords: Cadmium Telluride; Thin films; Tera-Hertz Generation; Carrier concentration; X ray Analysis; Phase transition

1 Introduction

Cadmium telluride (CdTe) is one of the most prominent polycrystalline materials for thin film solar cell because of its physical properties. It can be prepared with a high conductivity in both n and p type forms. CdTe is a member of the II–VI family of compound II-VI periodic group optically active chalcogenide semiconductor materials with immense applications in optoelectronics, photonics and bio-labelling applications.Intervention of nanoscience and nanotechnology has enabled the realization of low dimensional nanostructures of Cadmium chalcogenide (CdS, CdSe, or CdTe) with the enhanced surface area to volume ratio that has attracted major appreciation with their unique and enhanced electronic and optical properties[1-5].Being a direct bandgap semiconductor with the high atomic number and electron density, CdTe has been widely used in photovoltaic, sensors, diodes, rectifiers, and detectors[6–9] One of the interesting properties of CdTe is its high bond energy (5.75 eV)[10] which makes it a perfect candidate for space applications too. Looking at the material consumption point of view, the efforts are being made in the direction of the fabrication of ultra-thin film and small area devices[11]. Recently, Chu *et al.* have demonstrated that the solar cell efficiency of 8% from only 250 nm CdTe absorber layer[12]. The fabrication process also plays an important role in the final costing of the device. Though the conventional vacuum techniques lead to a better quality device, the low-cost alternatives are the area of interest to the researchers. CdTe has the possibility to be doped both n- and p-type and the variety of preparation techniques such as thermal evaporation which often preferred because it offers large possibilities to modify the deposition condition. The techniques like electrodeposition, spin coating, chemical bath deposition are being commonly used now a day for the synthesis of high-quality nanoparticles, thin films, or even large area devices.

Sergi *et al.* reported the effect of annealed temperature on the optical properties of P doped CdTe films [13-14]. Kasmorski *et al.* have reported the use of Auger analysis of CdSCuInSe2 thin-film used for the solar cells applications[15]. Pankove has nicely discussed the utility of five important properties in the deposition of CdS semiconductor films These studies were conducted by means of optical characterization, pH measurements, energy consumption tests, and chemical analysis[16]. Hans Batch and Dieter Krause have well discussed the art of deposition of semiconductor films on glass and their optical characterizations[17]. Sivaramakrishna *et al.* have explained the phenomena

*Corresponding author:
(E-mail: akcphys@gmail.com, akcsp@uohyd.ernet.in)

of instability in resistance and variation of the activation energy with thickness and deposition temperature in the case of $CdSe_{0.6}Te_{0.4}$ film[18].

The development of thin films has helped in solving many problems in non-linear optics. In the non-linear processes phase matching condition is one of the definitive criteria to achieve results. The coherent length plays a crucial role in this aspect. The growth of Nano-structure in making of thin films reduced the barrier of coherent length. This provided a new gate in developing efficient THz sources.

Efficient THz sources can be developed using thin films which are operated using optical rectification and photo-dember effect. Band-gap and the thickness of the material used in thin films plays a crucial role in production of commercial THz sources. Some interesting semiconductor or organic crystals such as ZnTe, $ZnGeP_2$, GaAs, GaP, BNA, DAST *etc*. are widely used for the THz generation. The CdTe in form of a single crystal or thin film that can be used for the generation of efficient THz signal in very effective manner[19-23]. However, in previous report the authors have presented the qualitative picture of THz generation from CdTe films. The report could not able to establish the role of carrier concentration with respect to annealed temperature and corresponding phase changes occurred in context of THz generation. In addition, the information of the efficiency was also not ascertained. The temperature at which the thin films were annealed also provides valuable information related to structural changes that is directly correlated to the efficiency of the generated THz signal.

However, second harmonics and THz generation from centrosymmetric materials are related to induced electric field based broken symmetry. Which is basically a surface phenomenon[24-26]. The entire process of generation from Centrosymmetry thin films is governed by second order nonlinearity and surface current induced due to third order nonlinearity and also known as Photo- dember effect. Equation (2 & 3) clearly represent the process of generation from the thin films.

$$P_i(\Omega) = \chi^{(2)}_{eff,ijk}(\Omega; \omega + \Omega, -\omega) E_j (\omega + \Omega) E^*_k(\omega) \quad \ldots (1)$$

$$\chi^{(2)}_{eff,ijk} = \chi^{(2)}_{ijk} + \chi^{(3)}_{ijk} E_{surf,l} \quad \ldots (2)$$

The generation of polarized waves in THz domain due to combined effect of Optical rectification process and effect of broken symmetry are explained using Eq.1 in which E and ω are electric field and frequency of excitation pulse, Ω is the frequency of the generated pulse and i, j, k are polarization directions. For efficient THz generation we should achieve a resonance condition between ω and Ω. In the current experiment we have used the excitation pumping source femto-seconds pulses which is responsible for the generation of ultra-short time based charge carriers that matches to time scale of THz signal.

In photo-dember process, χ^3 plays a very crucial role in generation of THz pulses which is shown in Eq.2. The value of the χ^3 depends on the symmetric nature of the crystalline thin film. The Centro-symmetry of the cubic structure increases the involvement of the process in generating efficient THz pulses. The decrease in symmetry of the crystalline structure reduces the value of χ^3 and affecting the strength of THz signal.

In the past, several groups have reported generation of THz signal using CdTe crystals and thin films and studied the effects of temperature in various parameters of CdTe crystal. This helped us to prove that at higher temperatures the refractive index, transmittance and formation of different states are varying with temperature. This also proved that CdTe can also be used as commercial efficient THz source.

In the present report, we have discussed the detailed characterization and optical behavior of CdTe thin films annealed at different temperatures. Further, we have observed the intensity and efficiency of output THz signal by CdTe thin film for different input powers at 800nm. We also observed the variation of physical structure and its effects on efficiency of the thin film when annealed at 4 different temperatures *i.e*. 27 , 200 , 300 and 400 ^oC, respectively.

2 Experimental Procedure

The experiment was carried out in three parts. In the first part, the CdTe films were deposited and annealed at different temperatures. The second part deals with the XRD characterization for structural analysis while, the third part covers the experimental details of THz generation and recording of generated signals with respect to incident laser power.

(I) Growth procedure of annealed CdTe thin films

The samples were prepared by a thermal evaporation method using a vacuum evaporation

(HINDHIVAC Vacuum coating unit, Model No: 12A4U), in high vacuum (10^{-6} Torr). The solid form of Cadmium (Cd) and Tellurium (Te) was used as source material and Glass slides were used as substrates to prepare cadmium telluride (CdTe) thin films of thickness around 50 nm. These films are deposited at a rate of 0.1 nm/sec on well-cleaned glass substrates. The substrates are pre-cleaned using chromic acid, acetone and distilled water through the systematic mechanism. The thickness and the rate of deposition of thin films were recorded using microprocessor-the controlled quartz crystal thickness monitor during deposition of films. The error in thicknessof the film is 0.2 nm.

(ii) XRD characterization of CdTe films

The XRD analysis was done for CdTe thin films annealed at different temperature using XRD X'pert PRO, PANalytical for its structural, morphological. In this the visible peaks were matched to known peaks of crystal structures. We determined the directional cosines of the crystalline structure in the thin film.

(iii) THz generation Setup and analysis

The Out-put THz radiation is observed by using a home-built THz radiation generation setup which is shown in the Fig.1 below.

THz radiation of CdTe films were measured using 800 nm wavelength pulses of 35 fs duartion at 1 kHz repition rate obtained from Ti:Sapphire laser amplifier. The incidient laser power was attenuated with λ/2 waveplate attenuator. The beam was focussed by 25 cm focal length lens and film was placed at loosly focus point. The film was rotated vertically using rotator to align it for the maximum generation of THz radiation. The genarted THz radiation is the mixture of unconveretd 800 nm wavelength which was separated using Teflon filter and silicon palte . The generated THz power is measured using pyrodetector (gentec Made) at room tempertaure. The output of the detector was fed to the lock-in amplifier and strength of the genearted power is mesured using computer. For increasing the signal to noise ratio (S/N) the laser pulses were chopped with 22 Hz range.

The incident laser power at 800nm was varied from 150 to 300 mW range with an increment of 25mW. The experiment is repeated for thin films annealed at different temperature.

The output radiation is characterized as a function temperature and incident input power. The carrier concentration is calculated from the standardized material parameters as a function of temperature. The efficiency and intensity were plotted with respect to incident power at different annealed temperature.

3. Results and Discussion

3.1 Result

The X-ray diffraction (XRD) results of the CdTe thin film deposited on the glass substrate at different annealing temperature are shown in Fig. 2. A crystalline cubic structure (confirmed with JCPDS #071-4163 and # 071-4162) and Anorthic (triclinic) structure were also revealed (confirmed with JCPDS

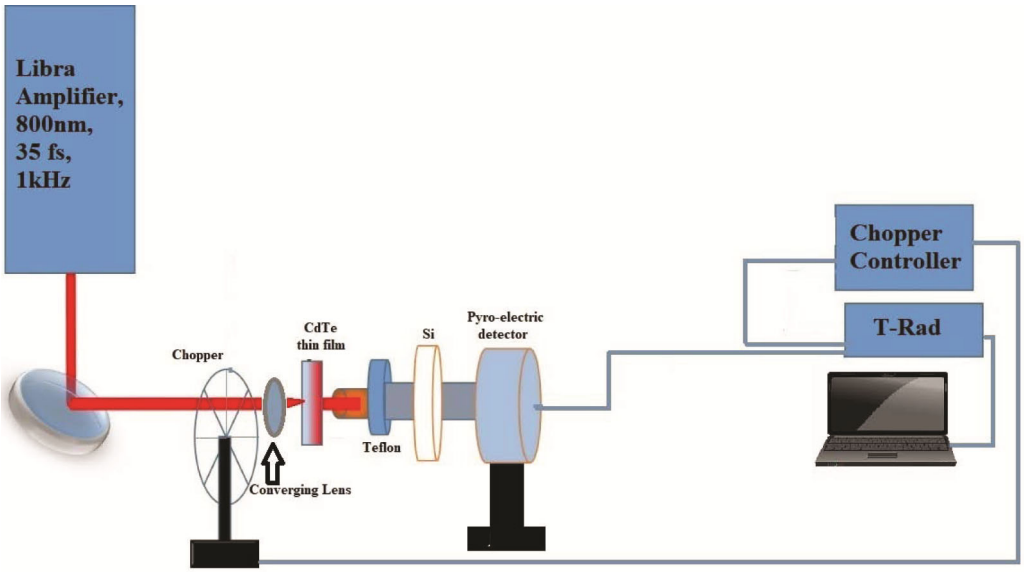

Fig. 1 — Schematic diagram Layout for THz generation and detection.

#055-0529). The 2θ values of 22.48°, 45.85° and 71.43° were matched with the cubic structure corresponding to (1 1 1), (3 1 1) and (4 2 2) index planes respectively. Peaks pointing at 22.43°, 32.88°, 45.85°, 55.65° and 71.41° correspond to the cubic structured index plane at (2 0 0), (2 2 0), (2 2 2) and (4 2 0) respectively. In addition, the peaks at 22.43° corresponds to dual crystalline phases *i.e.*, (111)/ (311) and (200)/220) index planes for cubic structures respectively. Fig. 2(d) shows the XRD graph of structured CdTe. The peaks at 27.94°, 32.90°, and 46.18° corresponds to the (2 0 1), (0 3 0), (1 4 2) planes for the crystal Anorthic (triclinic) structure. Overall, XRD graphs in Fig. 2(a) & (b) indicates that cubic phase. However, there were no peaks associated with the other compound of Cd or Te. In addition, the films exhibited a strong (1 1 1) plane peak, regardless of the thermal vacuum technique, which suggested that the CdTe crystallites had a cubic structure highly oriented with the (1 1 1) direction perpendicular to the glass substrate surface. Fig 1(a) & (b) show almost same peaks occurs but 300 °C show a mixed orientation (1 1 1) and (2 0 0) occurred. As the increase annealing temperature from 300 to 400 °C range, the intensity of the (1 1 1) peak get disappeared whereas at 300 °C two numbers of peaks appeared which clearly suggest the phase transition from cubic to anorthic (triclinic) structure. This indicates improvement of the crystallinity and/or increment of the degree of preferred orientation. Meanwhile, further increase of the Annealing temperature at 400°C resulted in smaller XRD peaks, indicating deterioration of the crystallinity.[23]

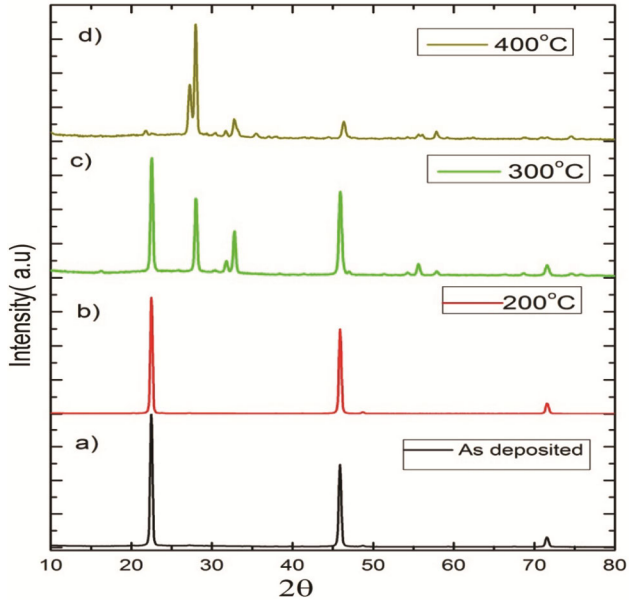

Fig. 2 — XRD pattern of the deposited CdTe thin film a) As-deposited b) 200 °C c) 300 °C d) 400 °C.

The carrier concentration was increased from $8*10^5$ to $8.013*10^{12}$ when annealed temperature is increased from 300K to 673 K. This indicates that carrier lifetime is getting decreased and more possibility of intra-band transitions.

The carrier concentrations are calculated using the standard equation. Which is given below:

$$n_i^2 = N_c N_v e^{\frac{-E_g}{k_B T}} \quad \ldots (3)$$

The intensity of the output THz radiation is increased with the increase in incident power. The drastic increase in the output power when the thin film is annealed at 200 °C is mainly due to increase in carrier concentration without any distortions in the film. The decrease in intensity after 200 °C is due to phase transitions from cubic to triclinic.

3.2 Discussion

Figure 2 shows that XRD spectra of CdTe films grown at different annealed temperature. This confirms the cubic structure in (1,1,1) between room temperature to 200 °C. But the phase started to transit from cubic (1,1,1) to triclinic phase (2,0,0) above 200 °C. This led to decrease the intensity of the THz generation for temperatures above than 200 °C.

Fig. 3 shows the increase in carrier concentration with respect to temperature. The curve shows exponential growth. This can be explained using Eq.No.3. The graph also shows a saturation behaviour at 400 °C temperature.

In addition, the observed optical energy band gap is located at approximately 1.5eV [26] which indicates the

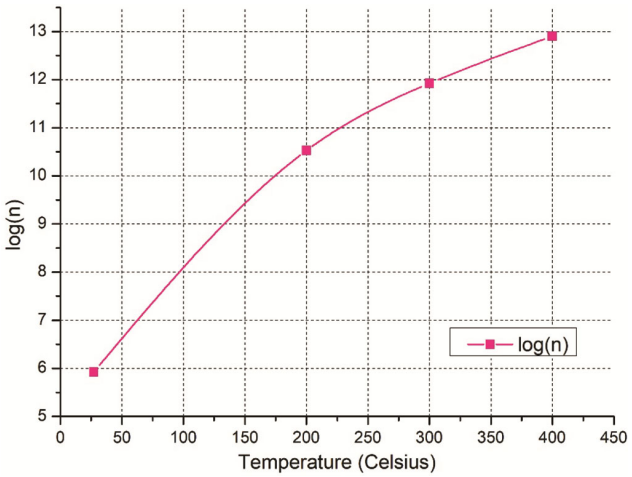

Fig. 3 — Shows the log (carrier concentration) *vs* temperature.

shift of Fermi energy level and also influenced the process of THz generation due to ultrafast transition. The increase in carrier concentration with respect to the temperature of annealed CdTe films resulted in enhancement of THz intensity. Fig.4 shows the intensity of generated THz radiation with respect to the incident power of femtoseconds pump laser beam. The intensity of generated signal was increased from 254.8nW/cm^2 to 1082.8nW/cm^2 at 200 ^{o}C annealed sample which is almost 3.7 times higher than the room temperature grown CdTe.

It is also shown in Fig. 5 that the efficiency of the generated THz signal is decreasing with respect to increase in the incident laser power below the temperature of 200 ^{o}C and showing a Gaussian behaviour above 200 ^{o}C. The decrease in efficiency is mainly caused due to formation of plasmons. The formation of plasmonic states is responsible for change in refractive index of the medium which also reduces the transmittance of the thin film. The phase transition above 200 ^{o}C also attributed to anomaly behaviour of efficiency of the thin film. It is also due to change of transmission behaviour *i.e.* drop in the transmission to change in the temperature due to high laser power density.

We have shown the role of symmetry in generating THz involving photo-dember effect in the CdTe thin-films annealed at different temperatures. The phase change after 200 ^{o}C from cubical to triclinic is losing the Centro-symmetry making the contribution of χ^3 less. This in turn reduces the power of recorded THz signal.

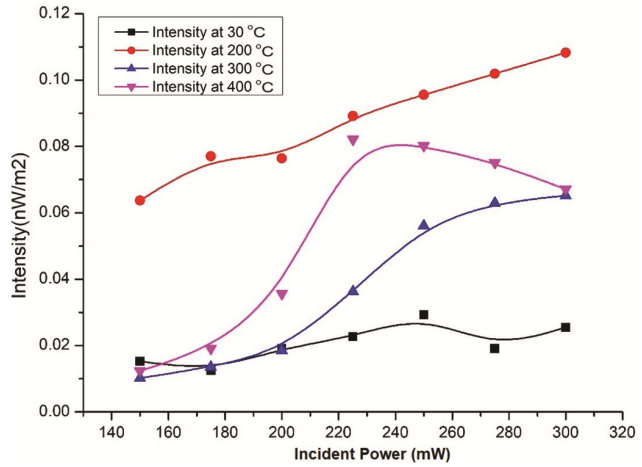

Fig. 4 — Depicts the variation of Intensity of THz radiation with incident power at different annealed temperatures.

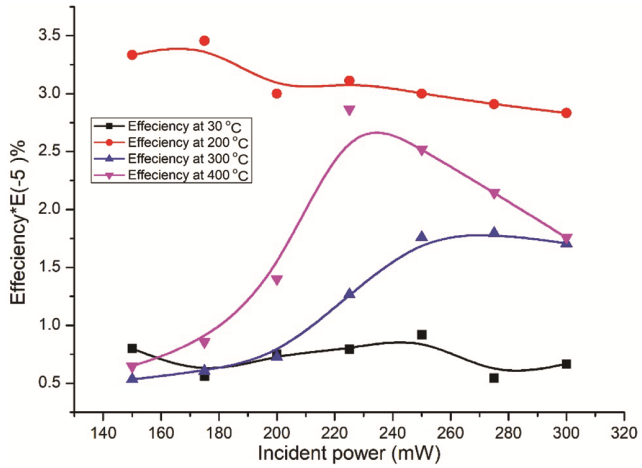

Fig. 5 — Shows the variation of Efficiency of the generated THz radiation with respect to the incident laser power at different annealed temperatures.

4 Conclusions

We have successfully deposited CdTe films using CVD technique and annealed them at different temperatures up to 400 ^{o}C. The XRD analysis proves that there is a change in phase of the thin film beyond 200 ^{o}C from cubic [mostly (1,1,1)] to triclinic [mostly (2,0,0)]. The intensity of the THz radiation is increased by 1.7 times with increase in incident power at as deposited temperature and at 200 ^{o}C The intensity of THz signal is showing Gaussian like behaviour for temperature above 200 ^{o}C, with increase in incident power. The change is crystal structure after 200 ^{o}C reduced the intensity of THz radiation compared to the lesser temperatures. The efficiency of the CdTe thin film is increased by 4.31 times when annealed at 200 ^{o}C than at room temperature. Above the temperature 200 ^{o}C efficiency is decreased. At all temperatures the efficiency of generation of THz radiation is decreased with increase in incident power. This may be attributed to formation irradiative phonon and plasmonic states in the film due to highly focused laser beam.

Acknowledgements

The authors would like to express their thanks to the funding agency Defence Research and Development Organization (DRDO), Ministry of Defence, Govt. of India for financial support under the grant No. DRDO/18/1801/2016/01038: ACRHEM-Phase-III and Dr. D. Ganesh for assistance during the experiment of THz generation.

Conflicts of Interest

Declare conflicts of interest or state “The authors declare no conflict of interest.”

References

1 Z Tang, N A Kotov & M Giersig, *Science*, 297 (2002) 237.
2 Ma C & Wang Z L, *Adv Mater*, 17 (2005) 323.
3 Kar S, Satpati B, Satyam P V & Chaudhuri S, *J Phys Chem B*, 109 (2005) 19134.
4 Zhao T, Fang X, Li L, Bando Y & Golberg D, *Nanoscale*, 2 (2010) 168.
5 Duan X, Huang Y, Agarwal R, Lieber C M C M & Fast C G, *Nature*, 421 (2003) 241.
6 Cola A & Farella I, *Appl Phys Lett*, 102 (2013), 113502.
7 Singh V P, Ericson O M & Chao J H, *J Appl Phys*, 78 (1995) 4538.
8 Chen M C & Bevan M J, *J Appl Phys*, 78 (1995) 4787.
9 Solanki C S, Solar Photovoltaics, Fundamentals and Applications (PHI Learning, 2009).
10 Sinha S, Chatterjee S K, Ghosh J & Meikap A K, *J Appl Phys*, 113 (2013) 123704.
11 Paudel N R, Wieland K A & Compaan A D, *Sol Energy Mater Sol Cells*, 105 (2012) 109.
12 Chu T L, Chu S S, Pauleau Y, Murthy K, Stokes E D & Russell P E, *J Appl Phys*, 54 (1983) 398.
13 Segui Y, Carrere F & Bui A, *Thin Solid Films*, 92 (1982) 303.
14 Moss T S, Optical properties of semiconductors, Butterworths, London, (1957).
15 Kasmorski L L, Cooper R B, White F R & Merrill A J, *IEEE Trans Electron Devices*, 24 (1977) 496.
16 Pankove J I, Optical processes in semiconductors (Dover Publisher Inc, New York, (1971).
17 Bach H & Krause D, Thin Films on Glass, Springer – Verlag Berlin, Heidelberg, (1997).
18 Sbastian P J & Sivaramakrishnan V, J Appl Phys, 65 (1989) 237.
19 Zhang X C, Jingzhou X, Introduction of THz wave photonics, (Spienger).
20 Dalapati P, Manik N B & Basu A N, *J Semiconduct*, 34 (2013).
21 Sze S M & Kwok K N, Physics of Semi-conductor devices, 3rd Edn, by Wiley (2003).
22 Kumari Archana, Chaudhary A K & Venkatesh M, *Appl Opt*, 59 (2020) 3417.
23 Mahendar M, Chaudhary A K, Damrala G & Gupta V, Workshop in Recent Advances in Photonics 2019 (2019) 1.
24 Shen Y R, The principle of Nonlinear Optics, Wiley-Interscience: New York, 1984.
25 Zhu L G, Kubera B & Mak F K, *Sci Rep*, 5 (2015) 10308.
26 Strauss A J, *Rev Phys Appl*, 12 (1977) 167.

Evaluation of cadmium telluride (CdTe) thin films grown at different annealing temperatures for efficient terahertz generation

M.Mahendar[(1)], A.K. Chaudhary[(1*)], Ganesh Damarla[(1)], and Vinay Gupta [(2)]

(1) Advanced Centre of Research in High Energy Materials, University of Hyderabad, Hyderabad 500046, India

(2) Dept. of Physics, University of Delhi, Delhi, India.

Corresponding authors e-mail: akcphys@gmail.com, anilphys@yahoo.com

***Abstract*— The paper reports the terahertz generation from polycrystalline CdTe thin films using 800 nm wavelength of 35 fs pulse duration at 1 kHz repetition rate obtained from Ti: sapphire laser amplifier. These films were deposited by thermal evaporation on a glass substrate and annealed at 200 and 300°C. The structural was investigated by XRD technique. Absorbance and transmittance were recorded in the wavelength (300- 800 nm). Optical studies showed that the optical energy gap decreases with increasing annealing temperatures. The results show that the film annealed at 200°C shows the highest generation of the order of 88 nW.**

Keywords— Cadmium Telluride (CdTe), XRD, Structural and Optical Properties, Terahertz generation

Introduction:

Far past two decades the field of terahertz generation and detection technology has been got much attention due to its potential applications in the field of homeland security, defence, etc. Since it possesses very low energy and has deep penetration ability from the organic and packing materials including cloths and semiconductors etc. Therefore, it is preferred over X-rays due to non-ionizing nature [1-3].

T-rays can be successfully generated from various types of optical and metallic materials available in the form of crystal, wafer and thin films. Some popular inorganic semiconductor and organic nonlinear crystals such as ZnTe, GaAs, CdTe, DAST, etc. are being used due to their higher nonlinear coefficients and good transmission in optical and THz domain along with with high or moderate damage threshold [4-6]. Since it is a direct bandgap semiconductor with the high atomic number and electron density, therefore, widely used in photovoltaic, sensors, diodes, rectifiers, and detectors. However, the generation of powerful THz generation by means of a simple experimental arrangement is still a challenging task and need a rigorous investigation of new materials in the form of film or crystals [7-10].

In the present study, we have evaluated the CdTe thin films annealed between 200-300°C temperature ranges for efficient THz generation using femtosecond laser. The generated THz signal is attributed to the transient surface surge current under the influence of ultra-short optical pulses and directly related to the structural and optical properties of the films. We also believe that the process of annealing of CdTe films modified the structure as well as the optical and band gaps, which help to generate the short lifetime surface charge current under the influence of femtosecond's laser pulses.

EXPERIMENTAL PROCEDURE:

Thin Cadmium Telluride films were prepared by a thermal evaporation method using vacuum evaporation (HINDHIVAC Vacuum coating unit, Model No: 12A4U), in high vacuum (10^{-6} Torr) on glass substrates. The solid form of Cadmium (Cd) and Tellurium (Te) with purity (99.999 %) was used as source material. Glass substrates were cleaned by a cleaning solution, rinsed in distilled water than pure alcohol in an ultrasonic cleaner. The deposition rate was 0.1 nm /min and the thickness of the films was fixed at as 50 nm. These samples were annealed at 200 °C and 300 °C temperatures and subjected to the XRD, UV-Visible spectrophotometer (Shimadzu-2600) for its structural and optical characterizations. Samples were subjected for THz generation using femtosecond laser as shown in Fig. 4. We have evaluated the potential of The efficiency of generated THz radiation of CdTe films were measured using 800 nm wavelength pulses of 35 fs duration at 1 kHz repetition rate obtained from Ti: Sapphire laser amplifier.

Results and Discussions:

Structural properties of the films were investigated by X-ray diffraction technique. The grain size (D) was calculated using the Debye-Scherrer equation (1) [11]

$$D = k\lambda/\beta \cos\theta \quad (1)$$

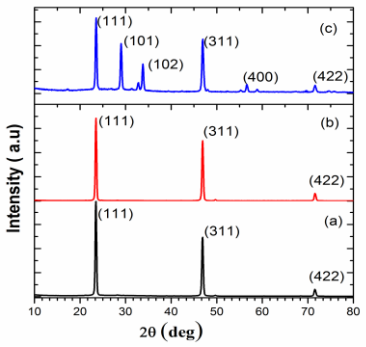

Figure 1 X-ray diffraction pattern of CdTe film annealed at a different temperature a) As Deposited b) 200°C c) 300°C.

XRD analysis data were obtained using a Philips X' pert pro diffract meter with Cu-Kα excitation wavelength of 1.54 Å. Figure 1(a) and 1(b) shows the X-ray diffraction patterns of as-deposited and annealed at 200°C for 30 minutes. The CdTe films were cubic Zinc blende structure and the main diffraction peak at 2θ = 23.47° which corresponds to preferred orientation along (111) plane. There are some weak reflections from the (311) and (422) planes. After annealing at 200°C for 30 minutes, the intensity of (111) peak decreased accompanying with an increase in (311) and (422) peaks observed a decrease in the intensity may be due to the change in stoichiometry These peaks correspond to the JCPDS (15-0770) data of cubic CdTe. However, in all the cases the intensities of the (311), (422) peaks are extremely low in comparison with the (111) peak, which indicates a preferential orientation of the crystallites in the (111) direction perpendicular to the substrate [12]. Fig.1(c) shows the x-ray diffraction pattern of CdTe film annealed at 300°C for durations of time 1 hrs. The corresponding peak at 2θ =23.49° belongs to the (111) plane of cubic and hexagonal phase overlap the presence of mixed phases cannot be ruled out. Hexagonal peaks corresponding (101), (102), and (400). This represents that randomness of the film increases which was revealed by a decrease in intensity of (111) and other peaks forms (101) (102) and (400) along with a decrease in average grain size at 300°C.shown in Table 1.

Table 1. Structural and Optical parameters of annealed CdTe thin film

Annealing temp[°C]	Grain Size [nm]	Bandgap [E_g][eV]
As Deposited	22.74	1.35
200°C	23.42	1.33
300°C	21.60	1.31

Optical Properties:

The optical transmittance and Absorbance of CdTe films with 50 nm thickness on glass substrates were measured by spectrophotometer. Figure 2(b) show the Absorbance spectra of the as-deposited films shows minimum absorption but broad peaks appearing around 470 to 540 nm are attributed to free carrier and Increasing Annealed temperature at 200°C shows the high absorption but same region appears in the broad peak. It is a clear cut indication of a shift in the optical band gap as well as the surface quality of the films. Annealed at 300°C temperature shows an exponential drop in absorption after crossing 400 nm wavelength. Fig. 2(a) shows the transmission behaviours of the CdTe films. It also reveals that CdTe films as-deposited have very low transmission i.e. 7% only while annealing at 200°C increases the level up to 15% and at 300°C it almost becomes 25%.

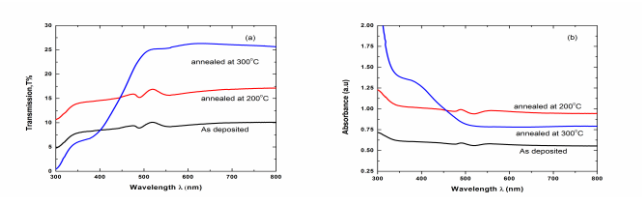

Figure 2. 2(a),2(b) Transmission, Absorbance Vs wavelength of CdTe of annealed at different temperatures a) As deposited b) 200 °C c) 300°C

Tauce has proposed as a mathematical equation to present the relationship between the optical energy gap and the energy of the incident photon [13]:

$$(\alpha h\upsilon)^2 \; \alpha \; (h\upsilon - E_g) \qquad (2)$$

Where hα is the optical absorption coefficient, A is a constant, hυ is the energy of the incident photon, E_g is the optical band gap and n is an index Which could take different values according to the electronic transition. The characteristics of $(\alpha h\upsilon)^2$ versus $(h\upsilon)$ were plotted for evaluating the bandgap (E_g) of the CdTe thin films, and extrapolating the linear portion near the onset of absorption edge to the energy axis as shown in figures 3(a), (b), (c) shows the value of E_g before and after annealing, it can be noticed that the value of the optical energy gap decrease as the annealing temperature increase, this could be attributed to the fact that an increase in annealing temperature at 200 and 300°C leads to minimizing structural imperfections. The grain size increases with annealing temperature, which decreases the bandgap and enhances the optical property of the film. Decrease of band gap with annealing temperature average grain size with annealing temperatures [14-15].

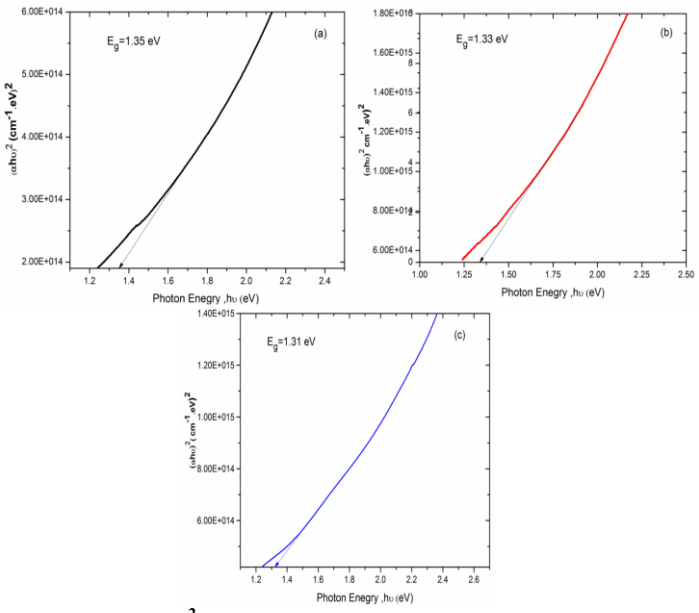

Figure 3 $(\alpha h\upsilon)^2$ Vs (hυ) for CdTe thin films annealed at a different temperature a) As-deposited (b)200°C (c) 300°C.

Terahertz generation:

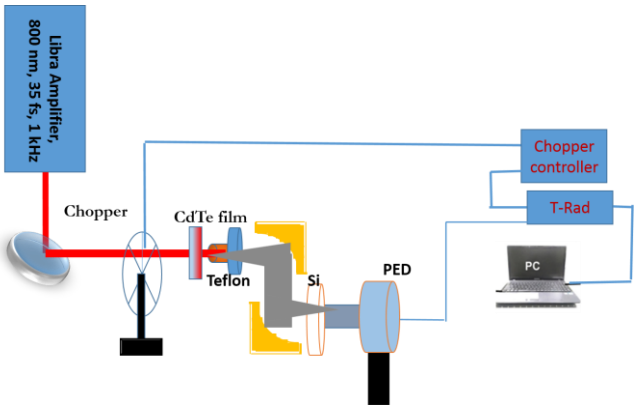

Figure 4.Experimental setup for THz generation and detection

Fig.4. Shows the curve between incident laser power vs the strength of the generated THz radiation in nW. It is interesting to note that maximum generated signal from the as-grown film is 20 nW while film annealed at 200°C is able to enhance the strength of the generated signal of the order of 88nW which is almost 4.4 times of the as-grown signal. The corresponding efficiency of the generated signal efficiency is of the order of 2.93 x10-5 %. Which is even comparable with the efficiency of the many nonlinear crystals such as BNA crystal grown from ethanol: methanol solution. The nature of the curve shows the possibility of further enhancement in the THz signal. But THz signals at 300°C is lower than the 200°C annealed films. It confirms two important aspects of the temperature (i) modification of the crystalline structure (ii) change in the optical absorption *and* bandgap properties of CdTe films. In addition, direct demonstration of THz signal from CdTe film under the measurable limit is attributed to the introduction of nonlinear absorption mechanisms in CdTe films. This is a clear-cut demonstration of surface phenomena and known as surface surge current effect. Since contribution due to optical rectification, the effect is more dominant in transmission mode, therefore, the possibility of OR effect is quite weak. It also shows the future potential of CdTe film as compared to other types of ferroelectric metallic films like Ni and other materials.

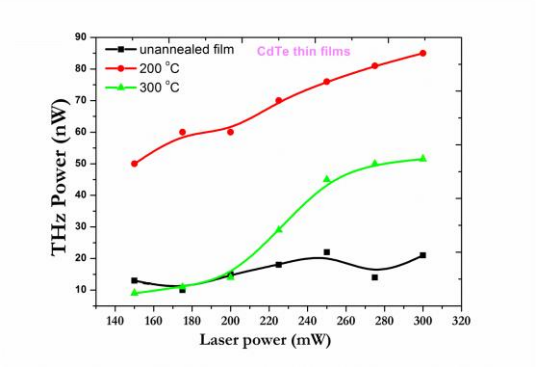

Figure 5: Laser power Vs THz Power for CdTe thin films different annealing temperature unannealed at 200°C 300°C.

Conclusions: In the present study, successfully generated the efficient THz radiation and investigated the effects of annealing temperature on the structural and optical properties of CdTe thin films deposited on glass substrates using thermal evaporation technique. From the XRD analysis and the cubic phase of the (1 1 1) direction perpendicular to the substrate surface became more dominant as the annealing temperature increased. It can be noticed that the value of the optical energy gap decrease as the annealing temperature increase, this could be attributed to the fact that an increase in annealing temperature at 200 and 300°C leads to minimizing structural imperfections. The CdTe film grown at room temperature generates weak THz radiation of the order of 20 nW at 300 mW incident power of laser .whereas film annealed at 200°C shows the highest generation of the order of 88nW at the same power, which is almost 4.4 times higher than the as-deposited film. The highest conversion efficiency of the generated THz signal is of the order of 2.93×10^{-5} % that can even be compared with the efficiency of the BNA crystal grown from an ethanol methanol solution.

ACKNOWLEDGEMENT :

The authors gratefully acknowledge the financial support provided by the DRDO, Ministry of Defence, and Govt. of India under ACRHEM Phase-III No.ERIP/ER/1501138/M/01/319/D(R&D).

REFERENCES

[1] 1.M. Tonouchi, Nat. Photonics 1 (2007)97–105

[2] 2. D. J. Funk, F. Calgaro, R. D. Averitt, M. L. T. Asaki, and A. J. Taylor, Appl. Spectrosc. 58 (2004) 428–431.

[3] J. A. Zeitler, K. Kogermann, J. Rantanen, T. Rades, P. F. Taday, M. Pepper, J. Aaltonen, and C. J. Strachan, Int. J. Pharm. 334(1-2) (2007) 78-84.

[4] G. Damarala, M. Venkatesh and A.K. Chaudhary,Applied Optics, 29, (2018) 8743 -8750.

[5] A. G. Davies, A. D. Burnett, W. Fan, E. H. Linfield, and J. E. Cunningham, Mater. Today 11 1(2008) 8–26.

[6] M. Venkatesh, K.S. Rao, T.S. Abhilash, S.P. Tewari, A.K. Chaudhary, Opt. Mater. 36 (2014) 596-601. doi:10.1016/j.optmat.2013.10.021.7.

[7] Ttreatment on the composition and semiconductivity of electrochemically deposited CdTe films J. Appl. Phys. 54, 398 (1983).

[8] Y. Segui, F. Carrere, A. Bui, Thin Solid Films 92, 303–310 (1982)

[9] 20. T.S. Moss, Optical properties of Semiconductors (Butterworths, London, 1957).

[10] The structure and optical properties of Cd1-x MnxTe thin films IEEE Trans. Electron Devices 24, 496 (1977).

[11] Eric Lifshin, X-ray Characterization of Materials, Wiley-VCH, NY, (1999) 37.

[12] B.Qi, D. Kim, D.L. williamson, J.U. Trefny, J. Electrochem. Soc. 143 (1996) 517.

[13] S. M. Alnaimi and M. N. Al. Dileamy, Determination of the Optical Constant of Cadmium Stannate Film, International Journal of Pure and Applied Physics, Vol.3(1), p. 30, (2007)

[14] .S. Deivanayaki, P; Jayamurugan, R. Mariappan, V. Ponnuswamy, Chalcogenide. Letters 7-3(2010) 159-163.

[15] J.J. Pankove, Optical Processes in Semiconductors, Prentice-Hall, Englewood Cliffs, NJ, 1971.

Study of nucleotides using Terahertz Time Domain Spectroscopy

M.Mahendar[(1)(2)], P.Naveen Kumar[(1)], A.K. Chaudhary[(1)*], SK.Ramiz Islam[(2)(3)], SoumenKanti Manna[(2)(3)]

(1) -Advanced Centre of Research in High Energy Materials, University of Hyderabad, Hyderabad 500046, India

(2)-Biophysics & Structural Genomics Division, Saha Institute of Nuclear Physics, Kolkata, 700 064, India.

(3)-HomiBhabha National Institute, Anushaktinagar, Mumbai, Maharashtra 400094

*1*Corresponding authors e-mail: akcphys@gmail.com, anilphys@yahoo.com*

Abstract:

We present the terahertz (THz) time-domain spectroscopy based study of ribo- and deoxyribonucleosides constituting RNA and DNA in an aqueous solution. These play pivotal roles in the biological information cascade and functioning of the cell. Terahertz spectroscopy is used to examine the low-frequency collective vibrational modes of the given molecules. THz fingerprint spectra of DNA and RNA molecules isolated from the cells could provide crucial information about the constituents and conformations. In addition, we also ascertained the interesting optical properties such as refractive index, absorption spectra, and extinction coefficients of these molecules in the spectral range of 0.1-2.0 THz.

Keywords—: DNA, RNA, Bases, Nucleosides, THz, R.I. Absorption Coefficients

Introduction: The recent development of THz technology has paved the way for its applications in the fields of medicine and biology[1,3]**.** The spectral range between 0.1-10 THz (3.3 cm^{-1}–333 cm^{-1}) is an important region for low-frequency dielectric relaxation and vibrational spectroscopy of liquids, such as water, methanol, ethanol, propanol, etc. [4,5].THz-Time domain Spectroscopy in combination with density functional theory (DFT) [6,12], can be used to study amino acids [13,18] and peptides [19,20] drugs and explosives [21-23].THz spectroscopy-based data analysis and characterization of molecules can enable us to investigate and interpret complex biochemical processes and be useful as a tool for medical diagnostics at the cellular and molecular levels.

The optical properties of macromolecules in the THz spectral range are due to the low-frequency vibration modes of large atomic groups present in the molecule. Such vibrational modes are sensitive to the intermolecular structure owing to their collective nature and allow the analysis of conformational states. The low-frequency vibrational modes play vital roles in biochemical reactions. The specificity of the THz spectra to various conformers and isomers of the substances under study has been reported by several groups. In addition, the THz absorption bands can be sensitive to mutations and the environment.

The application of THz spectroscopy in the study of Nucleo-bases, which are nitrogen-containing biological compounds remains limited. Their conjugates with ribose or deoxyribose sugar are known as ribo or deoxyribonucleoside, which can be phosphorylated to form corresponding nucleotides that polymerize to form RNA or DNA, respectively. Five nitrogenous bases are found in the biological system: Adenine (A), Guanine (G), Thymine (T), Cytosine (C), and Uracil (U). They form corresponding nucleosides Adenosine, Guanosine, Thymidine, Cytidine, and Uridine. Deoxynucleotides polymerize to form deoxyribonucleic acid (DNA) and ribonucleotides form ribonucleic acid (RNA).DNA contains A, T, G, and C, and RNA contains A, U, G, and C. Nucleic acid molecules serve as genetic material in biological organisms. THz techniques on hybridized DNA molecules have been performed in the past, but few experiments have addressed the binding state[24]. The importance of the refractive index of DNA molecules was highlighted by Brucherseifer and Nagel et al., who used the far-infrared absorption and index of refraction of a DNA sample to identify its hybridization state[25-26].

Chemical modification of these nitrogenous bases can modify the nature of information flow and thereby change the functional status of the cell. These modifications are highly regulated through a dedicated set of enzymes. These modifications have been reported in several diseases like diabetes, cardiovascular disease, neurodegenerative disease, cancers, etc. Several studies have also shown their prognostic and diagnostic values. Therefore, direct monitoring of the nucleobases and their chemical modification holds tremendous interest in the field of biochemistry. The commercially available authentic standards for modified bases, nucleosides, and nucleotides will be analyzed for orthogonal signatures, sensitivity, and dynamic range in an aqueous solution. Pure RNA and DNA-modified and unmodified oligos will be used to check the ability to identify/quantify modifications from intact oligos.

Experimental setup:

Terahertz time-domain spectroscopy (THz-TDS) experiment was carried out in reflection geometry by using the self-reference method [6]. THz-time domain system (TeraFlash-Toptica photonics, Germany) was used, which consists of an optical fiber coupled femtosecond laser and InGaAs/InAlAs photoconductive antennas for THz generation and detection. The femtosecond fiber-coupled laser was of 1.5 µm central wavelength with a repetition rate of 100 MHz, and the average output power was 80mW. Each of the molecules was purchased from Sigma-Aldrich (Germany) in the purest possible form and used without further purification or recrystallization. A 10 mg molecule powder from was mixed in 5ml of distilled water and sonicated for 15 min for a uniform sample mixture in aqueous media. A quartz plate of 2mm thickness was used as the reference material, and the reference signal was measured. The liquid sample was deposited on the quartz plate, and time-domain spectra were recorded, as shown in Fig 1. The complex refractive index ($\tilde{n} = n + ik$) of the liquid sample was calculated using the Eqn-1 as given below. The real part represents the refractive index(n), and the imaginary part represents the extinction coefficient (k).

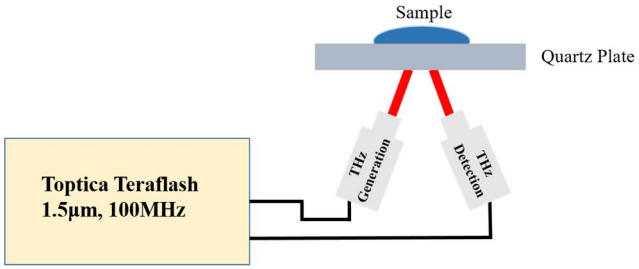

Fig 1: Schematic of the experimental setup

$$\tilde{n}(\omega) = \frac{\sqrt{n_q^2(1-\hat{r}_{qs})^2 + 4\hat{r}_{qs}\sin\theta^2}}{1+\hat{r}_{qs}} \qquad (1)$$

Where n_q is the refractive index of quartz, r_{qs} is the reflectance from the quartz-sample interface, and θ is the angle of incidence of THz radiation. The absorption coefficient α(ω) in cm^{-1} is related to the extinction coefficient k(ω) shown in Eqn- (2)

$$\alpha(\omega)=4\pi\upsilon k(\omega)/c \qquad (2)$$

Where 'c' is the velocity of light, 'υ is the frequency in the THz region

Results and Discussion:

The Time-domain spectra measured from different molecules are shown in Fig 1. The first peak represents the reflection of the THz signal from the air-quartz surface, and the second peak represents the reflection from the quartz-sample surface. The fast Fourier transform (FFT) of the time domain signal yields frequency domain spectra of these samples between 0.1 to 2 THz range, as shown in Fig 2.

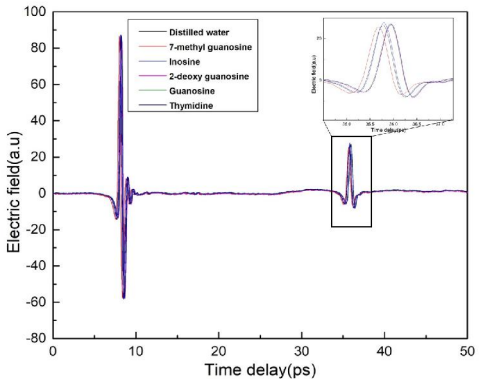

Fig 1: THz time-domain spectra of ribo & deoxyribonucleosides in aqueous solution.

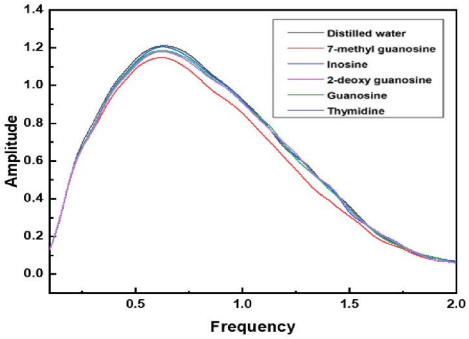

Fig 2: Shows frequency domain spectra of ribo & deoxyribonucleosides.

Optical parameters such as refractive index and absorption coefficients were measured and shown in Fig 3. The refractive index of the pure distilled water was measured and was found to vary from 3.5 and 2 between 0.1 to 2 THz range. Similarly, the refractive index of molecules mixed in water was also recorded and observed with similar types of change with some lower values of R.I. from 3.2 to 2 between 0.1 to 2.0 THz range. It is to be noted that each molecule has a distinct refractive index in the terahertz region and shows some characteristic variation at the 1.25 THz frequency range. The measured absorption spectra of molecules follow a similar pattern to water absorption spectra between the 0.1 to 1 THz range and the measurement at room temperature confirmed the presence of strong vibrational features observed in absorption spectra of ribo and deoxyribonucleoside molecules between the

1.0 to 2.0 THz range, as shown in Fig 4. The extinction coefficients were also measured, varying from 2.0 to 0.5 between 0.1 to 2.0 THz frequency range, as shown in Fig 4.

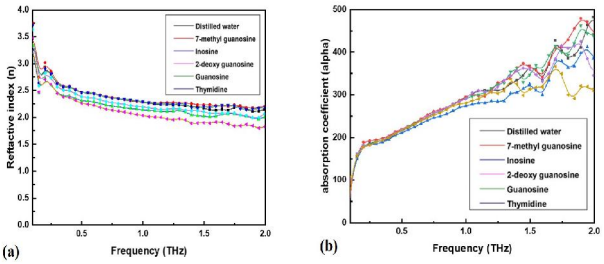

Fig 3: a) Refractive index of ribo & deoxyribonucleosides.
b) Absorption spectra of ribo & deoxyribonucleosides.

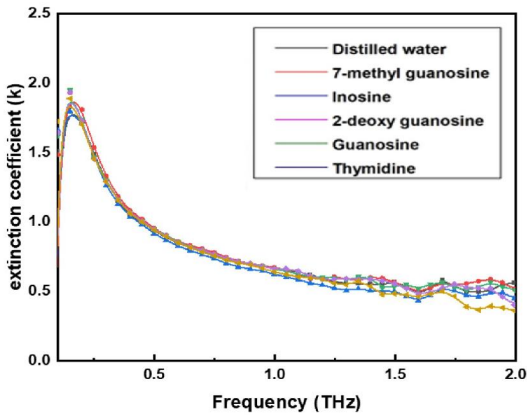

Fig 4: THz Extinction coefficient of ribo & deoxyribonucleosides.

Conclusions:

In the present work, we successfully recorded the distinguished spectral features of the ribo- and deoxyribonucleosides using the THz-TDS technique. Based on obtained experimental results and analysis, it is inferred that each molecule has a distinct absorption coefficient, refractive index, and extinction coefficient between 0.1 to 2.0 THz range. Terahertz spectroscopy requires only a small quantity of molecules to determine their characteristic optical properties, which may yield greater benefits, particularly as a probe for recording molecular dynamics, including the constituents and behaviors of DNA and RNA.

ACKNOWLEDGMENT:

The authors gratefully acknowledge the financial support provided by the DRDO, Ministry of Defence, and Govt. of India under ACRHEM Phase-III No.ERIP/ER/1501138/M/01/319/D(R&D).

REFERENCES

[1] B. M. Fischer, Phys. Med. Biol. 47, 3807 (2002)

[2] M. Semenov, T. Bolbukh, and V. Maleev, J. Mol. Struct. 408/409, 213 (1997).

[3] A. Rahman, B. Stanley, and A. K. Rahman, Proc. SPIE—Int. Soc. Opt. Eng. 7568, 756810 (2010)

[4] J. T. Kindt and C. A. Schmuttenmaer, J. Phys. Chem. 100, 10373 (1996).

[5] B. Reinhard, K. M. Schmitt, V. Wollrab, J. Neu, R. Beigang, and M. Rahm, Appl. Phys. Lett. 100, 221101 (2012).

[6] Jepsen, P. U., Cooke, D., & Koch, M. Laser & Photonics Reviews, 5(1), 124-166.

[7] R. M. Dreizler and E. K. U. Gross, Density Functional Theory an Approach to the Quantum Many-Body Problem (Springer, 1990).

[8] M. Orio, D. A. Pantazis, and F. Neese, Photosynth. Res. 102, 443 (2009).

[9] D. G. Allis, A. M. Fedor, T. M. Korter, J. E. Bjarnason, and E. R. Brown, Chem. Phys. Lett. 440, 203 (2007).

[10] T. M. Korter, R. Balu, M. B. Campbell, M. C. Beard, S. K. Gregurick, and E. J. Heilweil, Chem. Phys. Lett. 418, 65 (2006)

[11] M. D. King, W. D. Buchanan, and T. M. Korter, Anal. Chem. 83, 3786 (2011)

[12] D. G. Allis, D. A. Prokhorova, and T. M. Korter, J. Phys. Chem. A 110, 1951 (2006).

[13] M. D. King, P. M. Hakey, and T. M. Korter, J. Phys. Chem. A 114, 2945 (2010)

[14] B. Yu, F. Zeng, Y. Yang, Q. Xing, A. Chechin, X. Xin, I. Zeylikovich, and R. R. Alfano, Biophys. J. 86, 1649 (2004).

[15] J. Neu, C. T. Nemes, K. P. Regan, M. R. Williams, and C. A. Schmuttenmaer, Phys. Chem. Chem. Phys. 20, 276 (2018).

[16] J. Neu, H. Nikonow, and C. A. Schmuttenmaer, J. Phys. Chem. A 122, 5978–5982 (2018).

[17] M. R. C. Williams, A. B. True, A. F. Izmaylov, T. A. French, K. Schroeck, and C. A. Schmuttenmaer, Phys. Chem. Chem. Phys. 13, 11719 (2011).

[18] M. R. C. Williams, D. J. Aschaffenburg, B. K. Ofori-Okai, and C. A. Schmuttenmaer, J. Phys. Chem. B 117, 10444 (2013).

[19] M. Yamaguchi, K. Yamamoto, M. Tani, and M. Hangyo, in 2005 Joint 30th International Conference on Infrared and Millimeter Waves and 13th International Conference on Terahertz Electronics (IEEE, 2005), Vol. 2, pp. 477–478.

[20] M. Yamaguchi, K. Yamamoto, M. Tani, and M. Hangyo, in Infrared and Millimeter Waves, Conference Digest of the 2004 Joint 29th International Conference on 2004 and 12th International Conference on Terahertz Electronics, 2004 (IEEE, 2004), pp. 779–780.

[21] M. Lu, J. Shen, N. Li, Y. Zhang, C. Zhang, L. Liang, and X. Xu, J. Appl. Phys. 100, 103104 (2006).

[22] D Ganesh, E Narsimha Rao, M Venkatesh, K Nagarjuna,ACS omega 5 (6), 2541-2551(2020)

[23] R Koala, N Periketi, C Ghorui, S Mangali, AK Chaudhary, Journal of Molecular Structure, 1265 133449(2022)

[24] H. Urabe, and Y. Tominaga, J. Phys. Soc. Jpn. 50, 3543-3543 (1981).

[25] Brucherseifer M, Nagel M, Haring Bolivar P, Kurz H, Bosserhoff A and Buttner R 2000 ¨ Appl. Phys. Lett.77 4049.

[26] Nagel M, Haring Bolivar P, Brucherseifer M, Kurz H, Bosserhoff A and Buttner R 2002 ¨ Appl. Phys. Lett.80 154.

Development and Evaluation of Some Semi-Metallic Oxide (TeO2) and Semiconductor (CdTe) Films on Different Substrates for THz Device Applications

by Mahendar M

27.12.2022

Submission date: 26-Dec-2022 12:24PM (UTC+0530)
Submission ID: 1986649251
File name: Te_Films_on_Different_Substrates_for_THz_Device_Applications.pdf (4.38M)
Word count: 23397
Character count: 124255

Dr. Anil Kr. Chaudhary
Professor (Physics)
Advanced Centre of Research in
High Energy Materials (ACRHEM),
UNIVERSITY OF HYDERABAD
HYDERABAD-500 046. T.S. INDIA.

Similarity Screening Done @ IGM Library

Librarian / DL / AL
IGM Library (UOH)

Development and Evaluation of Some Semi-Metallic Oxide (TeO2) and Semiconductor (CdTe) Films on Different Substrates for THz Device Applications

ORIGINALITY REPORT

18%	10%	11%	4%
SIMILARITY INDEX	INTERNET SOURCES	PUBLICATIONS	STUDENT PAPERS

PRIMARY SOURCES

1	M. Mahendar, A. K. Chaudhary, Ganesh Damarla, Vinay Gupta. "Evaluation of cadmium telluride (CdTe) thin films grown at different annealing temperatures for efficient terahertz generation", 2019 Workshop on Recent Advances in Photonics (WRAP), 2019 Publication	7%
2	nopr.niscair.res.in Internet Source	4%
3	Submitted to University of Hyderabad, Hyderabad Student Paper	2%
4	ro.uow.edu.au Internet Source	1%
5	Chandan Ghorui, Kidavu V Arjun, P Naveen Kumar, Subhasis Das, Anil K Chaudhary, Yuri Andreev. "Comparative studies of terahertz-based optical properties in transmission/ reflection modes of GaSe: S and	1%

Similarity Screening Done @ IGM Library
Sub ID: 1986649251
Sub date: 26-12-2022
Librarian / DL / AL
IGM Library (UOH)

This to certify that out of 18% Similarity index the student has contribution from source 1 and 2 i.e. 11%. Therefore total index is 18-11 = 7% only

Dr. Anil Kr. Chaudhary
Professor (Physics)
Advanced Centre of Research in High Energy Materials (ACRHEM),
UNIVERSITY OF HYDERABAD
HYDERABAD-500 046. T.S. INDIA.

27.12.2022

measurement of its scattering losses due to surface roughness for efficient terahertz generation", Physica Scripta, 2022
Publication

6	docs9.chomikuj.pl Internet Source	<1 %
7	www.davidpublisher.com Internet Source	<1 %
8	worldwidescience.org Internet Source	<1 %
9	Namrata Dewan, K. Sreenivas, Vinay Gupta. "Properties of crystalline y-TeO2 thin film", Journal of Crystal Growth, 2007 Publication	<1 %
10	jih.uobaghdad.edu.iq Internet Source	<1 %
11	pubs.rsc.org Internet Source	<1 %
12	www.researchgate.net Internet Source	<1 %
13	Mingjie Tang, Qing Huang, Dongshan Wei, Guozhong Zhao et al. "Terahertz spectroscopy of oligonucleotides in aqueous solutions", Journal of Biomedical Optics, 2015 Publication	<1 %

es.scribd.com

14	Internet Source	<1 %
15	Xiaoping Tao, Yue Zhao, Shengyang Wang, Can Li, Rengui Li. "Recent advances and perspectives for solar-driven water splitting using particulate photocatalysts", Chemical Society Reviews, 2022 Publication	<1 %
16	www.creol.ucf.edu Internet Source	<1 %
17	Submitted to CSU, San Jose State University Student Paper	<1 %
18	Submitted to IIT Delhi Student Paper	<1 %
19	etheses.dur.ac.uk Internet Source	<1 %
20	inqueritos.iscsp.utl.pt Internet Source	<1 %
21	Madan Niraula. "Radical assisted metalorganic chemical vapor deposition of CdTe on GaAs and carrier transport mechanism in CdTe/n-GaAs heterojunction", Journal of Applied Physics, 1998 Publication	<1 %
22	saraswatgroup.stanford.edu Internet Source	<1 %

23	dyuthi.cusat.ac.in Internet Source	<1 %
24	Chandan Ghorui, A. M. Rudra, Udit Chatterjee, A. K. Chaudhary, D. Ganesh. " Efficient second-harmonic and terahertz generation from single BiB O crystal using nanosecond and femtosecond lasers ", Applied Optics, 2021 Publication	<1 %
25	juaps.uoanbar.edu.iq Internet Source	<1 %
26	"Heterogeneous Catalysts", Wiley, 2021 Publication	<1 %
27	Submitted to Monash University Student Paper	<1 %
28	eprints.kfupm.edu.sa Internet Source	<1 %
29	Yuan, N.Y.. "Structure, electrical and optical properties of N-In codoped ZnO thin films prepared by ion-beam enhanced deposition method", Journal of Crystal Growth, 20060415 Publication	<1 %
30	academic-accelerator.com Internet Source	<1 %
31	wrap.warwick.ac.uk Internet Source	<1 %

32	www.science.gov Internet Source	<1 %
33	mafiadoc.com Internet Source	<1 %
34	Metin, H.. "Characterization of chemically deposited ZnSe/SnO"2/glass films: Influence of annealing in Ar atmosphere on physical properties", Applied Surface Science, 20110515 Publication	<1 %
35	www.mpn-magic.com Internet Source	<1 %
36	www.nature.com Internet Source	<1 %
37	Colakoglu, T.. "Investigation of optical parameters of Ag-In-Se thin films deposited by e-beam technique", Journal of Non-Crystalline Solids, 20080715 Publication	<1 %
38	Sivasubramani Vediyappan, Anil Kumar Chaudhary, Venkatesh Mottamchetty, Raja Arumugam et al. "Evaluation of Linear and Nonlinear Optical Properties of D–π–A Type 2-Amino-5-Nitropyridinium Dihydrogen Phosphate (2A5NPDP) Single Crystal Grown by the Modified Sankaranarayanan–	<1 %

Ramasamy (SR) Method for Terahertz Generation", Crystal Growth & Design, 2019
Publication

39	Submitted to University of Kentucky Student Paper	<1%
40	Springer Series in Chemical Physics, 1996. Publication	<1%

Exclude quotes	On	Exclude matches	< 14 words
Exclude bibliography	On